

KMS Technologies – KJT Enterprises Inc.

An EMGS/rxt-company

Appendix 1 Derivations

extract from

Strack, K.-M., 1992, reprinted 1999
***Exploration with deep transient
electromagnetic:*** Elsevier, 373 pp.

This material is not longer cover by copyright. The copyright was released by Elsevier to Dr. Strack on November 5th, 2007.

The author explicit authorizes unrestricted use of this material as long as proper reference is given.

Appendix 1 Derivations

PROOF OF THE ITERATIVE DECONVOLUTION

A detailed discussion of the iterative deconvolution has been presented in Ioup and Ioup (1983). Here only the part of the derivation which is necessary for LOTEM is shown.

In the field, the signal $y(t)$ and the system response function $s(t)$ are measured. The wanted real transient is then $x(t)$, where $y(t)$ is a convolution of $x(t)$ with the system response functions $s(t)$.

$$\begin{aligned} y(t) &= s(t) * x(t) \\ &= \int_{-\infty}^{\infty} s(u) \cdot x(t-u) du \end{aligned} \quad (\text{A.1.1})$$

Following the convolution theorem (Bracewell, 1965) in the transform domain s for example yields

$$Y(s) = S(s) \cdot X(s) \quad (\text{A.1.2})$$

For the iterative deconvolution one now can define a van Cittert-iteration.

$$a_0 = y(t) \quad (\text{A.1.3})$$

$$\begin{aligned} a_1 &= a_0 + [y(t) - a_0 * s(t)] \\ &= y(t) + [y(t) - y(t) * s(t)] \end{aligned} \quad (\text{A.1.4})$$

$$\begin{aligned} a_2 &= a_1 + [y(t) - a_1 * s(t)] \\ &\vdots \\ a_m &= a_{m-1} + [y(t) - a_{m-1} * s(t)] \end{aligned} \quad (\text{A.1.5})$$

If you substitute equation (1.2) into equations (1.3) – (1.5), you get in the transform domain:

$$A_0(s) = Y(s) \quad (\text{A.1.6})$$

$$\begin{aligned} A_1(s) &= Y(s) + [Y(s) - Y(s)S(s)] \\ &= Y(s) [1 + (1 - S(s))] \end{aligned} \quad (\text{A.1.7})$$

$$\begin{aligned} A_2(s) &= A_1(s) + [Y(s) - A_1(s)S(s)] \\ &= Y(s) [1 + 1 - S(s) + 1 - S(s) - S(s) + S(s)^2] \\ &= Y(s) [1 + (1 - S(s)) + (1 - S(s))^2] \\ &\vdots \\ A_m(s) &= A_{m-1}(s) + [Y(s) - A_{m-1}(s)S(s)] \\ &= Y(s) [1 + (1 - S(s)) + (1 - S(s))^2 + \dots + (1 - S(s))^m] \\ &= Y(s) \sum_{i=0}^m (1 - S(s))^i \end{aligned} \quad (\text{A.1.8})$$

The series (1.8) converges for $(1 - S(s)) < 1$. This is always the case for transient electromagnetics, because the transients are causal and the system response function is normalized to 1. As limit of equation (1.8) we obtain:

$$\begin{aligned} \lim_{m \rightarrow \infty} A_m &= \lim_{m \rightarrow \infty} Y(s) \sum_{i=0}^m (1 - S(s))^i \\ &= \frac{Y(s)}{1 - (1 - S(s))} = \frac{Y(s)}{S(s)} = X(s) \end{aligned} \quad (\text{A.1.9})$$

It was proven that the van Cittert iteration (1.6) to (1.8) in the transform domain leads to the wanted quantity $X(s)$. That means that we will get $x(t)$ in the time domain and by doing so one can carry out the deconvolution.

SINGULAR VALUE DECOMPOSITION

The singular value decomposition has helped us to obtain a more objective estimate of the inversion parameters. It is well described in Lancos (1958) and Jackson (1972). Here we include a summary of the SVD for completeness and since it is one of the most frequently requested background details.

The goal is the solution of the linear system:

$$(J^T W^2 J + K^2 I) \Delta = J^T W^2 g \quad (A.2.1)$$

where J is the Jacobian, W the weighing matrix, I the identity matrix, K the damping factor, Δ the parameter difference vector and g the discrepancy vector (see chapter 4). For simplicity reason the weighing matrix may be omitted.

This goal can be reached by spectrally decomposing the Jacobian. After Lancos (1958) a spectral decomposition exists for every $n \times m$ matrix J with $\text{rang}(J) = p \leq \min(m, n)$ such that

$$J = U S V^T \quad (A.2.2)$$

S is a $m \times m$ diagonal matrix. Its elements contain the non negative roots of the eigenvalues of $J^T J$. With the maximum number of linear independent column (or row) vectors $\text{rang}(J) = p$, only p elements of S are different from zero (Jackson, 1972). The elements of S are ordered such that:

$$S_1 \geq S_2 \geq S_3 \dots \geq S_p > 0; S_{p+1}, \dots, S_m = 0 \quad (A.2.3)$$

U is a $n \times m$ matrix with p orthonormal data space eigenvectors in its columns corresponding to the non-zero eigenvectors.

V is a $m \times m$ matrix containing the eigenvectors of the parameter space in its columns.

This means, if V_j is a column vector of V with $j \leq p$ then

$$J^T J V_j = S_j^2 V_j$$

if U_i is a column vector of U with $i \leq p$ then

$$J J^T U_i = S_i^2 U_i$$

Since the column vectors are orthonormal the matrices U and V satisfy

$$U^T U = V^T V = V V^T = I_m \quad (A.2.4)$$

If we define two diagonal matrices S^* and T such that

$$S_{ij}^* = \begin{cases} \frac{1}{S_{ij}} & \text{for } S_{ij} > 0 \\ 0 & \text{otherwise} \end{cases} \quad (\text{A.2.5})$$

$$T_{ii} = \frac{S_{ii}^2}{S_{ii}^2 + K^2} \quad (\text{A.2.6})$$

the solution of equation (2.1) (without weighing matrix) is:

$$\Delta = V T S^* U^T g \quad (\text{A.2.7})$$

Proof: Substitute equation (2.7) in equation (2.1) (without weights).

$$\begin{aligned} (J^T J + K^2 I_m) V T S^* U^T g &= (V S^T U^T U S V^T + K^2 I) V T S^* U^T g = \\ &= (V S^2 V^T V T S^* U^T + V K^2 I T S^* U^T) g = \\ &= (V (S^2 T S^* + K^2 I T S^*) U^T) g = \\ &= (V (S^2 + K^2 I) T S^* U^T) g = \\ &= V S U^T g = I^T g \end{aligned} \quad (\text{A.2.7})$$

SOLUTION OF MAXWELL'S EQUATIONS USING SCALAR POTENTIALS

In this section we derive step by step the solution to Maxwell's equations which leads to the equations for the electromagnetic fields

We use the quasi-stationary Maxwell's equations:

$$\nabla \times \mathbf{E} = -\dot{\mathbf{B}} = \text{curl } \mathbf{E} \quad (\text{A.3.1})$$

$$\nabla \times \mathbf{H} = \mathbf{j} = \text{curl } \mathbf{H} \quad (\text{A.3.2})$$

$$\nabla \cdot \mathbf{D} = 0 \quad (\text{A.3.3})$$

$$\nabla \cdot \mathbf{B} = 0 \quad (\text{A.3.4})$$

and the material equations:

$$\mathbf{j} = \sigma \mathbf{E} \quad (\text{A.3.5})$$

$$\mathbf{B} = \mu \mathbf{H} \quad (\text{A.3.6})$$

$$\mathbf{D} = \epsilon \mathbf{E} \quad (\text{A.3.7})$$

where \mathbf{E} is the electric field, \mathbf{B} is the magnetic induction, \mathbf{H} is the magnetic field, \mathbf{j} is the current density and \mathbf{D} is the electric displacement. σ is the conductivity, $\mu \approx \mu_0 = 4\pi \cdot 10^{-7}$ Vs/Am is the magnetic permeability, and ϵ is the dielectric permittivity. Since \mathbf{j} and \mathbf{B} are both divergence-free, they can be decomposed into a toroidal mode (index E) and a poloidal mode (index M), which are described by scalar Debye potentials ϕ_E and ϕ_M :

$$\begin{aligned}\mathbf{B} &= \mathbf{B}_E + \mathbf{B}_M = \nabla \times \nabla \times (\mathbf{e}_z \phi_E) + \nabla \times (\mathbf{e}_z \sigma \mu_0 \phi_M) \\ \mathbf{j} &= \mathbf{j}_E + \mathbf{j}_M = -\nabla \times (\mathbf{e}_z \sigma \phi_E) + \nabla \times (\mathbf{e}_z \sigma \phi_M)\end{aligned}\quad (\text{A.3.8})$$

where \mathbf{e}_z is the unit vector in z-direction and \mathbf{j}_E is the toroidal current density. It has no vertical component and describes horizontal current loops. \mathbf{j}_M , the poloidal density, has no horizontal component and describes vertical current loops.

From equations (3.5) and (3.6) we get:

$$\begin{aligned}\mathbf{E}_E &= -\nabla \times (\mathbf{e}_z \dot{\phi}_E) & \mathbf{E}_M &= \frac{1}{\sigma} \nabla \times \nabla \times (\mathbf{e}_z \sigma \phi_M) \\ \mathbf{H}_E &= \frac{1}{\mu_0} \nabla \times \nabla \times (\mathbf{e}_z \phi_E) & \mathbf{H}_M &= \nabla \times (\mathbf{e}_z \sigma \phi_M)\end{aligned}\quad (\text{A.3.9})$$

Faraday's induction law (3.1) is already satisfied by \mathbf{E}_E , while \mathbf{H}_M satisfies Ampere's law (3.2). To satisfy (3.1) and (3.2) also with \mathbf{E}_M and \mathbf{H}_E , the two scalar functions ϕ_E and ϕ_M must be solutions of the differential equations

$$\begin{aligned}\nabla^2 \phi_E &= \mu_0 \sigma \dot{\phi}_E \\ \nabla \left(-\frac{1}{\sigma} \nabla (\sigma \phi_M) \right) &= \mu_0 \sigma \dot{\phi}_M\end{aligned}\quad (\text{A.3.10})$$

ϕ_E and ϕ_M are two independent solutions of Maxwell's equations. ϕ_E contains no vertical electric field component and is called the tangential electric polarization or TE mode. ϕ_M has no vertical component of the magnetic field and is called the tangential magnetic polarization or TM mode. The field components of \mathbf{E} and \mathbf{H} can be written:

TE mode	TM mode
$\mathbf{E}_{Ex} = -\frac{\delta}{\delta y} \dot{\phi}_E$	$\mathbf{E}_{Mx} = \frac{1}{\sigma} \frac{\delta^2}{\delta x \delta z} (\sigma \phi_M)$
$\mathbf{E}_{Ey} = \frac{\delta}{\delta x} \dot{\phi}_E$	$\mathbf{E}_{My} = \frac{1}{\sigma} \frac{\delta^2}{\delta y \delta z} (\sigma \phi_M)$
$\mathbf{E}_{Ez} = 0$	$\mathbf{E}_{Mz} = -\left(\frac{\delta^2}{\delta x^2} + \frac{\delta^2}{\delta y^2} \right) \phi_M$

$$\begin{aligned}
\mathbf{H}_{Ex} &= \frac{1}{\mu_0} \frac{\delta^2}{\delta x \delta z} \phi_E & \mathbf{H}_{Mx} &= \sigma \frac{\delta}{\delta y} \phi_M \\
\mathbf{H}_{Ey} &= \frac{1}{\mu_0} \frac{\delta^2}{\delta y \delta z} \phi_E & \mathbf{H}_{My} &= -\sigma \frac{\delta}{\delta x} \phi_M \\
\mathbf{H}_{Ez} &= -\frac{1}{\mu_0} \left(\frac{\delta^2}{\delta x^2} + \frac{\delta^2}{\delta y^2} \right) \phi_E & \mathbf{H}_{Mz} &= 0
\end{aligned} \tag{A.3.11}$$

These fields can be described by closed field lines. In particular, the field lines for \mathbf{j}_E , \mathbf{E}_E , \mathbf{B}_M and \mathbf{H}_M are in horizontal planes and are described by $\phi_E = \text{constant}$ or $\phi_M = \text{constant}$.

The equations (3.10) are only valid, if σ is continual. At layer boundaries, where σ is not continuous, one can derive the following constraints for the Debye potentials:

$$\phi_E, \frac{\delta \phi_E}{\delta z}, \sigma \phi_M \text{ and } \frac{1}{\sigma} \frac{\delta}{\delta z} (\sigma \phi_M) \text{ are continuous.} \tag{A.3.12}$$

In free space it can be assumed that $\sigma = 0$, and thus from the third constraint we get that $\phi_M(z=0) = 0$. This is another expression for the fact that there is no vertical current density at $z = 0$, which has the important consequence that

$$\phi_M = 0 \text{ in } z > 0, \text{ if all sources are in } z < 0 \text{ and } \sigma = \sigma(z). \tag{A.3.13}$$

This means that the induced currents flow in horizontal directions for the arbitrary sources in free space, which are inductively coupled to the layered half-space. On the other hand there are vertical currents, if the coupling of the source is galvanic which is the case for the LOTEM method.

To solve the differential equations (3.10), the scalar potentials ϕ_E and ϕ_M are decomposed into partial waves (Fourier components):

$$\phi_{E,M}(\mathbf{r}, t) = \iiint_{-\infty}^{\infty} f_{E,M}(z, \mathbf{k}, \omega) e^{i(\mathbf{k}\mathbf{r} + \omega t)} d^2 \mathbf{k} d\omega \tag{A.3.14}$$

where $\mathbf{k} = (k_x, k_y, 0)$ and $d^2 \mathbf{k} = dk_x dk_y$.

Substitution of (3.12) into (3.10) yields:

$$\begin{aligned}
 \text{TE-Mode:} \quad & \frac{d^2 f_E(z)}{dz^2} = \alpha^2(z) f_E(z) \\
 \text{TM-Mode:} \quad & \frac{d}{dz} \left(\frac{1}{\sigma} \frac{d}{dz} (\sigma f_M(z)) \right) = \alpha^2(z) f_M(z) ,
 \end{aligned} \tag{A.3.15}$$

$$\text{where} \quad \alpha^2(z) = k^2 + i \omega \mu_0 \sigma(z) , \quad k^2 = |\mathbf{k}|^2$$

$$\text{Using} \quad \frac{\delta}{\delta x} = i k_x , \quad \frac{\delta}{\delta y} = i k_y \quad \text{and} \quad \frac{\delta}{\delta t} = i \omega ,$$

we get for the frequency-wavenumber domain from (11):

$$\begin{aligned}
 \hat{E}_{Ex} &= \omega k_y f_E & \hat{E}_{Mx} &= i k_x \frac{d f_M}{dz} \\
 \hat{E}_{Ey} &= -\omega k_x f_E & \hat{E}_{My} &= i k_y \frac{d f_M}{dz} \\
 \hat{E}_{Ez} &= 0 & \hat{E}_{Mz} &= k^2 f_M \\
 \hat{H}_{Ex} &= \frac{i k_x}{\mu_0} \frac{d f_E}{dz} & \hat{H}_{Mx} &= i k_y \sigma f_M \\
 \hat{H}_{Ey} &= \frac{i k_y}{\mu_0} \frac{d f_E}{dz} & \hat{H}_{My} &= -i k_x \sigma f_M \\
 \hat{H}_{Ez} &= \frac{k^2}{\mu_0} f_E & \hat{H}_{Mz} &= 0
 \end{aligned} \tag{A.3.16}$$

where $(\hat{})$ stands for the frequency-wavenumber domain.

For the following it is useful to define the impedances:

$$Z_E(z, \mathbf{k}, \omega) = \frac{\hat{E}_{Ex}(z, \mathbf{k}, \omega)}{\hat{H}_{Ey}(z, \mathbf{k}, \omega)} = - \frac{\hat{E}_{Ey}(z, \mathbf{k}, \omega)}{\hat{H}_{Ex}(z, \mathbf{k}, \omega)} = i \omega \mu_0 \left(\frac{-f_E(z, \mathbf{k}, \omega)}{\frac{d}{dz} f_E(z, \mathbf{k}, \omega)} \right) \tag{A.3.17}$$

$$Z_M(z, k, \omega) = \frac{\hat{E}_{Mx}(z, k, \omega)}{\hat{H}_{My}(z, k, \omega)} = - \frac{\hat{E}_{My}(z, k, \omega)}{\hat{H}_{Mx}(z, k, \omega)} = i\omega\mu_0 - \frac{\frac{d}{dz} f_M(z, k, \omega)}{\sigma f_M(z, k, \omega)}$$

From the impedances (3.17) we define the reciprocal modified impedances:

$$\begin{aligned} B_{EM}(z, k, \omega) &= \frac{i\omega\mu_0}{Z_E(z, k, \omega)} = - \frac{\frac{d}{dz} f_E(z, k, \omega)}{f_E(z, k, \omega)} \\ B_M(z, k, \omega) &= \sigma Z_M(z, k, \omega) = - \frac{\frac{d}{dz} f_M(z, k, \omega)}{f_M(z, k, \omega)} \end{aligned} \quad (A.3.18)$$

In a horizontally layered half-space within the homogeneous isotropic layer m , f_E and f_M must satisfy the equations:

$$\begin{aligned} \frac{d^2 f_E}{dz^2} f_E(z) &= \alpha_m^2 f_E(z) \\ \frac{d^2 f_M}{dz^2} f_M(z) &= \alpha_m^2 f_M(z) \end{aligned} \quad (A.3.19)$$

$$\text{where } \alpha_m^2 = k^2 + i\omega\mu_0\sigma_m$$

From (3.12) follows that

$$f_E, \frac{d f_E}{dz}, \sigma f_M \text{ and } \frac{d f_M}{dz}$$

are continuous at the layer boundaries. Moreover, f_E and f_M should be 0 for $z \rightarrow \infty$.

The calculation of $f_E(z)$ and $f_M(z)$ will be done in two steps: first a recursive algorithm for the calculation of B_E and B_M at the layer boundaries h_m will be derived. The general solution for equation (3.19) is:

$$\begin{aligned} f_{E,M}(z) &= b_{E,M,m}^- e^{-\alpha_m(z-h_m)} + b_{E,M,m}^+ e^{\alpha_m(z-h_m)}, \text{ for } h_m \leq z \leq h_{m+1} \\ \text{and} \\ f_{E,M}(z) &= b_{E,M,n}^- e^{-\alpha_n(z-h_n)}, \text{ for } z \geq h_n, \end{aligned} \quad (A.3.20)$$

where n is the number of layers and h_n is the last layer boundary. For $z \geq h_n$ only the "−" part exists, because $f_{E,M} = 0$ for $z \rightarrow \infty$.

The solution is:

$$f(z) = (e^{-kz} + r_0 e^{kz}) f_0^e(k, \omega), \quad 0 \geq z \geq -\epsilon \quad (\text{A.3.24})$$

where the index "e" stands for "external".

The first term describes the source field:

$f_E^e(z, k, \omega) = f_0^e(k, \omega) e^{-kz}$, the second term is in the induced field.

Since f_E and $\frac{df_E}{dz}$ must be continual at $z = 0$, we get from equation (3.24)

$$r_0 = \frac{k - B_E}{k + B_E}; \quad B_E := \frac{-f_E'(0)}{f_E(0)}.$$

r_0 is the reflection coefficient and $B_E = B_{E1}$ is calculated recursively using equation (3.22). From equation (3.24) we get the relationship:

$$f_E(0) = f_E^e(0) \frac{2k}{k + B_E} \quad (\text{A.3.25})$$

Thus, for a known source potential $f_E^e(0)$ one can calculate $f_E(0)$, and from there $\phi_E(0)$ to determine \mathbf{E} and \mathbf{H} .

The sources of the TM mode are due to galvanic coupling. If $J_z^e(0)$ is the vertical current density at the surface, (3.11) yields:

$$J_z^e(0) = k^2 \sigma_1 f_M(0^+) \quad (\text{A.3.26})$$

In this case f_M has to satisfy:

$$\frac{d^2}{dz^2} f_M(z) = k^2 f_M \quad (\text{A.3.27})$$

and with $B_M := B_{M1} = -\frac{f_M'(0)}{f_M(0)}$ we get

$$f_M(0^+) = -\frac{k}{B_M} f_M(0^-) \quad (\text{A.3.28})$$

because $\frac{df_M}{dz}$ is continual at $z = 0$.

Together with equation (3.26) this yields:

$$f_M(0^-, k, \omega) = -\frac{B_M(k, \omega)}{\sigma_1 k^3} \hat{J}_z^e(0, k, \omega) \quad (\text{A.3.29})$$

In the following we use cylindric coordinates instead of cartesian coordinates which means: $(x, y, z) \rightarrow (r, \phi, z)$ via $x = r \cos \phi$, $y = r \sin \phi$, $z = z$.

Now we can use the Hankel transformation to calculate ϕ from f :

$$\begin{aligned}\phi(z, r, \omega) &= 2\pi \int_0^\infty f(k, z, \omega) J_0(kr) k dk \\ f(z, k, \omega) &= \frac{1}{2\pi} \int_0^\infty \phi(r, z, \omega) J_0(kr) r dr\end{aligned}\quad (\text{A.3.30})$$

where $r^2 = x^2 + y^2$

For the LOTEM method we have to consider a horizontal electric dipole (HED) which is described by a current I along the x -axis at $r = 0$ and the electric dipole moment D .

First we want to calculate the external potential $\tilde{\phi}_E^e$ for the TE mode (the "-" indicates that the potential is located in the frequency domain). To do this, we use Biot-Savart's law to calculate H_z , and using equation (3.16) we get

$$\tilde{H}_z^e(r, \omega) = -\frac{D y}{4\pi R^3} = \frac{1}{\mu_0} \frac{\delta^2}{\delta z^2} \tilde{\phi}_E^e(r, \omega), \quad (\text{A.3.31})$$

where $R^2 = r^2 + z^2$

This yields:

$$\frac{\delta^2}{\delta z^2} \tilde{\phi}_E^e(r, \omega) = -\frac{\mu_0 D(\omega)}{4\pi} \frac{\delta}{\delta y} \left(\frac{1}{R} \right)$$

and, using $\frac{1}{R} = \int_0^\infty e^{-k|z|} J_1(kr) dk$, we get

$$\begin{aligned}\tilde{\phi}_E^e(r, \omega) &= \frac{\mu_0 D(\omega)}{4\pi} \int_0^\infty e^{-k|z|} J_1(kr) \frac{dk}{k} \sin \phi \\ &= \frac{\mu_0 D(\omega) y}{4\pi (R + |z|)}\end{aligned}\quad (\text{A.3.32})$$

This results in the total TE potential (using equation (3.24)):

$$\tilde{\phi}_E(r, \omega) = \frac{\mu_0 D}{4\pi} \left(\frac{r}{R + |z|} - \int_0^\infty B_M(k) e^{-k|z|} J_1(kr) \frac{dk}{k} \right) \sin \phi \quad (\text{A.3.33})$$

For the TM mode we use the vertical current density at $z = 0$ in the wavenumber domain:

$$\tilde{J}_z^e(0, \mathbf{k}, \omega) = \frac{d i k_x}{4\pi^2}$$

and, using equation (3.29), we get for the total ϕ_M :

$$\tilde{\phi}_M(r, \omega) = \frac{-D(\omega)}{4\pi} \int_0^\infty B_M(k) e^{-k|z|} J_1(kr) \frac{dk}{k} \cos \phi \quad (\text{A.3.34})$$

To transform ϕ_E and ϕ_M to time domain, we write the step function

$$D(t) = \begin{cases} 0 & t < 0 \\ D_0 & t > 0 \end{cases} \quad \text{as}$$

$$D(t) = \frac{D_0}{2\pi i} \int_{-\infty}^{\infty} \frac{e^{i\omega t}}{\omega} d\omega$$

Finally, we calculate \mathbf{E} and \mathbf{H} in time domain from ϕ_E and ϕ_M using equation (3.16). The final results for E_x , E_y and $d/dt H_z$ are:

$$\begin{aligned} E_x^u(\mathbf{r}, t) = & \frac{-1}{2\pi i} \int_{-\infty}^{\infty} \frac{e^{i\omega t}}{\omega} \frac{-i\omega\mu_0 D_0}{4\pi} \int_0^\infty \left\{ \left(\frac{2B_M(\kappa, \omega) - B_M(\kappa, 0) - \kappa}{\kappa_1^2} \right. \right. \\ & \left. \left. - \frac{2}{B_E(\kappa, \omega) + \kappa} \right) \left(\left(\kappa J_0(\kappa, r) - \frac{2}{r} J_1(\kappa, r) \right) \cos^2 \phi + \frac{1}{r} J_1(\kappa, r) \right) \right. \\ & \left. - \frac{B_E(\kappa, \omega) - \kappa}{B_E(\kappa, \omega) + \kappa} J_0(\kappa, r) \right\} d\kappa d\omega - \frac{\rho_1 D_0}{4\pi r^3} (2 - 3 \sin^2 \phi) \end{aligned} \quad (\text{A.3.35})$$

$$\begin{aligned} E_y^u(\mathbf{r}, t) = & \frac{-2}{2\pi i} \int_{-\infty}^{\infty} \frac{e^{i\omega t}}{\omega} \frac{-i\omega\mu_0 D_0}{4\pi} \cos \phi \sin \phi \int_0^\infty \left(\frac{2B_M(\kappa, \omega) - B_M(\kappa, 0) - \kappa}{\kappa_1^2} - \right. \\ & \left. \frac{2}{B_E(\kappa, \omega) + \kappa} \right) \left(\kappa J_0(\kappa, r) - \frac{2}{r} J_1(\kappa, r) \right) d\kappa d\omega - \frac{3\rho_1 D_0 \cos \phi \sin \phi}{4\pi r^3} \end{aligned}$$

$$U_z^u(\mathbf{r}, t) = \frac{-1}{2\pi} \int_{-\infty}^{\infty} \mu_0 A e^{i\omega t} \frac{D_0 \cos \phi}{4\pi} \int_0^\infty \frac{B_E(\kappa, \omega) - \kappa}{B_E(\kappa, \omega) + \kappa} \kappa J_1(\kappa, r) d\kappa d\omega \quad (\text{A.3.36})$$

KMS Technologies – KJT Enterprises Inc.
6420 Richmond Ave., Suite 610
Houston, Texas, 77057, USA
Tel: 713.532.8144

Please visit us
<http://www.kmstechnologies.com>

This material is not longer covered by copyright. The copyright was released by Elsevier to Dr. Strack on November 5th, 2007.

The author explicitly authorizes unrestricted use of this material as long as proper reference is given.

KMS Technologies – KJT Enterprises Inc.

An EMGS/rxt-company

Appendix 2 Data Format Standards

extract from

Strack, K.-M., 1992, reprinted 1999
***Exploration with deep transient
electromagnetic:*** Elsevier, 373 pp.

This material is not longer cover by copyright. The copyright was released by Elsevier to Dr. Strack on November 5th, 2007.

The author explicit authorizes unrestricted use of this material as long as proper reference is given.

Appendix 2

Data Format Standards

INTRODUCTION

One of the basic problems with electromagnetic methods is the lack of compatibility between different systems and with other geophysical techniques. Thus, it is very important to use already existing standards, rather than making new ones. This means initially more development work since all possible options and sidekick developments should be considered. In the long run, the return of increased application of the techniques will be larger than fighting forever incompatibilities.

From the beginning the choice was made to use a seismic standard. The only one suitable for original records is the SEG Y standard (Barry et al, 1975). Using this standard also allows any seismic processing company to process electromagnetic data. This will bring a wealth of experience and new ideas into the processing and interpretation of EM data. The next step in standard would obviously be the adaption of the SEG 2 standard. At this stage this seems not feasible until sufficient users for the SEG 2 standard exist.

Transient electromagnetic data when recorded as original time series is in principle very similar to seismic data. The seismic source is substituted by the transmitter and the geophone traces by the transients. The need of a standard came about when larger scale LOTEM (a special transient EM configuration) measurements were conducted around the world.

This document describes the structure of the files as they are being used on the LOTEM Processing System (LOPS) software. At this stage, we have made the decision of either writing strictly SEG Y tapes or a structure conforming internally with the SEG Y standard adapted for the LOTEM Processing and Interpretation System (LOPIS). We strongly discourage you from using any other format, since the data will end up being non-interchangeable.

I would like to thank O. Engels, P.J. Bürger, J. Rossow for contributing all their thoughts and efforts to this standard. W. Schott spent countless hours checking the intermediate versions.

FILE FORMATS

On VAX machines the data is stored as binary random access file. The record size was selected to 256 bytes as a compromise between different field systems, number of real data points to be read into memory for selective stacking (1 record) and already existing computer standards. The selection for 256 bytes was made as being half of the VAX default record size. Even this moderate size gives you considerable storage problems when selectively stacking 1000 transient (i.e. reading 1000 records with 64 real words equals 256 kbytes of data). Effectively this can only be handled by virtual addressing operating systems.

There are three kinds of files used within VAX-based LOPIS: a raw or prestacked processed data file with 50 transients per file, a stacked data file with one transient per file, and an ASCII data file obtained after conversion to logarithmically spaced data. The latter is only of interest within LOPS and thus not discussed here. The prestack data file and the poststack data file have now the same format. This allows us to use any number of data points without changing the format.

On a PC the file format is identical to the VAX format except for the way the PC writes internally real numbers. Thus only binary files from the VAX must be converted to the PC format.

Format of a LOPS Data File

The example record numbers are calculated for 1024 data points. The respective values are given for 2048 data points in brackets in table A2.1. The record pointer is calculated from the number of data points in the file header. A graphic illustration is shown in figure A2.1

Table A2.1: Record structure for a LOPS data file containing several individual transients.

VAX RECORD No.	CONTENT:
1-15	File header information
16	Trace header of 1st transient
17-32(48)	Data of 1st transient
33(49)	Trace header of 2nd transient
34-49(50-81)	Data of 2nd transient
...	...
...	...
<EOF>	

This file format is presently used by LOPS. It is possible to have a variable file length. The standard maximum size (50 transients in a file) is:

- 865 records or 433 blocks for 1024 data points
- 1665 records or 833 blocks for 2048 data points.

Format of a LOPS Stacked Data File

The shown record numbers are calculated for 1024 data points. The respective values are given for 2048 data points in table A2.2 in brackets. The record pointer is calculated from the number of data points in the file header. A graphic illustration is shown in figure A2.1

Table A2.2: Record structure for a LOPS data file containing a stacked transient.

VAX RECORD No.	CONTENT:
1-15	File header information
16	Trace header of transient
17-32(48)	Data of transient
33-48(49-80)	Standard deviation of data
...	...
...	...
<EOF>	

Because there is only one transient in file, the file size can be calculated to

- 48 records or 24 blocks for 1024 data points.
- 80 records or 40 blocks for 2048 data points.

NOTE

There are two coordinate systems in use. One is the absolute coordinate system used in the survey area. Please, use only rectangular coordinate systems. In FRG x (EAST) is the RECHTSWERT and y (NORTH) is the HOCHWERT. The second system is the reference coordinate system based on the transmitter with the origin (0,0) at the transmitter center. For this x, y coordinates are being used. When the transmitter information is available before acquisition the transformation can be done during the acquisition phase. Otherwise, it must be done during processing. E1 and E2 mark the respective electrode positions of the grounded wire dipole transmitter (source).

When the file contains records of an entire array the respective receiver position of the traces must be known. If the file contains single records at one site, the reference receiver position from the file header may be used.

NOTE

Under a record we include all data recorded simultaneously during one source sweep (pulse, current switch etc). This means the i-th transient of a spread builds one record. Under a trace we include each individual transient recorded at each receiver site.

Fig.A2.1: Graphic illustration of the file records structure of LOTEM SEGY standard data files. Here the implementation for the VAX is shown (after Engels, pers. comm.).

The bytes positions 0001–3200 hold a 40x80–byte card image file header as summarized in table A2.3. In this card image file header the acquisition comments are written in the byte positions 0001–1520 and the processing comments in byte position 1521–3200. The above is contained as mask in block data for read and write. Internal read/write will have to fill the empty places. For the DEMS IV system, the acquisition comments (WDUM(70–100)) are written in the file header beginning with byte 894 and the processing comments beginning byte position 1537. None of the comments is presently written into the header. Future acquisition systems should do so.

Table A2.3: Card image header mask as defined by the SEG Y standard modified for TEM data.

Use free spaces for your entry. The information is best coded in a block data module.

```

----- CARD IMAGE NUMBER
0000000001111111112222222222333333333344444444445555555555666666666677777777778
1234567890123456789012345678901234567890123456789012345678901234567890
-----
C 1 CLIENT          COMPANY          CREW NO
C 2 LINE            AREA              MAP ID
C 3 REEL NO         DAY-START OF REEL  YEAR   OBSERVER
C 4 INSTRUMENT: MFG  MODEL            SERIAL NO
C 5
C 6 SAMPLE INTERVAL  SAMPLES/TRACE  BITS/IN  BYTES/SAMPLE
C 7 RECORDING FORMAT  FORMAT THIS REEL  MEASUREMENT SYSTEM
C 8 SAMPLE CODE: FLOATING PT  FIXED PT  FIXED PT-GAIN  CORRELATED
C 9 GAIN TYPE: FIXED  BINARY  FLOATING POINT  OTHER
C10 FILTERS: ALIAS  HZ NOTCH  HZ BAND  -  HZ SLOPE  -  DB/OCT
C11 SOURCE: TYPE    LENGTH    BEARING    AREA
C12 COMMENTS:
C13
C14
C15
C16
C17
C18
C19
C20 PROCESSING:
C21
C22
C23      !! THE CARD IMAGE IS AVAILABLE THROUGH COMMON!!!
C24
C25
C26
C27
C28
C29
C30
C31
C32
C33
C34
C35
C36
C37
C38
C39
C40

```

SEG Y uses header bytes 3261 to 3600 as optional information. The file header should contain only the information which is not essential for the processing of a trace. If the header is needed, the information in these bytes should also be in the trace header. There must be an IBG (Interblock Gap) after byte 3200. Table A2.4 shows the definition of the file header sorted by bytes.

The coordinates given in meters cannot be represented as INTEGER*2, because their values are too large when using European GKK/UTM coordinates with 6 digits. This difference is presently under investigation.

NOTE

There must be an IBG between the card image header and the optional header. Otherwise IBGs are ONLY between traces. This means data and trace header are NOT separated (see SEG Digital Tape Standards, SEG 1980; Barry et al, 1973).

NOTE

Variables are I*2 or I*4, except for the card image header. Bold face text gives important comments not directly part of the header explanation. RFU means that this variable is presently not used but already reserved for future use. Do not use these variables for your implementation. *Not used, dummy* marks presently unassigned bytes in the header. You may use these bytes for your specific implementation. Reference to LOPS variables is only given when these are different. generally for simplicity it is tried to keep the same variable names as in SEG Y.

Table A.2.4: File header record and byte definition for TEM data adopting SEG Y standard.

VAX REC.	byte position	SEG Y variable	variable type	LOPS present variable name	LOPS meaning
1	0001-0256	C		CARDIMAGE(0001-0256)	--
2	0257-0512	A		CARDIMAGE(0257-0512)	--
3	0513-0768	R		CARDIMAGE(0513-0768)	--
4	0769-1024	D		CARDIMAGE(0769-1024)	WDUM(70-100)
acquisition comments at byte 894-925					
5	1025-1280	I		CARDIMAGE(1025-1280)	--
6	1281-1536	M		CARDIMAGE(1281-1536)	PROCC(1-200)
processing comments, 1537 up					
7	1537-1792	A		CARDIMAGE(1537-1792)	--
8	1793-2048	G		CARDIMAGE(1793-2048)	--
9	2049-2304	E		CARDIMAGE(2049-2304)	--
10	2305-2560	H		CARDIMAGE(2305-2560)	--
11	2561-2816	E		CARDIMAGE(2561-2816)	--
12	2817-3072	AD		CARDIMAGE(2817-3072)	--
13	3073-3200	ER		CARDIMAGE(3073-3200)	--
HERE MUST BE AN IBG (interblock gap) on magnetic tapes					
3201		SURNUM	I*4		survey id number. i.e. 8601. year, sequential.
3205		LINENO	I*4		line number.
3209		REELNO	I*4		tape reel number.
3213		TRAREC	I*2		no. of traces per record.
3215		AUXREC	I*2	IFILSOU	source code.
3217		DT	I*2		srate in micro s. this reel.
3219		IDELTO	I*2		srate in micro s. original.
3221		NDAT	I*2		no. of samples per trace.
3223		NDATO	I*2		no. of samples per trace. original.
3225		SCODE	I*2		data sample format (i.e. 1=R*4, 2=I*4, 3=I*2, 4= other).
3227		CDPFOLD	I*2		not used, dummy
3229		TRACSOR	I*2		trace sorting, RFU
3231		ISTACK	I*2		no. of sums per trace.
3233-3248 reserved for mixed frequency EM systems					
3233		SFSTART	I*2		sweep frequency at start. RFU

3235	SFEND	I*2	sweep frequency at end, RFU
3237	SWLENG	I*2	sweep length in ms, RFU
3239	SWCODE	I*2	sweep type code, RFU
3241	SWTRACE	I*2	sweep trace number, RFU
3243	TAPSTAR	I*2	taper length at start, RFU
3245	TAPEND	I*2	taper length at end, RFU
3247	TAPTYPE	I*2	taper type code, RFU
3249	ICORR	I*2	correlated traces, RFU (0=yes; 1=no)
3251	IGAIN	I*2	gain recovery (0=yes;1=no).
3253	AMPREC	I*2	not used, dummy
3255	IMEAS	I*2	meas. unit: 0=meters,1=feet.
3257	IMPSIG	I*2	not used, dummy
3259	VIBCOD	I*2	not used, dummy

SEGY optional file header 3261-3600

3261	--	I*2	ISTYPE	type of survey: 1=seismic (def.); 2=radar; 3=LOTEM.
3263	--	I*2	ITIMSC	time scale: 1=pico s; 2=nano s; 3=micro s (default); 4= milli s; 5=sec.
3265	--	I*2	ITYPREC	type of recording: 1=finite length (def.); 2= continuously.
3267	--	--	--	not used, dummy
3269	--	--	--	not used, dummy
3271	--	--	--	not used, dummy
3273	--	I*2	ITLEN	trans.length (see byte 3263).
3275	--	I*2	ITLEAD	lead time (see byte 3263).
3277	--	I*2	IVPERD	micro volts/division of ADC
3279	--	I*2	TRIGPOL	trigger reference polarity (1=positive, 2=negative, 0=undefined).
3281	--	I*2	ISRCELE	elev. of source center (see byte 3255).
3283	--	I*2	ISRCLN	transmitter length (see byte 3255).
3285	--	I*2	ICURREN	source current in Amperes.
3287	--	I*4	JGKK(1)	transmitter coor. EAST E1.
3291	--	I*4	JGKK(2)	transmitter coor. NORTH E1.
3295	--	I*4	JGKK(3)	transmitter coor. EAST E2.
3299	--	I*4	JGKK(4)	transmitter coor. NORTH E2.
3303	--	I*4	JGKK(5)	receiver coor. EAST.
3307	--	I*4	JGKK(6)	receiver coor. NORTH.
3311	--	I*4	JXCOOR	x-coor. of receiver ref.
3315	--	I*4	JYCOOR	y-coor. of receiver ref.
3319	--	I*4	JZCOOR	elevation of rec. ref (see byte 3255).
3323	--	I*2	IRECREP	receiver reference (i.e. n= n-th receiver in spread).
3325	--	I*2	--	not used, dummy
3327	--	I*2	--	not used, dummy

Notch filter settings bytes 3329-3360 (0=out; 1=in)

14	3329	--	I*2	IA50S1	amplifier 50 Hz sett. 1.
	3331	--	I*2	IA50S2	amplifier 50 Hz sett. 2.
	3333	--	I*2	IA50S3	amplifier 50 Hz sett. 3.
	3335	--	I*2	IA50S4	amplifier 50 Hz sett. 4.
	3337	--	I*2	IA50S5	amplifier 50 Hz sett. 5.
	3339	--	I*2	IP50S1	preamplifier 50 Hz sett. 1.
	3341	--	I*2	IP50S2	preamplifier 50 Hz sett. 2.
	3343	--	I*2	IP50S3	preamplifier 50 Hz sett. 3.
	3345	--	I*2	IA16S1	amplifier 16 2/3 Hz sett. 1.
	3347	--	I*2	IA16S2	amplifier 16 2/3 Hz sett. 2.
	3349	--	I*2	IA16S3	amplifier 16 2/3 Hz sett. 3.
	3351	--	I*2	IA16S4	amplifier 16 2/3 Hz sett. 4.
	3353	--	I*2	IA16S5	amplifier 16 2/3 Hz sett. 5.
	3355	--	I*2	IP16S1	preamplifier 16 2/3 Hz.
	3357	--	I*2	IP16S2	preamplifier 16 2/3 Hz.

3359	--	I*2	IP16S3	preamplifier 16 2/3 Hz.
3361	--	I*2	ILAMP	lowpass frequency amplifier.
3363	--	I*2	ILPAMP	lowpass frequency preamp.
3365	--	I*2	IAGAIN	amplifier gain setting.
3367	--	I*2	IPGAIN	preamplifier gain setting.
3369	--	I*2	YEAR	year file created.
3371	--	I*2	MONTH	month file created., 0=
				sequential days in 3373.
3373	--	I*2	DAY	day file created.
3375	--	I*2	HOURL	hour file created.
3377	--	I*2	MINUTE	minute file created.
3379	--	I*2	SECOND	second file created.
3381	--	I*2	ITIMBA	time base: 1=local; 2=GMT;
				3=other.
3383	--	I*2	ISPEC	spectrum switch: 1=spectra,
				0=raw data.
3385	--	I*2	NSTACK	number of traces in this file (proc.)
3387	--	I*2	IASTACK	average number of stacks.
3389	--	I*2	MINSTK	min. no. of stacks (proc.)
3391	--	I*2	MAXSTK	max. no. of stacks (proc.)
3393-3584	--	--	--	not used, dummy
15 3585-3600	--	--	--	not used, dummy
record filler				VAX spare: non SEGY

TRACE HEADER STRUCTURE

Suppose the number of data points is NDAT. The record pointer of the n-th trace (MOLD for LOPS) is calculated by:

$$\text{REC} = (\text{MOLD} - 1) * (\text{NDAT} / 64 + 1) + 16$$

where 64 is the number of REAL data points per record. We have defined the record length on the VAX to be 256 bytes long (equals 64 real numbers). The value of 1 is added for the trace header of each trace and the value of 16 is added for the file header of each file. The definition of the trace header is given in table A2.5.

The time base is referred to the default onset (IONSET) which is in most instances 20% of the total trace length. Once the onset (IONSET in sample number) is known, this is set to be zero reference time. The pretrigger and delay time is referenced to this time (and corresponding sample number).

(All values are either INTEGER*4 or INTEGER*2 defined by its length.)

Table A.2.5: Trace header byte allocation table for TEM data adopting SEG Y standard.

byte pos. length	SEG Y variable	LOPS present value	LOPS meaning
001 4	TRACNO		trace number within line, numbers increase for add. reels.
005 4	TRAREEL		trace number in reel.
009 4	ORIREEL	JORREC	original record number.
013 4	TRAORI		trace number within original record.
017 4	ENEPT	ISRCNUM	source point number.
021 4	CDPENS		gather number. RFU
025 4	TRENSNM		num. code for current trace within one gather. RFU.
029 2	TRACID		trace id: 01-31 reserved for seismic data. 32=unknown. 33=LOTTEM data raw.34=system response. 35=LOTTEM data stacked. 36=LOTTEM logarithmic (equidist.) data.
031 2	NSTACK		number of stacked traces yielding this one.
033 2	HORSTAC		number of horizontal stacks yielding this trace. RFU
035 2	USAGE		data code: 1=production. 2=test.
037 4	OFFSET		source to receiver (this trace) offset (ref. coord. syst.)
041 4	JZCOOR		receiver elevation (depending on byte 69-70).
045 4	SRCELE		source center elevation (depending on byte 69-70).
049 4	SRCDPE		source length (depending on byte 69-70).
053 4	DATELE		receiver datum elevation (depending on byte 69-70).
057 4	DATSRCE		source center datum elevation (depending on byte 69-70).
061 4	WATDEPS	JCURREN	source current in amperes.
065 4	WATDEPG		not used, dummy
069 2	SCALAR		scale factor for bytes 41-60 (negative = divisor).
071 2	SCALAR1		scale factor for bytes 73-88 (negative = divisor).
073 4	SRCCOX	JXREF	receiver x coordinate w.r.t. reference receiver (depending on byte 71-72).
077 4	SRCCOY	JYREF	receiver y coordinate w.r.t. reference receiver in m (depending on byte 71-72).
081 4	GRPCORX		receiver x-coordinate (depending on byte 71-72).
085 4	GRPCORY		receiver y-coordinate (depending on byte 71-72).
089 2	CORUNI		coordinate system used: 1=length. 2= seconds of arc.
091 2	WEAVEL		not used, dummy
093 2	SUBVEL		not used, dummy
095 2	UPTSRC		not used, dummy
097 2	UPTGRP		not used, dummy
099 2	SRCSTA		not used, dummy
101 2	GRPSTA		not used, dummy
103 2	TOTSTAT	IAMEXP	amplifier gain setting (if binary. exponent only).
105 2	LAGTIA	IONSET	number of samples before onset.
107 2	LAGTIB	IPRETRIG	pretrigger in base time scale.
109 2	DELAYT		delay time in base time scale of synchronization trigger.
111 2	MUTETS		mute time start. RFU
113 2	MUTETE		mute time end. RFU
115 2	NDAT		number of data points (samples) in this trace.
117 2	DT		sample interval (depending on file header byte 3263-3264).
119 2	GAININS		gain type: 1=fixed; 2=binary; 3=IFP.
121 2	GAINCON	IPAEXP	preamplifier gain setting (if binary. exponent only).
123 2	INIGAIN		initial gain in db.
125 2	ICORR		correlated traces (0=yes: 1=no). RFU
byte 127-140 reserved for mixed frequency EM systems			
127 2	SFSTART		sweep frequency at start. RFU
129 2	SFEND		sweep frequency at end. RFU
131 2	SWLENG		sweep length in ms. RFU
133 2	SWCODE		sweep type code. RFU
135 2	TAPSTART		taper length at start. RFU
137 2	TAPEND		taper length at end. RFU
139 2	TAPTYPE		taper type code. RFU

141	2	ALIASF		alias filter frequency (0=not used).
143	2	ALIASSL		alias filter slope (0=passive).
145	2	NOTCHF		notch filter base frequency (0=not used).
147	2	NOTCHSL		notch filter slope (0=passive).
149	2	HIPASS		high pass filter frequency (0=not used).
151	2	LOPASS		low pass filter frequency (0=not used). amplifier.
153	2	HIGHPSL		high pass filter slope (0=passive).
155	2	LOWPASL		low pass filter slope (0=passive). amplifier.
157	2	YEAR		year of data recording.
159	2	DAY		day of data recording.
161	2	HOURL		hour of data recording.
163	2	MINUTE		minute of hour recording.
165	2	SECOND		second of minute recording.
167	2	TIMBASE		time basis: 1=local, 2=GMT, 3=other.
169	2	TRAWEI		trace weighting factor.
171	2	GRPROL	MONTH	month of data recording (0=sequential days in 159).
173	2	GRPONE		station no. of first trace in original record.
175	2	GRPLAST		station no. of last trace in original record.
177	2	NUMGRP		number of receivers per group, RFU
179	2	OVRTRAV	IRCVCD	receiver coil code.

SEG Y optional trace header 181-240

181	2	--	ILOPAPA	low pass filter frequency (0=not used). preamplifier.
183	2	--	ILOPAPS	low pass filter slope (0=passive). preamplifier.
185	2	--	JSTATI	station number increment, used when more than one transient occurs at the same site (multiple transmitters, tests, etc.).
187	2	--	IRECSTAT	receiver station number.
189	2	--	FFID	field file identification
191	2	--	IA16S(1)	amplifier 16 2/3 Hz setting 1.
193	2	--	IA16S(2)	amplifier 16 2/3 Hz setting 2.
195	2	--	IA16S(3)	amplifier 16 2/3 Hz setting 3.
197	2	--	IA16S(4)	amplifier 16 2/3 Hz setting 4.
199	2	--	IA16S(5)	amplifier 16 2/3 Hz setting 5.
201	2	--	IREMTOT	total number of remote units.
203	2	--	NCHAN	nos of receivers per spread.
205	2	--	IA50S(1)	amplifier 50Hz setting 1.
207	2	--	NFIRST	first channel number.
209	2	--	IA50S(2)	amplifier 50Hz setting 2.
211	4	--	IEDL	length of dipole, if 215 =1 or 2 or receiver equivalent area in square units otherwise.
215	2	--	IFIELD	0-HZ, 1-EX, 2-EY, 3-HX, 4-HY.
217	2	--	ISYSTEM	receiver system code.
219	2	--	ICHAN	recording channel in use.
221	2	--	IPHYSADD	physical address of remote unit.
223	2	--	IA50S(3)	amplifier 50Hz setting 3.
225	2	--	IA50S(4)	amplifier 50Hz setting 4.
227	2	--	IA50S(5)	amplifier 50Hz setting 5.
229	2	--	IP50S(1)	preamplifier 50 Hz setting 1.
231	2	--	IP50S(2)	preamplifier 50 Hz setting 2.
233	2	--	IP50S(3)	preamplifier 50 Hz setting 3.
235	2	--	IP16S(1)	preamplifier 16 2/3 Hz setting 1.
237	2	--	IP16S(2)	preamplifier 16 2/3 Hz setting 2.
239	2	--	IP16S(3)	preamplifier 16 2/3 Hz setting 3.

KMS Technologies – KJT Enterprises Inc.
6420 Richmond Ave., Suite 610
Houston, Texas, 77057, USA
Tel: 713.532.8144

Please visit us
<http://www.kmstechnologies.com>

This material is not longer covered by copyright. The copyright was released by Elsevier to Dr. Strack on November 5th, 2007.

The author explicitly authorizes unrestricted use of this material as long as proper reference is given.

KMS Technologies – KJT Enterprises Inc.

An EMGS/rxt-company

Appendix 3 Useful Information

extract from

Strack, K.-M., 1992, reprinted 1999
***Exploration with deep transient
electromagnetic:*** Elsevier, 373 pp.

This material is not longer cover by copyright. The copyright was released by Elsevier to Dr. Strack on November 5th, 2007.

The author explicit authorizes unrestricted use of this material as long as proper reference is given.

Appendix 3

Useful Information

GLOSSARY

A-type curve – an apparent resistivity curve exhibiting an increasing resistivity for a 3-layer model: ($\rho_1 < \rho_2 < \rho_3$)

Analog modeling – in order to simulate the real geologic situation, a model can be built in the laboratory using metal or other materials. When scaling down the geometry the conductivity must also be scaled to simulate as close as possible the field situation. This type of scale modeling is called analog modeling.

Archie's formula – an empirical formula relating the resistivity of a formation with the resistivity of the formation fluid, the formation porosity and the pore space filled by the pore fluid. The constants associated with this formula are empirical and may change with rock type. Archie's law should only be applied to single member rocks (i.e. clean sand).

Anisotropy – a volume element is electrically anisotropic when the resistivity of a layered medium is different in horizontal and verti-

cal direction, i.e. the medium has different longitudinal and transverse resistivity. A sedimentary layer-cake is typically anisotropic due to its depositional history.

Bipolar continuous waveform – see *current waveform*

Bipolar waveform – see *current waveform*

Calibration factor – a constant which for the magnetic components of TEM only depends on the distance between transmitter and receiver. This factor can be used to compensate for inaccuracies in field parameters as well as corrections due to current channeling and static shifts.

Coefficient of anisotropy – the square root of the ratio of vertical and horizontal resistivity $\sqrt{\frac{\rho_v}{\rho_h}}$

Clock rate – time length of one clock pulse or time between clock pulses. Typically the clock rate is half of the repetition rate.

Conductance – see *total conductance*.

Conductance referencing – a correction procedure where the total conduc-

tance of a layer or layer-cake is kept fixed and the thickness and resistivity are adjusted. Usually, the resistivity is selected to be the average resistivity and the thickness is adjusted accordingly keeping the total conductance to be the same.

Controlled source electromagnetics – a terminology grouping all electromagnetic techniques which use their own transmitter. Examples are transient electromagnetics (TEM) and controlled source audio EM (CSAMT).

CSAMT – Controlled Source Audio Magnetotelluric method. A technique similar to magnetotellurics in the audio frequency range (1 Hz to 20 kHz) using as source excitation a transmitter which is at least five times the skin depth away from the receiver.

Cumulative conductance – see *total conductance*.

Cultural noise – electromagnetic noise caused by man and the effects of industrialization and civilization (i.e. power lines etc).

Current waveform – the shape of the current as a function of time as injected by the transmitter. To avoid effects caused by the polarization of the electrodes for LOTEM a bipolar waveform is being used. This waveform has the shape of a positive and negative square wave separated by an off-time. A bipolar continuous waveform is obtained when the off-time is negligible (polarity reversing transmitter).

Electrical anisotropy – see *anisotropy*.

EM 37 – shallow transient EM system developed by Geonics Ltd. of Canada.

Equivalence – see *layer equivalence*.

H-type curve – An apparent resistivity curve exhibiting a decrease resistivity second layer ($\rho_1 > \rho_2 < \rho_3$).

Inversion – a procedure to derive from the field data an earth model which is consistent with the data and describes the subsurface.

Joint inversion – when inverting two independent data sets simultaneously to obtain one resulting model, one calls this process joint inversion. Usually the data vector has the length of both data sets while the model parameter vector remains of the same length as for ordinary inversion methods.

K-type curve – An apparent resistivity curve exhibiting an increase resistivity of the second layer ($\rho_1 < \rho_2 > \rho_3$).

Layer-cake – a combination of different layers building one unit. Typically used in sedimentary environment because of its depositional process.

Layer equivalence – a procedure to reduce a multi-layer model (derived from a well log) to a simpler model containing less layers. Usually the thickness of the layers, h_i , is maintained. Then from the total thickness, H_T , the average resistivity is calculated using a formula derived from the total conductance.

LNC – Local Noise Compensation technique. A noise compensation

$$\rho_{\text{average}} = H_T / \sum_{i=1}^n \frac{h_i}{\rho_i}$$

method using a base station to obtain a high quality base stack. This is then used to calculate the noise for the entire measuring time. The noise of the base station is then subtracted from the individual records of a mobile receiver. This technique can only be used, when the noise at the base station and at the mobile receiver is correlated (spatially constant).

Longitudinal resistivity – The resistivity of a medium measured with horizontal current flow. The resistivity in lateral direction.

LOTEM – Long Offset Transient Electromagnetics. A transient electromagnetic sounding technique using an earthed wire transmitter and several components of the electromagnetic field at the receiver which yield independent information on the resistivity structure of the subsurface.

Magnetotellurics – an electromagnetic depth sounding method using the natural electromagnetic fields as source and measuring 5 components (H_x , H_y , H_z , E_x , E_y) of the electromagnetic field.

MT – see *magnetotellurics*.

Nonseismic methods – a terminology referring to the geophysical techniques used for oil exploration other than reflection seismics (i.e. gravity, magnetics, electromagnetics etc.).

Offset – distance between transmitter and receiver center position.

Off-time – the time between current switching when no current is flowing in the transmitter

PRBS – Pseudo Random Binary Sequence; an electromagnetic technique where the transmitter signal code in a PRBS fashion. The intention of this technique is to overcome the noise in the same manner as done with vibroseis in reflection seismic (see Duncan et al, 1980).

Q-type curve – an apparent resistivity curve showing a decreasing resistivity for a 3-layer model: ($\rho_1 > \rho_2 > \rho_3$).

Periodic noise – electromagnetic interference noise caused by power lines from the AC grid and AC railroad. The noise is of sinusoidal nature and can usually be filtered out by digital filters or analog notch filters during recording. In general geophysics called "high-line noise".

Ramp time – the time the transmitter current requires to go from one constant current state to the other.

Repetition rate – the full cycle between source signals of the same shape and polarity.

Reversal – the term reversal describes a transient signal which crosses the reference DC-level during signal duration. Reversals are not theoretically possible for layered structures for the LOTEM H_z component and are indicative of faults, pipelines and the like.

SIROTEM – shallow transient EM system developed by the Scientific and Industrial Research Organization of Australia.

Spitter – a mechanical device used to pick up wire while driving. A spitter is a common device for seismic and deep EM cable crew. Similar devices are also used in several countries in a reversed mode to eject rubber bullets.

Sporadic noise – electromagnetic noise. It can be seen on the recorded trace as a spike. This type of noise is caused by pumps, machinery, surges on the AC grid and others.

Static shift – in electromagnetics analogous to seismic distortion of the data caused by near surface inhomogeneities. Strictly speaking static shift refers to shifts of the curves (mainly in amplitude) which can be interpreted with a model different from the true earth. Since this is usually not known before the interpretation, sometimes one refers to 3-D distortions as static shifts.

System response – the response of the acquisition including transmitter and receiver component to an ideal spike input signal. The output signal as recorded $y(t)$ consists of the system response $s_y(t)$ convolved with the input signal $x(t)$: $y(t) = s_y(t) * x(t)$

TDEM – Time Domain ElectroMagnetics. see *TEM*.

TEM – Transient ElectroMagnetics. An electromagnetic technique in the time domain. using a transmitter to generate a secondary electromagnetic field in the subsurface.

This secondary electromagnetic field is being measured when no additional induction currents are being generated.

Total conductance – the integral conductance of a layer-cake, i.e.

$$S = \int_0^z \sigma dz$$

Transverse resistance – The resistivity of a medium for currents crossing the layer boundary.

Transverse resistance referencing – a correction procedure where the transverse resistance of a layer-cake is kept fixed and the thickness and resistivity are adjusted. Compare *Conductance referencing*.

UTEM – University of Toronto EM system. A transient EM sounding and profiling system developed at the University of Toronto and now being primarily used by Lamontagne Geophysics Ltd. of Canada. See *TEM*.

Walkaway test – test measurement usually carried out to check out the transmitter quality. Selected receiver sites are usually measured perpendicular to the center of the transmitter starting at a few hundred meters and changing in offset up to several tens of km.

Z – transform – The Z – transform may be thought of as $Z = e^{i\omega t}$, which is an easy way to relate time to a domain that can be similarly treated as the frequency domain (Sheriff, 1984).

LOTTEM FIELD OBSERVER'S LOG SINGLE SITE SYSTEMS

DATE:		SOURCE CODE:		STACKED DATA FILE NAME:																		
PROJECT:		LENGTH:		m		SAMPLING RATE:				Hz												
CREW CHIEF:		CURRENT:		A		AMPLIFIER S/N:																
OPERATORS:		CLOCKRATE:		sec		PREAMPLIFIER S/N:																
SYSTEM:		BEARING: EX:		EY:		CLOCK S/N:																
TX - COORD.		ELECTRODE 1 x:		ELECTRODE 1 y:		ELECTRODE 2 x:				ELECTRODE 2 y:												
CURVE ID (i.e. 01ABHZ)	coordinates		Gain	LP	BQ	Notches	AMPLIFIER			LP	BQ	Notches	PREAMPLIFIER			LP	BQ	Rec. code	Time in	Time out	Samp rate Hz	PROCESSING SYSTEM response name
	X	Y					ELEV. (Z)	N	M				50	16	2/3							
COMMENTS:																						
COMMENTS:																						
COMMENTS:																						
COMMENTS:																						
COMMENTS:																						

CLOCK DRIFT MEASUREMENT LOG

Survey Area: _____	Operator: _____	Date: _____
Crew Chief: _____		
Master clock: _____ used as reference: _____ synchronize at: _____ , file name: _____ day month year hour min		
SYSTEM A: Synchronization at: _____ day - month- year hour - min		Clock rate (sec): _____ file name: _____
Measurement of clock drift at: _____ day - month- year hour - min	Drift (ms): _____	Calculated Accuracy per second: _____
SYSTEM B: Synchronization at: _____ day - month- year hour - min		Clock rate (sec): _____ file name: _____
Measurement of clock drift at: _____ day - month- year hour - min	Drift (ms): _____	Calculated Accuracy per second: _____
Signature of Operator: _____		

FILE CONVENTION:

survey code —————→ **A**
 receiver code —————→ **F**
 day of survey (starting at 01) —————→ **01**
 transient code, increments
 for different settings,
 repeats etc. —————→ **A**
 clock # of signal source —————→ **1**
 clock drift measurements —————→ **.CL**
 clock # of trigger source —————→ **1**

AF01A1.CL1

LOTEM TRANSMITTER RECORD SHEET

Project: _____	Operator: _____	Date: ___. ___. 199__
Transmitter: _____	Crew Chief: _____	

CHART - RECORDER			
voltage		speed	
10 mvolts <input style="width: 20px;" type="checkbox"/>	1 volt <input style="width: 20px;" type="checkbox"/>	2 <input style="width: 20px;" type="checkbox"/>	
20 mvolts <input style="width: 20px;" type="checkbox"/>	2 volts <input style="width: 20px;" type="checkbox"/>	6 <input style="width: 20px;" type="checkbox"/>	
50 mvolts <input style="width: 20px;" type="checkbox"/>	5 volts <input style="width: 20px;" type="checkbox"/>	20 <input style="width: 20px;" type="checkbox"/>	
100 mvolts <input style="width: 20px;" type="checkbox"/>	10 volts <input style="width: 20px;" type="checkbox"/>	60 <input style="width: 20px;" type="checkbox"/>	
200 mvolts <input style="width: 20px;" type="checkbox"/>	20 volts <input style="width: 20px;" type="checkbox"/>		
500 mvolts <input style="width: 20px;" type="checkbox"/>	50 volts <input style="width: 20px;" type="checkbox"/>		
cm per hour <input style="width: 40px;" type="checkbox"/>		cm per min. <input style="width: 40px;" type="checkbox"/>	

Type: _____ kVA	GENERATOR	3 phases <input style="width: 20px;" type="checkbox"/>
Output: _____ Volts		1 phase <input style="width: 20px;" type="checkbox"/>
Cycles: _____ Hz		

CHECK LIST	
Cooling of switchbox <input style="width: 20px;" type="checkbox"/>	2 cables from electrodes <input style="width: 20px;" type="checkbox"/>
Remote control <input style="width: 20px;" type="checkbox"/>	Clock connection <input style="width: 20px;" type="checkbox"/>
Power cable <input style="width: 20px;" type="checkbox"/>	Generator not grounded <input style="width: 20px;" type="checkbox"/>

RUNNING TIME		
time on	time off	comments

CURRENT RECORDING			
time	High (+)	Low (-)	comments
08:00	_____ Ampere	_____ Ampere	
09:00	_____ Ampere	_____ Ampere	
10:00	_____ Ampere	_____ Ampere	
11:00	_____ Ampere	_____ Ampere	
12:00	_____ Ampere	_____ Ampere	
13:00	_____ Ampere	_____ Ampere	
14:00	_____ Ampere	_____ Ampere	
15:00	_____ Ampere	_____ Ampere	
16:00	_____ Ampere	_____ Ampere	
17:00	_____ Ampere	_____ Ampere	
18:00	_____ Ampere	_____ Ampere	

Inversion Statistics

There are several ways to evaluate the reliability of the inversion result. For LOTEM we have found that the SVD analysis works best. In particular, the inversion statistics allow full adjustment to the sensitivity of the LOTEM method and are thus particularly suited. In the development of inversion statistics we followed closely the paper by Raiche et al (1985) and Jupp and Vozoff (1975). As an example of what the individual parameters mean we give a description of the statistics below. In the interpretation chapter 4 we refer to these statistics in many different places.

The following is the explanation for the statistics output from the inversion program we use. The list is in alphabetical order and included here because the terminology is needed for the following inversion examples.

APRE – The average predicted residual error (APRE) is used to determine the model with the least number of layers which is still consistent with the data. For this model, APRE has a sharp minimum compared with the models with more or fewer parameters.

Confidence bounds – Confidence bounds for the physical parameters can be obtained by tracing back the uncertainties in the measured data towards the physical parameters. They are the same for the physical parameters what the damped error multipliers are for the eigenparameters. The standard deviation of the fit is taken as the uncertainty of the data. When calculating the *confidence bounds* it is advisable to use 95% confidence intervals for data with high signal to noise ratio and 68% for noisy data. Also when calculating the *confidence bounds*, for LOTEM for deep applications, one should calculate them with damped multipliers (Cramer–Rao Multipliers). This means that only the well resolved parameters will be varied and not randomly all parameters.

Correlation matrix – This symmetric N by N matrix shows the correlation between any two parameters. The correlation matrix is calculated from the covariance matrix of measurement and theoretical curve.

Covariance matrix – The covariance matrix indicates, how the fit between the calculated curve ('solution') and the measured curve ('data') transforms into confidence bounds for the solution.

Cramer–Rao multipliers – The Cramer–Rao multipliers for the original parameters transform the fitting error between data and calculated curve over to confidence bounds for the physical parameters. They are the same for the physical parameters what the (damped) error multipliers are for the eigenparameters. In fact they are obtained from the (damped) error multipliers through a transformation back into the physical parameter space. This may be done damped or undamped.

Deviation of mean – The standard deviation of mean value shows, how good the mean of each data point is in relation to the calculated value. This factor gives an estimate of the statistical probability of the calculated values.

Damping factors – The damping factors indicate the influence of the transformed parameters (eigenparameters) on the calculated curve. They show more directly the influence of the corresponding parameter combination on the curve than the spectral values (or singular values SV).

Damped error multipliers – The damped error multipliers for the transformed parameters are calculated as the ratio of the damping factor divided by the spectral value (singular value, SV). They are used in the calculation of the correction vector for the eigenparameter during each iteration (if damped error bounds were selected in the inversion setup). Hence they indicate the change of the parameters during the last iteration. When the program has converged properly onto a solution then these multipliers should be small for all parameters. If they turn out to be large, then the convergence criterion was probably set too high so that the program stopped even though there had been clear changes in the parameters.

Importance – The importance of the physical parameters is also called 'damping factors of the original parameters' in the statistics output of the inversion program. They are nothing more than the damping factors of the eigenparameters transformed back into the physical parameter space. Hence, they give the influence of the real parameters on the solution and are therefore called 'importance' of the parameters. They are a tool to judge the reliability of a parameter which has resulted from the inversion (see also 'damping factor' and 'normalized spectral value' or 'normalized singular value', SV).

Inverse Jacobian – The generalized inverse of the Jacobian matrix is also called 'data influence matrix'. It indicates how a small change in the measured data would influence the inversion result without actually doing another inversion. This matrix is therefore of interest for the inversion of synthetic data during a feasibility study and survey design.

Jacobian – The normalized Jacobian matrix is a measure for the change in the i -th data point, when the j -th parameter is varied. Hence this matrix is also called parameter influence matrix or sensitivity matrix. A parameter is only well resolved by the measurement if the data points depend strongly on this parameter, in other words: if the Jacobian has large entries in the corresponding column. Furthermore, each column of the Jacobian indicates the time window, in which the corresponding parameter is predominantly resolved by looking at the variation in the data. The columns are ordered thus: first the resistivities, then the thicknesses, then (in the joint case) the calibration factor(s). If you do a joint inversion MTHZ, the entries in the calibration factor column must be zero in the part which belongs to the MT data. The same applies to HZEX and HZEY.

Noise-to-signal ratio – The noise-to-signal ratio (NSR) is a measure for the quality of the data. It shows how well the inversion algorithm can pick up variations of the data from the model. The NSR is calculated from the standard deviation, the number of data points, number of parameters, the model data and their mean value.

Number of effective parameters – The number of effective parameters is calculated as the sum over the damping factors. It shows how many parameters can effec-

tively be resolved. The fewer parameters contribute to the solution, the smaller is this number. On the other hand, if all parameters are important then this number of effective parameters should be only slightly smaller than the actual number of parameters.

Number of iterations – The number of iterations that were completed before convergence. Linear problems would converge after just one iteration. The higher the non-linearity of the problem, the more complicated is the correlation among the parameters. This requires more and more iterations. The number of iterations depends also on the number of the parameters and the starting model.

Scale factor – The scale factor is defined as the largest SV. It allows to obtain the true values from the normalized values by a simple multiplication.

Spectral values – The normalized spectral values (SV, also called Singular Values from the Singular Value Decomposition, SVD) are a measure for the importance of the corresponding combination of N parameters for the solution. If the normalized SV is greater than about 0.1 then the corresponding damping factor is close to 1.0 and the corresponding parameter combination strongly influences the solution. If the normalized SV is much smaller than 0.1 then the damping factor becomes very small and it is dominated by the Marquardt factor. The corresponding parameter combination loses its influence on the calculated curve and hence it becomes unimportant. The ratio between the biggest and the smallest SV is a measure for the condition of the Jacobian matrix just as in any true eigenvalue problem.

Standard deviation – The standard deviation is a measure for the difference between the model curve and the data curve. It is a measurement for the goodness of fit of the two curves.

U – matrix – The U-matrix contains the eigenvectors of the data space. The product U times its transpose gives the information content of each measured data point.

V – matrix – The V-matrix sets up the relation between the physical and transformed parameters. Its columns are the eigenvectors of the parameter space. These eigenvectors represent combinations of the physical parameters (thickness, or resistivity). We consider only the logarithms of the resistivity and thicknesses. Each of the eigenvectors indicates which combinations of parameters are resolved. For example, suppose the entry for the thickness of the second layer is large positive (0.7) while the entry for the resistivity of the second layer is large negative (–0.7). Since we consider logarithms, this means that the conductivity – thickness product of the second layer is resolved with this eigenparameter. However, if the eigenvalue (singular value, SV) of that eigenparameter is small, then the eigenparameter does not contribute much to the solution – in other words, it is not important. Which combination of parameters contributes to the solution (that means which eigenparameter is actually resolved) can be only seen from the corresponding eigenvalue or SV and the damping factor which is calculated from the SV.

KMS Technologies – KJT Enterprises Inc.
6420 Richmond Ave., Suite 610
Houston, Texas, 77057, USA
Tel: 713.532.8144

Please visit us
<http://www.kmstechnologies.com>

This material is not longer covered by copyright. The copyright was released by Elsevier to Dr. Strack on November 5th, 2007.

The author explicitly authorizes unrestricted use of this material as long as proper reference is given.

KMS Technologies – KJT Enterprises Inc.
An EMGS/rxt-company

Appendix 4
Documentation of the Forward Modeling
Program MODALL

extract from

Strack, K.-M., 1992, reprinted 1999
Exploration with deep transient
electromagnetic: Elsevier, 373 pp.

This material is not longer cover by copyright. The copyright was released by Elsevier to Dr. Strack on November 5th, 2007.

The author explicit authorizes unrestricted use of this material as long as proper reference is given.

Appendix 4

Documentation of the Forward Modeling Program MODALL

MODALL is a program for interactive transient EM (LOTTEM optimized) forward modeling. It has many different options built in for a variety of modeling setups. This documentation explains how to use the program. The user should be familiar with the content of the chapter 6 of this book. The enclosed program is for demonstration of the material in this book only. It is by no means a competition to commercial software.

This documentation starts first to describe the content of the distribution diskette. The main part of this description covers the menu explanations. In each menu you can change different parameters. To control the program you use the commands specified in each menu explicitly. In general you use <SPACE> to continue and "Q" to go back one menu. The structure of the menus is as follows:

SOFTWARE INSTALLATION

The software is distributed on a 3,5 inch floppy diskette in the back of the book. The diskette contains the following files:

MODALL.EXE	<i>executable file</i>
MODALL.MEB	<i>menu interface data file</i>
MODALL.DEF	<i>default data file</i>
README.1ST	<i>latest documentation</i>

To use the software, copy the above files to your path on the hard disk and execute it from there by typing: **MODALL**

Then follow the instructions on the screen.

DESCRIPTION OF THE MENUS

You invoke MODALL by simply saying MODALL. Make sure you have the MODALL.DEF file in your default path. The first program pages will inform about the copyright of the software and the user responsibilities.

From the DEFAULT SETUP menu you will be guided through a number of different menus. Eventually, you will get back to the DEFAULT SETUP screen. You can only leave the program from this screen.

MODALL menus

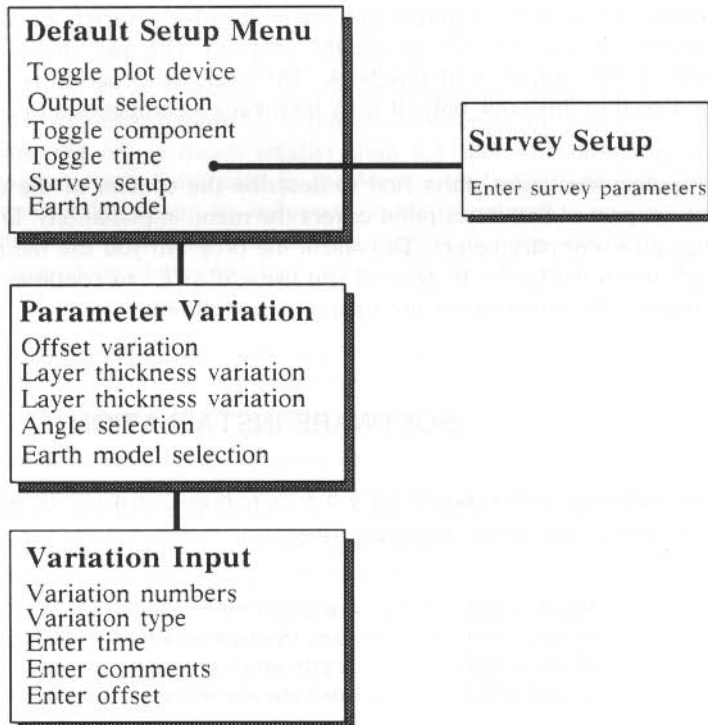


Fig. A4.1: Main menu structure for the program MODALL (subscreens are not shown).

☞ DEFAULT SETUP MENU

This menu shows you the defaults used for the modeling and allows you to change them. To do this, you can go into the SURVEY SETUP, or the OUTPUT SETUP or

you can change the basic earth model by pressing "M". The program handles the defaults by using your file MODALL.DEF

In this menu you have the option to toggle several setups. When you press the corresponding key, you will get the next option displayed on the screen. See TOGGLE for further information.

TOGGLE

In the DEFAULT SETUP menu you may toggle:

- ☐ Output for plot:
 - Terminal
 - Printer: EPSON, HPGL, PLOTCALL
- ☐ Field component: HZ, EX, EY
- ☐ Y-axis:
 - Measured voltage in VOLTS
 - Early time apparent resistivity
 - Electric field (for EX and EY)
 - Early + late time apparent resistivity (for HZ only)
 - All time apparent resistivity (for HZ only)
 - Early + late + all time apparent resistivity (for HZ only)
- ☐ X-axis:
 - Real time in seconds
 - Russian normalized time $(\sqrt{2.E7*PI*RHO*T}/H1)$

SURVEY SETUP

The SURVEY SETUP menu allows you to select all basic survey parameters needed for calculation of the measured voltage. These are:

- ☐ Equivalent area of receiver coil (for HZ)
- ☐ Length of receiver dipole (for EX & EY)
- ☐ Source length in meters
- ☐ Source current in Amperes
- ☐ Angle between transmitter and offset vector (in degrees)

OUTPUT SETUP

In this menu you can decide the format of your output file:
You can choose between:

- ☐ ASCII output file out_name.PRT
- ☐ No output file

You can enter an individual filename, but it is recommended that you keep the proposed extensions. If you vary a parameter, so that you calculate different curves,

the program will produce one output file for each curve. The file extension for every output file after the first one will be out_name.PR1, out_name.PR2 etc.

EARTH MODEL

The basic earth model is shown in the DEFAULT SETUP menu. You can change it by pressing **M**. You will then be asked for the layer number, the resistivities and thicknesses. Default values can be used by typing a comma instead of the value.

▣ PARAMETER VARIATIONS

This menu allows you to select the parameter you like to vary. You can choose:

- ☐ Offset
- ☐ Angle between transmitter and offset vector
- ☐ Resistivity or thicknesses of individual layers
- ☐ Earth models with different layer numbers

This means, you can see different curves on one Plot. See VARIATION INPUT for an example.

▣ VARIATION INPUT

This menu allows you to enter the different values of the parameter you have specified in the PARAMETER VARIATIONS menu. Maximum number of variations is 10

EXAMPLE: Base Model:

Resistivities: **10.**, **1000.**, **100.** (Ohm-m)

Thicknesses: **200.**, **2000.** (m)

2nd layer resistivity varied, 3 variations:

1000., **2000.**, **3000.** (Ohm-m)

In this menu you can also change:

- ☐ Minimum calculation time
- ☐ Comments on the plot
- ☐ Default offset

Note: The default offset is not used if offset is the varied parameter.

☞ MODEL VARIATIONS

This menu allows you to enter different models to be presented on one plot. This is a helpful option if you select models with different number of layers. Make sure that you have non-zero values in all models you use. Maximum number of models is 4. The menu consists of two pages. In this menu you can also change:

- ☐ Minimum calculation time
- ☐ Comments on the plot
- ☐ Default Offset

EXAMPLES

MODALL is an interactive self explanatory forward modeling package. You should not need specific help examples. Here we have included two test runs with the appropriate outputs. The first example generates a magnetic field forward model and the second example the corresponding electric field.

MODALL EXAMPLE 1: Magnetic field models

This example calculates a magnetic field response and displays it as apparent resistivities. The following sample session contains only the important variable information of the screen. The specific input (screen variables) is printed in bold face. You move from screen to screen using the space bar unless you have modified the parameters.

Type **MODALL**

The program starts and you will see:

START UP SCREEN

DEFAULT setup menu

```
Plots on TERMINAL
Output file,  OFF
Field component: HZ
X-axis in REAL time
Y-axis: EARLY and LATE TIME APPARENT RESISTIVITY
3 layers
Resistivities: 100  10  100
Thicknesses:  1000 500

press  <SPACE>
```

PARAMETER VARIATION SELECTION

Default: 3 Offset variations

H_z - component selected

press <SPACE>

VARIATION Input menu

Number of variations: 3

03 Offset variations

5000 10000 15000

Minimum time: 0.001

Comments: H-type examples

Default offset: 10000

HZ component selected

...working

MODALL now calculates the field for the parameters you have selected and will then display a plot on your terminal.

OFFSET VARIED
VARIATIONS: 5000, 10000, 15000
BASE MODEL: 3 LAYERS
RESISTIVITIES: 100.0, 10.0, 100.0 OHM-M
THICKNESSES: 1000, 500 m
COMMENTS: H-type example

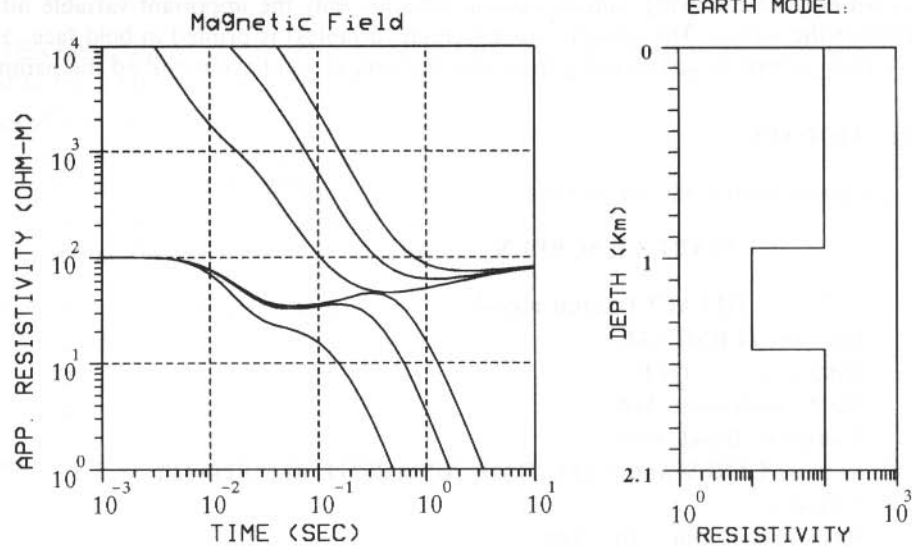


Fig. A4.2: Example plot for the MODALL program calculating the magnetic field response for three different offsets.

MODALL EXAMPLE 2: Electric field models

This example calculates a electric field response and displays it as measured voltage. The following sample session contains only the important variable information of the screen. The specific input (screen variables) is printed in bold face. You move from screen to screen using the space bar unless you have modified the parameters. Use the online help of MODALL for further information:

Type **MODALL**.

The program starts and you see.

START UP SCREEN

DEFAULT setup menu

Plots on **TERMINAL**
 Output file, **OFF**
 Field component: **EX**
 X-axis in **REAL** time
 Y-axis: **MEASURED VOLTAGE**
 3 layers
 Resistivities: **100 10 100**
 Thicknesses: **1000 500**

press **<SPACE>**

PARAMETER VARIATION SELECTION

Default: 3 Offset variations
EX - component selected

press **<SPACE>**

VARIATION Input menu

Number of variations: 3
03 Offset variations
5000 10000 15000
 Minimum time: 0.001
 Comments: **H-TYPE EXAMPLES, EX**
 Default offset: **10000**
EX component selected

press **<SPACE>**

...working

MODALL now calculates the field for the parameters you have selected and will then display a plot on your terminal.

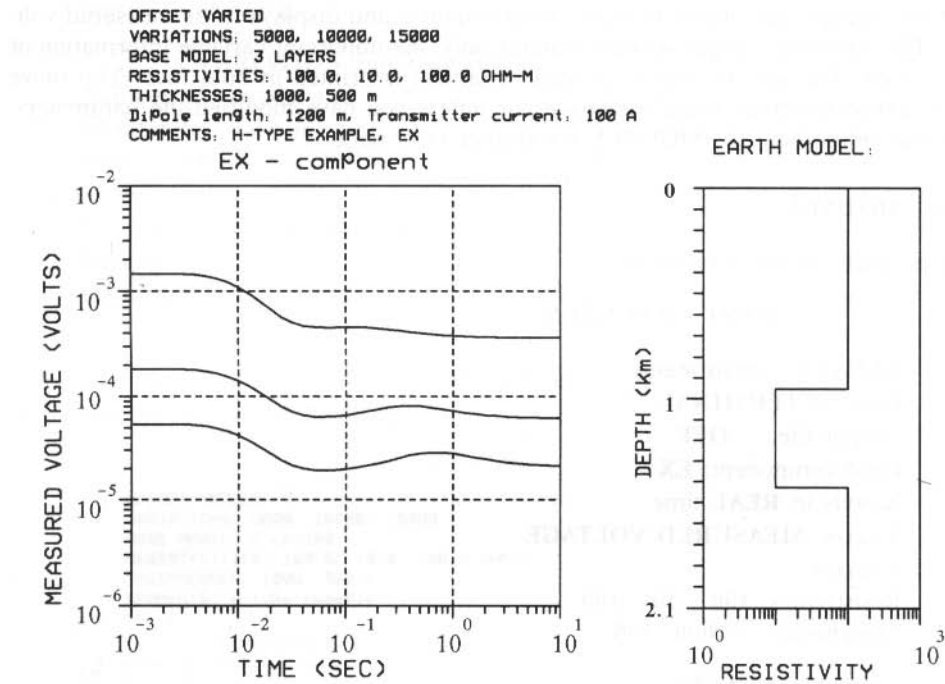


Fig. A4.3: Example plot for the MODALL program calculating the electric field response for three offsets.

KMS Technologies – KJT Enterprises Inc.
6420 Richmond Ave., Suite 610
Houston, Texas, 77057, USA
Tel: 713.532.8144

Please visit us
<http://www.kmstechnologies.com>

This material is not longer covered by copyright. The copyright was released by Elsevier to Dr. Strack on November 5th, 2007.

The author explicitly authorizes unrestricted use of this material as long as proper reference is given.

KMS Technologies – KJT Enterprises Inc.

Appendix 5 List of Figures, Tables, Symbols and References

extract from

Strack, K.-M., 1992, reprinted 1999
***Exploration with deep transient
electromagnetic:*** Elsevier, 373 pp.

This material is not longer cover by copyright. The copyright was released by Elsevier to Dr. Strack on November 5th, 2007.

Appendix 5

List of Figures, Tables, Symbols and References

LIST OF FIGURES

Fig.1.1:	Location of the case histories shown in this book. The numbers represent the chapters where the case histories can be found.	1
Fig.1.2:	Signal and source waveforms in frequency and time domain systems (after Nekut and Spies, 1989)	7
Fig.1.3:	Historical tree of the different organizations involved in deep transient electromagnetics.	8
Fig.1.4:	Conceptual information flow of geophysical necessities to obtain information about the subsurface. The shaded areas mark the focus of this book.	10
Fig.1.5:	Ranges of resistivity for consolidated and unconsolidated sedimentary rocks (modified after Angenheister, 1982).	13
Fig.1.6:	Resistivity versus temperature / depth of the pore fluid for different salt concentrations (after Schlumberger, 1987).	14
Fig.1.7:	Dependency of the resistivity versus geologic age (after Vozoff 1989 pers. comm.).	14
Fig.1.8:	Resistivity anisotropy as a result of horizontal bedding during cyclic deposition. ...	15
Fig.1.9:	Simulation of an anisotropic model for the LOTEM method for the magnetic field derivative (top) and electric field (bottom) responses. The half space has a resistivity of 10 Ωm and all measurements are taken at 7 km offset. The anisotropic model includes two embedded resistive layers (each 50 m thick, 1000 Ωm resistivity) at a depth of 2000 m and 2250 m.	16
Fig.1.10:	Example of longitudinal resistivities (top) and electrical anisotropies (bottom) for two formations across an area in the Denver-Julesberg Basin, USA (after Keller, 1971).	17
Fig.1.11:	Example of an induction log as for the definition of the interpretation model. The dashed line shows the interpreted starting model.	18
Fig. 2.1:	Typical LOTEM transmitter and receiver setup (single site system).	22
Fig. 2.2:	<i>Smoke rings</i> for a grounded dipole in a half-space with 200 Ωm resistivity. The different frames mark different times after current turn off. The contours represent lines of equal electric field strength. The dashed lines mark opposite polarity.	23

Fig. 2.3: System of <i>smoke rings</i> for a grounded wire dipole on a two-layer earth model. The contours represent lines of equal electric field strength. The dashed lines mark opposite polarity.	23
Fig. 2.4: Comparison of the diffusion process of induction currents 10 ms after current turn off for a half-space and a two-layer earth model.	24
Fig. 2.5: Example of an early and late time apparent resistivity curve for a homogenous half-space with 10 Ωm resistivity.	29
Fig. 2.6: Example of an early and late time apparent resistivity curve for a three-layer earth model with the second layer being highly resistive.	30
Fig. 2.7: <i>Resistivity transforms</i> for the models from figure 2.5 (left) and 2.6 (right).	31
Fig. 2.8: <i>All time apparent resistivity curves</i> by Stoyer for a two-layer model (after Strack, 1985).	32
Fig. 2.9: <i>All time apparent resistivity curves</i> for a four-layer model using Strack's least square formulation (after Strack, 1985).	33
Fig. 2.10: Magnetic fields for two half-spaces with the resistivities of 30 Ωm and 1 Ωm and for a two-layer model with the same resistivities (30 Ωm , 1 Ωm ; first layer thickness = 400 m) for offsets of 1 km, 5 km and 9 km.	34
Fig. 2.11: <i>All time apparent resistivity curves</i> for a three-layer model with varying second layer resistivity (after Karlik and Strack, 1990).	35
Fig. 2.12: <i>All time apparent resistivity curves</i> for the three-layer model used by Yang (see figure 2.10) (Karlik and Strack, 1990). Left is the <i>all time apparent resistivity</i> curve derived from the magnetic field and on the right the corresponding curve by Yang. Both curves are calculated for an offset of 1km.	36
Fig. 2.13: <i>All time apparent resistivity curves</i> for a four-layer model used for figure 2.9 (after Karlik and Strack, 1990).	36
Fig. 2.14: Field data of an early and late time apparent resistivity curve (left) and the respective <i>all time apparent resistivity curve</i> (after Karlik and Strack, 1990).	37
Fig. 2.15: <i>Source image</i> for a two-layer model.	40
Fig. 2.16: <i>Source image</i> for a three-layer model.	41
Fig. 2.17: Earth model (top) and the <i>source imaging</i> (center) and <i>interval imaging</i> (bottom) results.	42
Fig. 2.18: 3-D model and profile location used to calculate the synthetic data for the <i>source imaging</i>	43
Fig. 2.19: <i>Source image</i> of the synthetic data for the 3-D model shown in figure 2.18	44
Fig. 3.1: <i>Black Box</i> concept for the signal path.	48
Fig. 3.2: Combination of noise sources with the true signal.	48
Fig. 3.3: Example of a selectively stacked transients with (left) and without (right) time domain deconvolution of the system response.	51
Fig. 3.4: Schematic of the pole-zero technique in the complex plane for the construction of a digital recursive filter.	53
Fig. 3.5a-c: Example of a digital recursive notch filter applied to synthetic data. For all figures the noise - free synthetic input signal is superimposed for comparison. The bottom two curves are the results of applying the digital notch filter with different bandwidths to the top curve. For figure 3.5a, periodic 16 2/3 Hz noise is added to a sinusoid which abruptly starts, and ends with a step discontinuity.	

The synthetic curve in figure 3.5b represents an ideal theoretical transient. Figure 3.5c is the theoretical transient from figure 3.5b convolved with the impulse response of the recording system and transmitter, thus representing a real transient (after Strack et al, 1989).

Fig. 3.6:	Digital recursive, true amplitude notch filter applied to transient data. The left curve shows the original field data and the right curve the same data after filtering (after Strack et al, 1989).	55
Fig. 3.7:	Example of a single transient contaminated with periodic noise. The left column shows the single record before and after filtering with a lockin digital filter. On the right side the respective amplitude responses are shown.	56
Fig. 3.8:	Ten raw transients from Germany distorted by sporadic noise (after Strack et al, 1989).	57
Fig. 3.9:	Upper transient is the result of a straight average summation with poor signal-to-noise ratio. This stacking technique is improved by eliminating all amplitudes outside two standard deviations of the average ($-\sigma$, $+\sigma$) from the selective stack as shown in the lower transient (after Strack et al, 1989).	59
Fig. 3.10:	Stacked data using the <i>symmetric rejection</i> selective stack technique with a cutoff 20% at both ends of the sorted amplitudes. The shaded areas represent the amplitudes which are all kept, all others are rejected (after Strack et al, 1989).	60
Fig. 3.11:	Stacked data using the <i>area-defined rejection</i> selective stack technique with an area (shaded) defined as 60% to keep (after Strack et al, 1989).	61
Fig. 3.12:	Comparison of the selective stacking algorithm (bottom) with a straight averaging of the signal (top) using the same data (after Walker et al, 1982).	62
Fig. 3.13:	Sketch of the symmetry within the current behavior of a DC-monopole used to visualize the effect of the calibration factor (after Hördt, 1989).	66
Fig. 4.1a:	FORWARD modeling functional diagram.	74
Fig. 4.1b:	INVERSE modeling functional diagram.	74
Fig. 4.2:	Model of a horizontally layered earth made up of M layers with respective resistivities and thicknesses.	75
Fig. 4.3:	Error ridge trace as function of the estimated model parameters (after Menke, 1984).	79
Fig. 4.4:	The function $T^{(N)}(\lambda) = \frac{\lambda^{(2N)}}{1 + \lambda^{(2N)}}$ for $N = 1, 2, 3, \infty$ (after Jupp and Vozoff, 1975)	82
Fig. 4.5:	Synthetic data example for LOTEM and MT joint inversion for a K-type model (left) and inversion results on the right. The joint inversion result here is the same as the true model (after Hördt, 1989).	85
Fig. 4.6:	V matrices for the individual and joint inversion of LOTEM and MT data using K-type synthetic data (after Hördt, 1989).	86
Fig. 4.7:	LOTEm (top left) and MT (bottom left) synthetic data for an A-type model. On the right inversion result are shown with the parameter importances below (after Hördt, 1989).	88
Fig. 4.8:	Field data for LOTEM (top) and MT (bottom) measured at the same site in North-Western Germany with the synthetic curves for the joint inversion result (after Hördt, 1989).	89
Fig. 4.9:	Comparison of the individual inversions and the joint inversion with the well log (after Hördt, 1989). The reduced well log was derived from blocking of the original laterolog (Büchter, 1983).	90

- Fig.4.10: Inversion results for the same survey line. The top shows the results of the individual inversions using the same starting model for all data. The middle is the same line when the inversion result of the previous station was used as starting model for the next station. The bottom frame shows the results of the same procedure after eliminating station 3 (after Petry, 1987). 93
- Fig.4.11: Inversion results for the same data as in figure 4.10 using soft bounds (bottom) and hard bounds (top) *profile inversion* (after Petry, 1987). 95
- Fig.4.12: Interpreted resistivity section using the individual inversion results (top). At the bottom of the figure the data (squares) and synthetic curves are shown sequentially starting from the left side of the profile. 96
- Fig.4.13: Interpreted resistivity section for the *profile inversion* without parameter bounds. At the bottom of the figure the data (squares) and synthetic curves are shown sequentially starting from the left side of the profile. 97
- Fig.4.14: Interpreted resistivity section using the profile inversion with bounds. At the bottom of the figure the data (squares) and synthetic curves are shown sequentially as indicated by the arrows. 98
- Fig.4.15: Comparison of *Occam inversion* with layered earth inversion. The left frame shows the field data (squares) with the theoretical curves for the inversion results on the right (smooth curve) (after Schruth, 1990). 101
- Fig.4.16: Example of an *Occam inversion* compared with the layered earth inversion result. 101
- Fig.4.17: Display of observed field data showing a reversal. The top is the linear display of the stacked transients and the bottom a logarithmic display after apparent resistivity conversion. The crosshatching represents the 95% confidence interval. 103
- Fig.4.18: Classification of the field data distortions of a LOTEM survey in Utah. The left curve shows a reversed voltage at early times (1) and the right curve at late times (4). The two middle curves show mid-time distortions with a reversed voltage on the left (2) and a strong depression on the right (3) (modified after Stoyer and Damron, 1986). 104
- Fig.4.19: Synthetic distorted curve inferred for the Milford data (after Tsubota, 1979; Stoyer and Damron, 1986). The response of the conductor is negative for all times and responsible for the late time reversal. The conductor response is superimposed on the half-space response which is positive for all times. 105
- Fig.4.20: Station locations, faults and location of the modelled conductor for the Milford LOTEM survey (after Stoyer and Damron, 1986). Sounding 4 exhibiting a late time reversal is shown as example. 106
- Fig.4.21: Simulation of a fault zone using an analog modeling experiment. The resulting shapes of the signal are used to classify the distorted responses (Stoyer and Damron, 1986). The station numbers are used as classification reference. 106
- Fig.4.22: Interpreted *fault zone map* using the classification (bold numbers) for the distorted transients from figure 4.21 (after Stoyer and Damron, 1986). The large numbers refer to the curves shown in figure 4.18. The dotted line shows Stoyer and Damron's 1986 interpretation of the location of the fault. 107
- Fig.4.23: Survey map showing the location of distorted data (shaded areas). The shaded area in the north-eastern part exhibits reversals, two examples of which are shown in the figure (after Stephan, 1989). The dashed lines make the railroad and power lines. 108
- Fig.4.24: Possible fault maps for the Haltern Survey area using Damron's classification for distorted signals from figure 4.21 (after Stephan, 1989). 108

- Fig.4.25: Field array and model for the conductive plate program simulating a sedimentary environment and the synthetic transients (semi-logarithmic axes) at the respective receiver sites. The conductive plate is laterally homogeneous (Weidelt, pers. comm.). The negative signals are displayed by area fill. 110
- Fig.4.26: Geometric setup for the conductive plate program with lateral inhomogeneities. The model parameters simulate a sedimentary environment. The resulting synthetic transients (semi-logarithmic axes) are shown at the bottom. 111
- Fig.4.27: The three-dimensional response of a conductor near the receiver is calculated using the integral equation method. The top shows the section and plan view of the earth model. The data set on the bottom left shows the synthetic data for the 3-D model in comparison with the respective one-dimensional curve. On the bottom right a real field data set exhibiting the same characteristics is shown. The different location in time of the notch in both diagrams is caused by the model scaling and the fact that the detailed resistivity structure underneath the three-dimensional measurements is not known. 112
- Fig.4.28: Model profile over a conductive body from 3-D modeling (after Newman, 1989). 113
- Fig. 4.29: Two-dimensional model setup for the axial conductor model of the Milford area, Utah. At the bottom of the figure a comparison between the synthetic and field data is shown. Both data sets are displayed as resistivity transforms. (after Kriegshäuser, 1991). 114
- Fig. 4.30: Three-dimensional model setup (right) for part of the Milford survey. On the left the resistivity transform are shown for the modeled and field data. 115
- Fig.4.31: Plan view and cross section of the 3-D model to test the effect of conductive bodies underneath one electrode of the transmitter. For two stations the 3-D response (squares) and the 1-D response (solid lines) is shown on the right (after Newman, 1989). 118
- Fig.4.32: Interpretation results for the 3-D data of figure 4.31 using a 1-D inversion program (after Newman, 1989). 119
- Fig.4.33: Geometric setup and calculated data for a conductor embedded in a layered earth with the transmitter located on top of the conductive patch (after Newman, 1989). 120
- Fig.4.34: Interpretation results for the 3-D data of figure 4.33 using a 1-D inversion program (after Newman, 1989). 121
- Fig.4.35 The 3-D model used to compare the forward modeling routines. For the thin-sheet program the conductive body is infinitesimally thin, with a conductance of 100 S. For the two other programs (integral equation and finite difference, SLDM) the body is 25 m thick, with a resistivity of 0.25 Ωm (after Hördt et al, 1992). 123
- Fig. 4.36: Comparison of calculated data for the configuration of figure 4.35. Upper row: The solid line is the result using thin-sheet modeling. The squares are the results using the integral equation (IE) method. Lower row: The solid line is the result using the spectral Lanczos decomposition method (SLDM). The squares are the results using the IE method (after Hördt et al, 1992). 124
- Fig. 5.1: Typical setup of the long offset transient electromagnetic sounding system. 128
- Fig. 5.2: Block diagram of the hardware building blocks for a LOTEM transmitter and receiver systems. 129
- Fig. 5.3: Takeout and connector of the LOTEM induction coil which is made up of a 160 m long seismic cable. On the right side of the figure the preamplifier is displayed. 130

Fig. 5.4: LOTEM preamplifier showing on the left side of the preamplifier the calibration unit and on the right side the preamplifier control panels.	131
Fig. 5.5: Digital ElectroMagnetic System (DEMS IV) which is the heart of the LOTEM system. Here the original prototype is shown.	132
Fig. 5.6: Digital ElectroMagnetic System (DEMS IV) in a commercial version.	132
Fig. 5.7: Two possible bipolar transmitter current waveforms.	133
Fig. 5.8: Principal schematic of an electromechanical switchbox (after Strack, 1985).	134
Fig. 5.9: Standard construction generator used for LOTEM test surveys in Germany.	134
Fig. 5.10: 400 Hz 30 KVA generator as commonly used for mining applications. Connected to the generator can be solid state 25 KVA switchbox giving maximum output current of up to 50 Ampere (peak-to-peak).	135
Fig. 5.11: Principal block diagram of a synchronization clock.	136
Fig. 5.12: Front plate of a simple synchronization clock.	137
Fig. 5.13: Front panel diagram of a multi-purpose synchronization clock.	137
Fig. 5.14: Typical field layout for a multichannel transient EM system.	139
Fig. 5.15: Voltages responses for different offsets for deep crustal application.	140
Fig. 5.16: Ten single magnetic field measurements (time derivatives) recorded consecutively.	141
Fig. 5.17: Example of the experiment for comparison of the DC-level effect before and after stack.	142
Fig. 5.18: Effect of slight inaccuracies in the determination of the DC-level on the apparent resistivity curves. The notches in the perturbed curves represent the times when the signals become negative (negative values are displayed as absolute values).	143
Fig. 5.19: Principal block diagram of the microprocessor controller DC-bias circuit of the TEAMEX system.	144
Fig. 5.20: System units for a single site LOTEM system where electromagnetic noise can influence the signal.	144
Fig. 5.21: Example of an interpreted resistivity depth section where the noise in the signal can still be seen in the scattering of the depth to the conductor (shaded) (after Strack et al, 1990).	145
Fig. 5.22: Block diagram of the TEAMEX multichannel system.	146
Fig. 5.23: Comparison of the different system responses of the DEMS IV and the TEAMEX systems. The graphs show the TEAMEX data in comparison with the real earth model convolved with the TEAMEX system response (bottom) and the DEMS IV system response (top).	147
Fig. 5.24: Comparison of the DEMS IV and TEAMEX measurements at the same site. On the left are the resistivity transforms and on the right the Occam inversion models.	148
Fig. 5.25: Comparison of a single site processed data set (left) with the same data after noise processing (right) using multiple receivers.	148
Fig. 5.26: Photograph of a remote unit of the TEAMEX multichannel system.	149
Fig. 5.27: Block diagram of the principal building blocks of the LOTEM data processing and interpretation workstation.	150
Fig. 5.28: Arrangement of six individual electrode pits at one end of the main cable. A fence is required to protect bystanders.	151

Fig. 5.29: Preparation of transmitter electrodes. Top: preparation of electrode pit. Bottom: connection to main cable.	152
Fig. 5.30: Simplified circuit diagram for initial transmitter check out.	153
Fig. 5.31: Block diagram of the daily synchronization control setup.	154
Fig. 5.32: System setup of the LOTEM equipment to record the system response. The top shows the setup using only the switchbox which is done in the laboratory and the bottom shows the setup including the entire system.	155
Fig. 5.33: Two system responses for two different receiver systems measured in the field using the entire transmitter and receiver system.	156
Fig. 5.34: Cable winder ("spitter") which permits the pick-up the 25 mm ² transmitter cable (1–5km) in ten minutes.	157
Fig. 5.35: Receiver site for single site systems for continuous electric field and continuous magnetic field measurements.	159
Fig. 5.36: Multichannel layout for split spread and roll along configurations.	160
Fig. 5.37: Basic field setup for the LNC technique using two receivers (after Stephan, 1989).	162
Fig. 5.38: Selectively stacked transient at the base station, which is termed 'base stack' (after Stephan and Strack, 1991).	163
Fig. 5.39: Two examples of the processing sequence for the LNC technique (left column: sporadic noise; right column: periodic noise; data taken in Germany). Top: noise at the base station. Second row: raw transient of control measurement with a different receiver system. Third row: noise-compensated data. Bottom: compensated data without clock drift correction (after Stephan and Strack, 1991).	164
Fig. 5.40: Comparison between uncompensated (upper frame) and noise compensated (lower frame) stacked transients of the control measurement at the base station (German survey) (after Stephan and Strack, 1991).	166
Fig. 5.41: Receiver location map of the field test in China (after Stephan and Strack, 1991).	167
Fig. 5.42: Comparison between uncompensated (upper frame) and noise – compensated (lower frame) stacked transients of the control measurement at the base station (China survey) (after Stephan and Strack, 1991).	167
Fig. 5.43: Comparison between uncompensated (upper frame) and noise – compensated (lower frame) resistivity transform of two measurements in China. Left side: control measurement B27 at the base station. Right side: mobile receiver station B31, 3.3 km away from the base station (after Stephan and Strack, 1991).	168
Fig. 5.44: Comparison between four examples of the raw data (left column) and compensated data (right column) of the mobile station B31 (after Stephan and Strack, 1991).	169
Fig. 5.45: Change in $S/(S+N)$ ratio for all receiver locations as a function of distance from the base station (China survey) (after Stephan and Strack, 1991).	170
Fig. 6.1: Cumulative conductance for the blocked well log from table 6.1 for a four-layer model (top) and a five-layer model (bottom).	175
Fig. 6.2: Simulated LOTEM data for the blocked model without reduction (10 layers) in comparison with the reduced model (5 layers).	177
Fig. 6.3: Simulated LOTEM data for the two different reduction models (5 layers and 4 layers).	177
Fig. 6.4: Apparent resistivity curves for three different transmitter–receiver offsets (5, 10 and 15 km) for the ten-layer model.	179

Fig. 6.5: Apparent resistivity curves for three different thicknesses of the third layer. The absence of this part of the target was simulated as an invisibly thin (1m) layer. 180

Fig. 6.6: Apparent resistivity curves for three different resistivities of the fourth layer. 180

Fig. 6.7: Induced voltage in the receiver coil (signal level) for three different resistivities of the fourth layer. 181

Fig. 6.8: Blocked electrical log for the well in the survey area in Australia. 185

Fig. 6.9: Two way travelttime contours of the top of the dolorite unit. 185

Fig. 6.10: Seismic section indicated in figure 6.9. the dark area marks the dolorite unit. 186

Fig. 6.11: Two-dimensional section view of the model used for the computation of the transient responses shown in the upper half of the figure. 188

Fig. 6.12: Plan view of the two-dimensional section displayed figure 6.11 and the location of the profile of which selected data sets are shown. 189

Fig. 7.1: Survey layout of the 1987 (top) and the 1988 (bottom) LOTEM survey. 194

Fig. 7.2: Representative well log derived from borehole measurements within the survey area. 195

Fig. 7.3: Cumulative conductance analysis to define the resistivity layer boundaries from the well logs (after Stephan et al, 1991). 196

Fig. 7.4: Comparison of two Occam inversion results with a layered earth model. 197

Fig.7.5: Seismic reflection line for the survey area (after Stephan et al, 1991). 197

Fig. 7.6: Processing steps for individual raw signals of the magnetic field (left; site A09) and the electric field (right; site B11). The top shows a single record of the raw field data. The second row are the amplitude spectra used for the quality control. Following are the digitally filtered records. At the bottom the further smoothed individual signals are displayed (after Stephan et al, 1991). 198

Fig. 7.7: Selectively stacked magnetic field transient from figure 7.5 and the corresponding resistivity transform curve (left).On the right the measured electric field transient is displayed both linearly and logarithmically (after Stephan et al, 1991). 199

Fig. 7.8: Inversion results of the field data shown in figure 7.6 and figure 7.7 (after Stephan et al, 1991). 200

Fig. 7.9: Interpreted resistivity cross section through well nos.1 and 2 of figure 7.1 (after Stephan et al, 1991). 201

Fig.7.10: Comparison of unconstraint inversion of magnetic field measurements at the same sites using three different transmitters (after Stephan et al, 1991). 202

Fig. 7.11: Comparison of inversion of the electric and magnetic field measurements at two sites (after Stephan et al, 1991). 202

Fig. 7.12: Resistivity contour map of the second conductive layer (top) and contour map showing the near top of Carboniferous (after Stephan et al, 1991). 203

Fig. 7.13: Geologic map for the survey area including the structural interpretation (after Stephan et al, 1991). 204

Fig. 7.14: Location map of the Colorado School of Mines test area (heavy border) (after Harthill, 1968). 205

Fig. 7.15: Generalized geoelectric-geologic cross section for the CSM test area (after Harthill, 1968). 206

Fig. 7.16: Apparent resistivity curves for the LOTEM measurements over the CSM test area (after Strack, 1985). 207

Fig. 7.17: LOTEM field data (dots) and theoretical curves (solid line) for the generalized geoelectric model in figure 7.15 (after Strack, 1985).	208
Fig. 7.18: Generalized geographic location map of the LOTEM survey area in the Sydney Basin (after Strack, 1984).	209
Fig. 7.19: Survey plan of the LOTEM receiver and transmitter sites (after Strack, 1984).	210
Fig. 7.20: Simplified general geological north-south cross section of the Sydney Basin (after Strack, 1984).	211
Fig. 7.21: Simplified shallow geologic west-east cross section of the Sydney Basin (after Strack, 1985).	211
Fig. 7.22: Selectively stacked LOTEM transients of the eight receiver sites (after Strack, 1984).	212
Fig. 7.23: Inversion result for receiver site 1 (after Strack, 1985).	212
Fig. 7.24: Interpreted geological section in comparison with the results from BMR bulletin 149 (after Strack, 1984).	213
Fig. 7.25: Comparison of inversion results with other geophysical techniques and well log data (modified after Vozoff et al, 1984).	214
Fig. 7.26: Basemap showing the LOTEM and MT stations in the Münsterland survey area. The shaded area denotes the 3-D region. The creeks are indicated for orientation.	216
Fig. 7.27: Inversion results along profile ML8701 with the data sets around the 3-D anomaly. The squares correspond to the measured, the solid lines to the calculated data. Data sets B03 and A01 show layered behavior, the other data sets show 3-D effects. Station A05 includes a sign reversal on a linear scale. On the logarithmic scale in the figure the absolute values are shown. The positive and negative data for site A05 are indicated by "+" and "-".	217
Fig. 7.28: Physical explanation of the 3-D effects observed in the field data. The upper part of the figure schematically shows the behaviour of currents and magnetic fields when the 1-D structure is disturbed by a local conductive body. The squares are the receiver locations on the surface. The lower part shows the apparent resistivity for different times along the profile over the body in comparison with the 1-D response.	218
Fig. 7.29: The "best fit" thin-sheet inversion model (plan view). The map corresponds to the shaded area in figure 7.26.	220
Fig. 7.30: The 3-D model (plan view) used for the simulation with the IE program. The midpoint and the strike of the conductive body are the same as for the thin-sheet model in figure 7.29. The body extends from the surface down to 300 m depth. Data fit for the model configuration is displayed at the bottom. The squares correspond to the measured data, the solid line is the calculated curve. The bottom shows a comparison of data set A05 with the calculated curve of location "Test". It gives a better fit than the calculated curve at the location of site A05.	221
Fig. 7.31: Top: The 3-D model (plan view) used for the simulation with the SLDM program. Bottom: Schematic 3-D sketch of the 3-D SLDM model (after Hördt et al, 1992).	223
Fig. 8.1: Transmitter and receiver survey plan (partial) of the European test. Station numbers start with 0 at the well, going positive in the western and negative in the eastern direction (after Strack et al, 1989b).	230
Fig. 8.2: Comparison of inversion results at station -2 for two different transmitter locations displayed on a log-linear scale (after Strack et al, 1989b).	231

Fig. 8.3: Intermediate results from the data processing at one station of the test profile in figure 8.1. The magnetic response (time derivative of the magnetic field) is shown on the left column and the electric field signal on the right (after Strack et al, 1989b).	232
Fig. 8.4: Inversion results based on the magnetic response data using both transmitters. The depth to the top of the resistive region (shaded) is resolved but not its resistivity or thickness (after Strack et al, 1989b).	233
Fig. 8.5: Inversion results based on the electric field data using both transmitters. The depth to the top of the resistive region (shaded) is resolved, as is its resistivity (after Strack et al, 1989b).	234
Fig. 8.6: Resolution analysis for the resistive layer parameters using the normalized Jacobian as a measure of sensitivity. The magnetic field (bottom two curves) is almost insensitive to changes in the target layer resistivity, whereas the electric field (top two curves) is very sensitive to both thickness and resistivity variations (after Strack et al, 1989b).	234
Fig. 8.7: Basemap of the Australian survey (after Strack et al, 1989b).	235
Fig. 8.8: Geological cross section for the Canning Basin LOTEM survey area (after Strack et al, 1989b).	236
Fig. 8.9: Canning Basin LOTEM survey plan (after Strack et al, 1989b).	236
Fig. 8.10: Well log with blocked model (heavy line) for the well Kora-1 in figure 8.9 (after Strack et al, 1989b).	237
Fig. 8.11: Seismic section for line 4 which was used to fix the geologic structure for the inversion (after Strack et al, 1989b).	237
Fig. 8.12: Resistivity variations within units, obtained from magnetic transient data by fixing all layer thicknesses according to seismic information and inverting for the best fitting resistivity values. Confidence in Unit i values is poor because it is resistive (after Strack et al, 1989b).	238
Fig. 8.13: Resistivity variations within units. They were obtained from magnetic and electric transient data by fixing all layer thicknesses according to seismic information and inverting for the best fitting resistivity values using joint inversion. The statistical confidence in the resistive unit i is much greater than in figure 8.12 (after Strack et al, 1989b).	239
Fig.8.14: Resistivity versus percentage sandstone for unit e. The relationship is derived from the well log and used to convert the interpreted resistivity values to sand-to-shale ratios (after Strack et al, 1989b).	239
Fig.8.15: Resistivity section in terms of sand-to-shale ratios, reflecting porosities under the assumption that salinity and water saturation do not vary laterally same within a clastic unit. The percentage sandstone values were derived using the calibration curve and the scales along the axis from figure 8.14 (after Strack et al, 1989b).	240
Fig. 8.18: Seismic section for line 3220 with three interpreted reflectors.	241
Fig. 8.17: Contour map derived from seismic information of the top of the Triassic. The south-western part of the seismic line 3220 shows a depression. At the bottom a geological section along a perpendicular seismic line is shown.	242
Fig. 8.18: Survey plan of the LOTEM survey near Tai Xing, PRC.	243
Fig. 8.19: Two reduced induction logs. The blocked one represents the blocked preserving the lithology and the dashed one considers LOTEM layer resolution.	243
Fig. 8.20: Synthetic LOTEM curves for the magnetic and electric field responses for porosity (thus resistivity) variations in the Permian limestone.	244

Fig. 8.21: Resistivity section derived from one-dimensional inversions for the LOTEM profile. Superimposed are the seismic reflectors.	245
Fig. 9.1: Reproduction of an original strip chart record from the Cabora Bassa line ultra deep resistivity measurement. The information leading to the labeling of the figure was supplied by S. Joubert (pers. comm.).	248
Fig. 9.2: Example of a processing display of the Cabora Bassa DC-resistivity measurements. The bottom shows the complete time series after digitization. The top left frame displays the resulting stack after picking windows out of the time series and stacking them (courtesy S. Joubert, CSIR)	248
Fig. 9.3: Magnetic field transients measured over the Southern extension of the Canadian Shield (after Sternberg, 1979).	249
Fig. 9.4: Electric field transients measured over the Southern extension of the Canadian Shield (after Sternberg, 1979).	250
Fig. 9.5: Interpreted model range for the explanation of the transient soundings over the southern extension of the Canadian Shield the (after Sternberg, 1979).	251
Fig. 9.6: Example of an interpreted profile for the Pacific North-West (after Keller et al, 1984).	252
Fig. 9.7.: Regional geologic map of Southern Germany with LOTEM and deep reflection seismic survey locations. geologic key: a: Tertiary and Quaternary basin and graben fill; b: Tertiary volcanic rocks; c: Permian to Triassic sediments; d: Devonian (Rhenish Shield); e: Alpine orogen; f: Jurassic sediments (Swabian Alb); g: crystalline Hercynian basement. Map notation: K – Köln, F – Frankfurt, M – Munich, Str – Strasbourg, Ka – Karlsruhe, B – Basel, Stu – Stuttgart. A basemap of the LOTEM survey areas (squares) is shown in figures 9.12 and 9.21 (after Strack et al, 1990).	253
Fig. 9.8: Representative data set for the 1986 LOTEM survey in the Oberpfalz area, Germany. The different displays show the different processing steps.	254
Fig. 9.9: Interpreted resistivity cross section for the LOTEM survey near the location of the German continental drill hole.	255
Fig. 9.10: Resistivity test for the Oberpfalz model (Oberpfalz site15), illustrating that the data require a conductive last layer in 10 km depth.	256
Fig.9.11: Minimum conductor thickness test for the 1986 LOTEM data (Oberpfalz site 15), showing that the data requires a minimum thickness of the conductor being 250 m.	256
Fig. 9.12: Basemap for the Black Forest survey (after Strack et al, 1990).	257
Fig. 9.13: Seismic section showing the bright spot at 9.5 km depth and the laminated lower crust of the Black Forest beginning at 14 km. The bar on top marks the location of the LOTEM survey (after Strack et al, 1990).	258
Fig. 9.14: Data processing sequence from the Black Forest survey (site 12). Two consecutive recordings versus time at one receiver site show slightly different noise characteristics. The filtered data from all recordings (250 transients) at this site were then selectively stacked to yield the bottom transient (after Strack et al, 1990).	259
Fig.9.15: Interpreted E–W resistivity profile 8605 (E–E' 9.12) (after Strack et al, 1990). .	260
Fig.9.16: Interpreted resistivity sections 8601 and 8602 derived from 1–D inversions. Note the apparent dip of the conductor to the NW. The error bars are the 68% confidence limit.	260

Fig. 9.17: Representative comparison of independent 1-D inversions for closely spaced stations with two different transmitter locations (after Strack et al, 1990).	261
Fig. 9.18: Resistivity test (left) and minimum thickness test (right) carried out for the evaluation of the existence of the conductor in the Black Forest LOTEM data.	262
Fig. 9.19: Histogram of the depth to last conductor from all inversions to the Black Forest data.	263
Fig. 9.20: A comparison of reflection profile data, velocities from seismic modeling of wide angle data, and EM depth soundings (after Lüschen et al, 1987).	263
Fig. 9.21: Site location map of the LOTEM test survey in the Urach Geothermal Area (after Strack et al, 1990).	264
Fig. 9.22: Existing geophysical information (seismic and magnetotellurics) for the Urach Geothermal Area (after Berkthold et al, 1982) with a low velocity region. The LOTEM survey covered 7 km directly over the region.	265
Fig. 9.23: Data processing sequence for the Urach survey (site 6). The polarity of the signal is selected by the first transmitter pulse and all consecutive signals are adjusted to it. The data processing follows that of figure 9.14 (after Strack et al, 1990).	265
Fig. 9.24: Interpreted LOTEM resistivity depth section from one-dimensional inversions along traverse UL8601. Mesozoic and younger Paleozoic sediments from 0 to 1600 m are above resistive crystalline basement (gneisses). The crosshatching and shading of corresponding resistivity units is used to aid geologic correlation (after Strack et al, 1990).	266
Fig. 9.25.: Comparison of inversion result and induction log at the Urach geothermal well site. The shaded part marks the confidence bounds. LOTEM station 10 is 400 m from well U III apart (after Strack et al, 1990) and its interpretation given by the dashed line.	267
Fig. 9.26: Last layer resistivity test for Urach LOTEM station 6. The upper and lower curves represent early and late time resistivity transform curves for the respective models on the right. The circles represent the observed data and the solid/dashed lines the synthetic curves derived from the model on the right (after Strack et al, 1990).	267
Fig. 9.27: General geologic features around the Kaapvaal craton in terms of their resistivities.	268
Fig. 9.28: Basemap of the LOTEM survey including the most important deep DC-resistivity soundings.	269
Fig. 9.29: Top: Geoelectric section from Pietersburg to north of Dendron along the seismic reflection profile. Resistivity values are $k \Omega m$. Bottom: Line drawing of the seismic reflection pattern in the Pietersburg-Dendron section of the profile (after De Beer et al, 1991).	269
Fig. 9.30: Voltage responses for different transmitter to receiver offset using an average model for the conductor near the base of the Kaapvaal craton.	270
Fig. 9.31: Response resulting after convolving the data of figure 9.30 with a measured system response taking filters and transmitter waveform into account.	271
Fig. 9.32: Representative data set from the LOTEM survey. The left four frames show four single records. The right frame displays the result after removing the DC-level from all the records and stacking the data using an extended median stacking technique.	272
Fig. 9.33: Early and late time apparent resistivities for stations DE04 and DE05 (see figure 9.28). The field data are represented by the points and the theoretical curve for	

the inversion results by the solid line through the data points. The dashed line represent a half-space response when the conductor is absent (after De Beer et al, 1991).	272
Fig. 9.34: Error ellipse for an χ^2 fit better than 7% for different resistivities and depths of the conductor.	273
Fig. 9.35: The earth models interpreted for LOTEM sounding data for DE05 and DE04 as shown in figure 9.33 (after De Beer et al, 1991).	273
Fig. 9.36: The depth to the deep crustal conductor in the Kaapvaal craton and SMZ as determined by ultra-deep Schlumberger soundings at sites 32, 37, 34, 36 and 38 and LOTEM soundings at DE05 and DE04 (after De Beer et al, 1991).	274
Fig. 9.37: Percentage change of the mean monthly resistivity measured by Wenner arrays in the Tangshan area (after Qian et al, 1983).	275
Fig. 9.38: Contour map of the resistivity anomalies in the Beijing-Tianjin-Tangshan area (after Qian et al, 1979).	276
Fig. 9.39: Distribution of earthquakes with magnitudes above 4 after the Tangshan earthquake. Open circles represent aftershocks while the closed ones are earthquakes appearing to be unrelated to the aftershocks (after Qian et al, 1979).	276
Fig. 9.40: Basemap of the LOTEM survey near the Tangshan area, PRC.	277
Fig. 9.41: Representative stacked transient (FB15) for the survey in the Tangshan area, PRC.	278
Fig. 9.42: Selectively stacked transients at the control site in the Tangshan area, PRC.	278
Fig. 9.43: Inversion results for the measurements at the control site in the Tangshan area, PRC.	279
Fig. 9.44: Resistivity depth sections for profile F8801. The top section displays the results as they are given by the inversion. The bottom section shows the same results after adjusting for the fact that the inversion resolved only the first layer conductance and not the individual layer parameters (conductance referencing).	280
Fig.A1.1: Source configuration for the TE mode.	293
Fig.A2.1: Graphic illustration of the file records structure of LOTEM SEGY standard data files. Here the implementation for the VAX is shown (after Engels, pers. comm.).	300
Fig.A4.1: Main menu structure for the program MODALL (subscreens are not shown).	318
Fig.A4.2: Example plot for the MODALL program calculating the magnetic field response for three different offsets.	322
Fig.A4.3: Example plot for the MODALL program calculating the electric field response for three offsets.	324
Fig.A7.1: Example of colour resistivity sections derived with <i>Occam inversion</i> . The top section shows the display of the inversion results as they are output. The center frame shows the same data after filtering it with a lowpass filter with a width of half of the total depth. This filter is applied horizontally. For the bottom frame only every third data set was used simulating sparse measurements.	367
Fig.A7.2: Comparison of different inversions using single sets of the synthetic data. On the left column the starting model was without the resistive unit, on the right column the resistive unit was included from the beginning on. Both layer thickness and layer resistivity were allowed to vary during the fitting procedure.	367

Fig.A7.3: Comparison of different inversions using single sets of the synthetic data. On the left column the starting model was without the resistive unit, on the right column the resistive unit was included from the beginning on. The layer resistivities were allowed to vary during the fitting procedure, while the layer thicknesses were forced to stay at the preset values. This simulates the use of a priori information from seismics. 367

Fig.A7.4: Comparison of different *joint inversions* using combinations of the synthetic data sets for increased resolution. On the left column the starting model was without the resistive unit, on the right column the resistive unit was included from the beginning on. The layer resistivities were allowed to vary during the fitting procedure, while the layer thicknesses were forced to stay at the preset values. This simulates the use of a priori information from seismics. 367

Fig.A7.5: Geoelectrical model (top) and inversion results for the joint inversion (along a profile) of the electric and magnetic field components keeping the structure fixed from the seismic a priori information (middle).In addition to the procedures for the center frame, for the bottom frame the bottom and top resistivities were kept fixed. 370

Fig.A7.6: Comparison of current flow patterns for a conductive layer (left, 1 Ω m, 500 m thick) and a resistive layer (right, 400 Ω m, 500 m thick) embedded at 2 km depth in a half space of intermediate resistivity (20 Ω m). The colours represent areas of equal current density. The induction currents are flowing perpendicular to the plane of the figure. The dashed lines are the contours of the return currents with opposite sign. Time increases from top to bottom on both sides, from 0.01 s to 1 s. In both cases vertical and lateral moveout can be observed, but is faster for the resistive case on the right. 370

Fig.A7.7: Plan view time-slices of the charge density distribution at the top of the second layer for the conductive (left) and resistive (right) models of figure 2. The difference in resistivity of the second layer (left – 1 Ω m-m; right – 400 Ω m-m) causes a charge distribution of opposite sign, which points in the direction of the vertical electric field. The transmitter dipole is sketched in the center of each frame. 371

Fig.A7.8: LOTEM current image of a profile parallel to a seismic line for the case history from Tai Xing, China. The seismic section is superimposed. Note that the LOTEM source image was done with only about 30 data sets. 371

LIST OF TABLES

Table 1.1: Different constants to be substituted in Archie’s formula when lithology of a rock is known (after Keller, 1988). 12

Table 3.1: Data processing modules which can be applied to LOTEM data. The X marks when this module should be applied prestack or poststack. 68

Table 5.1: Task list of the daily routine tasks of a LOTEM crew. 158

Table 6.1: Example for a simplified electric well log: resistivities, thicknesses and lithology. 174

Table 6.2: Reduction models resulting from different degrees of reduction of the geoelectric model. Left: five-layer model, right: four-layer model. 176

Table 6.3: Resistivity models used for the resolution study 183

Table 6.4:	Data of a blocked electrical log maintaining the lithological boundaries.	191
Table A2.1:	Record structure for a LOPS data file containing several individual transients.	298
Table A2.2:	Record structure for a LOPS data file containing a stacked transient.	299
Table A2.3:	Card image header mask as defined by the SEGY standard modified for TEM data. Use free spaces for your entry. The information is best coded in a block data module.	300
Table A2.4:	File header record and byte definition for TEM data adopting SEGY standard.	301
Table A2.5:	Trace header byte allocation table for TEM data adopting SEGY standard. ..	305

CONVENTIONS AND LIST OF SYMBOLS

VECTORS and MATRICES

- g** – bold lower case symbols represent vectors, except for σ (in chapter 4) which is not written bold face.
- J** – bold capitals represent matrices (e.g Jacobian matrix containing the derivations of the model function with respect to the model parameters).
- *** – denotes the convolution operator.
- y** – data vector containing the field observations.
- e** – error vector.
- f** – model function vector containing the model function values at the same points as the field observation.
- g** – discrepancy vector.
- j** – current density.
- p** – model parameter vector.
- p₀** – initial model vector.
- q** – parameter difference vector.
- q, r** – transformed parameters.
- B** – magnetic induction.
- D** – electric displacement; diagonal matrix containing parameter weights.
- E** – electric field intensity.
- H** – magnetic field.
- I** – identity matrix.
- I_w** – weighed Jacobian matrix.
- S, T** – matrices containing information about the eigenparameters.
- U, V** – othogonal matrices for the SVD.
- W** – weighting matrix.

SCALARS

- A** – receiver equivalent area (for magnetic sensors).
- BE, BH** – reciprocal modified impedances.
- D₀** – dipole moment (= current times transmitter length).
- dl** – transmitter dipole length.
- f** – model function.
- F** – formation factor.
- hi** – thickness of the *i*-th layer.
- H_x, H_y, H_z** – magnetic field components.
- H(z)** – *z* transform of transfer function.
- J₀, J₁** – Bessel functions of zeroth and first order.
- K, v** – controlling factors for the inversion.
- l** – receiver electric dipole length.
- M** – number of layers.
- m** – number of model parameters.
- n** – number of data points.
- p_i** – model parameters.
- R₁, R₂** – roughness for the resistivity versus depth function.
- r** – offset between transmitter center and receiver center. Radius vector in the *Z*-plane.
- s** – fraction of pore volume. Cumulative conductance
- s(t)** – system response function.
- t** – time values.
- U_z** – voltage induced in an induction coil.
- V_x, V_y** – voltage measured between electric field sensors in *x* and *y* direction.
- V_x** – volume fraction of shale.
- x, y** – *x*, *y* coordinates. *x* is taken parallel to the transmitter dipole.
- x(t)** – input function.

- $y(t)$ – output function.
 $X(z)$ – z transform of input function.
 $Y(z)$ – z transform of output function.
 z – z -transform variable.
 z_n – zeroes on the z -plane.
 z_p – poles on the z -plane.
 Δ – parameter difference vector.
 κ – $\text{SQRT}(i\omega\mu\sigma)$; frequency wavenumber.
 ϵ – dielectric permittivity.
 η – proportionally factor relating real parts of poles and zeroes with each other.
 λ_{ii} – normalized eigenvalues
 μ_0 – $4\pi \cdot 10^{-7}$ Vs/Am magnetic permeability.
 ρ – resistivity.
 $\rho_a^{\text{E.T.}}$ – early time apparent resistivity.
 $\rho_a^{\text{L.T.}}$ – late time apparent resistivity.
 ρ_u – horizontal resistivity.
 ρ_w – resistivity of pore fluid.
 ρ_x – resistivity of shaly rock fraction.
 σ – conductivity; standard deviation.
 Φ_E, Φ_M – Debye potentials.
 ϕ – porosity; angle between transmitter and offsets.
 ω – angular frequency.
 τ – normalized time.

REFERENCES

- Andrieux, P., and Wightman, W. E. 1984, *The so-called static corrections in magnetotelluric measurements*, 54th Ann. Mtg., Expanded Abstracts, Soc. Expl. Geophys., 43–44.
- Abramowitz, M., and Stegun, I.A., 1964, *Handbook of mathematical functions with formulas, graphs, and mathematical tables*, National Bureau of Standards, Applied Mathematics Series 55.
- Angenheister, G., ed., 1982, *Physical properties of rocks*, Landolt-Börnstein, New series: 1b, Springer Verlag.
- Archie, G. E., 1942, *The electrical resistivity log as an aid in determining some reservoir characteristics*, Trans. Am. Inst. Min. Metallurg. Petr. Eng. 146, 54–62.
- Barnet, C.T., 1984, *Simple inversion of time-domain electromagnetic data*, Geophysics 49, 925–933.
- Barringer, A.R., 1962, *A new approach to exploration—The INPUT airborne electrical pulse prospecting system*, Min. Congress Journal 48, 49–52.
- Barry, K.M., Cavers, D.A. Kneak, C.W., 1975, *Recommended standards for digital tape formats*, Geophysics 40, 344–352.
- Bartelsen, H., Lüschen, E., Krey, Th., and Meissner, R., Schmoll, J., and Walter, Ch., 1982, *The combined seismic reflection-refraction investigation of the Urach geothermal anomaly*, in Haenel, R., (ed.), *The Urach geothermal project*: E. Schweizerbart'sche Verlagsbuchhandlung, 247–262.
- Barton, J.M., Jr., and Key, R.M., 1981, *The tectonic development of the Limpopo Mobile Belt and the evolution of the Archaean cratons of southern Africa*, in: Kröner, A., (ed.), *Precambrian Plate Tectonics*, Developments in Precambrian Geology 4, 185 – 212.
- Barton, J.M., Jr., 1983, *Our understanding of the Limpopo Belt – a summary with proposals for future research*. Spec. Publ. Geol. Soc. S. Afr. 8, 191 – 203.
- Behr, H.-J., Engel, W., Franke, W., Giese, P., and Weber, K., 1984, *The Variscan belt in Central Europe: main structures, geodynamic implications, open questions*, in Zwart, H.J., Behr, H.J., and Oliver, J., Eds., *Appalachian and Hercynian Fold Belts*, Tectonophysics 109, 15–40.
- Berkman, E., Orange, A., and Smith, R. D., 1983, *Seismic and magnetotellurics combined: a case history of the South Clay Basin Prospect*, 53rd Ann. Mtg., Soc. Expl. Geophys., Expanded Abstracts, 65–67.

- Berkthold, A., Hänel, R., and Wohlenberg, J., 1982, *A model of the Urach geothermal anomaly as derived from geophysical investigations*, in Haenel, R., (ed.), *The Urach geothermal project: E. Schweizerbart'sche Verlagsbuchhandlung*, 401–412.
- Blohm, E.K., Worzyk, P., and Scriba, H., 1977, *Geoelectric deep soundings in southern Africa using the Cabora Bassa power line*, *J. Geophysics* **43**, 665 – 679.
- Boerner, D.E., 1992, *Deep Controlled Source Electromagnetic Sounding: Theory, Results, and Correlation*, Geophysical Surveys (in press).
- Boerner, D.E., and West, G.F., 1989, *A generalized representation of the electromagnetic fields in a layered earth*, *Geophys. J.* **97**, 529–548.
- Bortfeld, R.K., Gowin, J., Stiller, M., Baier, B., Behr, H.-J., Heinrichs, T., Dürbaum, H.J., Hahn, A., Reichert, C., Schmoll, J., Dohr, G., Meissner, R., Bittner, R., Milkereit, B., and Gebrande, H., 1985, *First results and preliminary interpretation of deep-reflection seismic recordings along profile DEKORP 2–South*, *J. Geophys.* **57**, 137–163.
- Bracewell, R.N., 1965, *The Fourier transform and its applications*, McGraw-Hill Book Company, New York.
- Büchter, C., 1983, *Die Verteilung der elektrischen Leitfähigkeit im Bereich der Bohrung Münsterland 1: Ein Vergleich zwischen magnetotellurischen Untersuchungen, elektrischen Bohrlochmessungen, geoelektrischen Tiefensondierungen sowie Messungen der Leitfähigkeit an Gesteinsproben*, Diplom thesis, Universität Münster, (unpublished).
- Chen Leshou, Cai Gang, Ma Tao, 1988, *Two-dimensional inversion of magnetotelluric sounding data; in: An overview of exploration in China*, Soc. Expl. Geophys. Geophysical References 3, Tulsa.
- Clarke, J., Gamble, T.D., Goubau, W.M., Koch, R.H., and Miracky, R.F., 1983, *Remote-reference magnetotellurics: equipment and procedures*, *Geophys. Prosp.* **31**, 149–170.
- Constable, S.C., Parker, R.L., and Constable, C.G., 1987, *Occam's inversion: A practical algorithm for generating smooth models from electromagnetic sounding data*, *Geophysics* **52**, 289–300.
- Coward, M.P., and Fairhead, J.D., 1980, *Gravity and structural evidence for the deep structure of the Limpopo Belt, Southern Africa*, *Tectonophysics* **68**, 31 – 43.
- Christopherson, K.R., 1990, *Applications of magnetotellurics to petroleum exploration in Papua New Guinea*, in Carman, G. J. and Z., eds., *Petroleum exploration in Papua New Guinea*, Proc. 1st PNG Petroleum Conv., Port Moresby.
- Damron, L.A., 1986, *Physical modeling of lateral variations of resistivity in transient electromagnetics*, M.Sc. thesis T-3008, Colorado School of Mines.
- De Beer, J.H., and Stettler, E.H., 1988, *Geophysical characteristics of the southern African Continental Crust*, *J. Petrol. (Special Lithosphere Issue)*, 163 – 184.
- De Beer, J.H., LeRoux, C.L., Hanstein, T., and Strack, K.-M. 1991, *Direct current resistivity and LOTEM model for the deep structure of the northern edge of the Kaapvaal craton, South Africa*, *Physics of the Earth and Planetary Interior* **66**, 51 – 61.
- Dey, A., 1972, *Finite source electromagnetic response of layered and inhomogeneous earth models*, Ph.D. thesis, University of California, Berkeley.
- Dolan, W.M., 1970, *Geophysical detection of deeply buried sulfide bodies in weathered regions*, *GSC Economic Geology Rep.* **26**, 336–344.
- Druskin, V.L., and Knizhnerman, L.A., 1988, *A spectral semi-discrete method for the numerical solution of 3D nonstationary problems in electrical prospecting*, *Physics of the solid Earth* **24**, 63 – 74.
- Du Toit, M.C., van Reenen, D.D., and Roering, C., 1983, *Some aspects of the geology, structure and metamorphism of the Southern Marginal Zone of the Limpopo Metamorphic Complex*, Spec. Pub. Geol. Soc. S. Afr. **8**, 121 – 142.

- Duncan, P.M., Hwang, A., Edwards, R.N., Baileys, R.C., Garland, G.D., 1980, *The development and applications of a wide band electromagnetic sounding system using a pseudo-noise source*, *Geophysics* **45**, 1276–1296.
- Eadie, T., 1981, *Detection of hydrocarbon accumulations by surface electrical methods: a feasibility study*, *Research in Applied Geophysics* **15**, University of Toronto.
- Earth Technology Corporation, 1985, *Mapping hydrocarbon-brine contacts*, technical report.
- Edwards, R.N. and Gomez-Trevino, E., 1979, *Magnetometric resistivity (MMR) anomalies of two-dimensional structures*, *Geophysics* **44**, 947–958.
- Edwards, R.N., Lee, H., and Nabighian, M.N., 1978, *On the theory of magnetometric resistivity methods*, *Geophysics* **43**, 947–958.
- Ensley, R.A., 1984, *Comparison of P- and S-wave seismic data: A new method for detecting gas reservoirs*, *Geophysics* **49**, 1420–1431.
- Flis, M. F., Newman, G. A., and Hohman, G. W., 1989, *Induced-polarization effects in time-domain electromagnetic measurements*, *Geophysics* **54**, 514–523.
- Fuchs, K., Bonjer, K.-P., Gajewski, D., Lüschen, E., Prodehl, C., Sandmeier, K.-J., Wenzel, F., and Wilhelm, H., 1987, *Crustal evolution of the Rhinegraben area, Exploring the lower crust of the Rhinegraben rift by unified geophysical experiments*, *Tectonophysics* **141**, 261–275.
- Fullagar, P.K., 1989, *Generation of conductivity-depth pseudo-section from coincident loop and in-loop TEM data*, *Exploration Geophysics* **20**, 43–45.
- Gamble, T.D., Goubau, W.M., and Clarke, J., 1979, *Magnetotellurics with a remote magnetic reference*, *Geophysics* **44**, 934–948.
- Gomez-Trevino, E., and Edwards, R.N., 1979, *Magnetometric resistivity (MMR) anomalies of two-dimensional structures*, *Geophysics* **44**, 947–958.
- Gomez-Trevino, E., and Edwards, R.N., 1983, *Electromagnetic soundings in the sedimentary basin of southern Ontario – A case history*, *Geophysics* **48**, 311–330.
- Gough, D.I., 1986, *Seismic reflectors, conductivity, water and stress in the continental crust*, *Nature* **323**, 143–144.
- Gunderson, B.M., Newman, G.A., and Hohmann, G.W., 1986, *Three-dimensional transient electromagnetic responses for a grounded source*, *Geophysics* **51**, 2117–2130.
- Haak, V., and Hutton, R., 1986, *Electrical resistivity in continental lower crust*, in: Dawson, J.B., Carswell, D.A., Hall, J., and Wedepohl, K.H., (eds.), *The nature of the lower continental crust*, *Geol. Soc. Spec. Pubs.* **24**, 35–49.
- Haenel, R., (ed.), 1982, *The Urach geothermal project*, E. Schweizerbart'sche Verlagsbuchhandlung.
- Harthill, N., 1968, *The CSM test area for electrical surveying methods*, *Geophysics* **33**, 675–678.
- Helbig, K. and Mesdag, C.S., 1982, *The potential of shear-wave observations*, *Geophys. Prosp.* **30**, 413–431.
- Hördt, A., 1989, *Ein Verfahren zur "Joint Inversion" angewandt auf "Long Offset Transient Electromagnetics" (LOTEM) und "Magnetotellurik" (MT)*, Diplom thesis – geophysics, University of Cologne, (unpublished).
- Hördt, A., Jödicke, H., Strack, K.-M., Vozoff, K., and Wolfgram, P.A., 1992, *Inversion of long-offset transient electromagnetic soundings near the borehole Münsterland I, Germany, and comparison with MT measurements*, *Geophys. J. Int.*, (in press).
- Hördt, A., Druskin, V.L., Knizhnerman, L.A., Strack, K.-M., 1992, *Interpretation of 3-D effects in long-offset transient electromagnetic (LOTEM) soundings in the Münsterland area / Germany*, *Geophysics* (in press).
- Hohmann, G.W., 1971, *Electromagnetic scattering by conductors in the earth near a line source of current*, *Geophysics* **36**, 101–131.
- Hohmann, G.W., 1975, *Three-dimensional induced polarization and electromagnetic modelling*, *Geophysics* **40**, 309–324.
- Inman, J.R., 1975, *Resistivity inversion with ridge regression*, *Geophysics* **40**, 798–817.
- Ioup, G.E., and Ioup, J.W., 1983, *Iterative deconvolution*, *Geophysics* **48**, 1287–90.

- Jackson, D.D., 1988, *Interpretation of inaccurate, insufficient, and inconsistent data*, Geophys. J. R. astr. Soc. **28**, 97–109.
- James, B.A., and Zerilli, A., 1991, *An introduction to transient EM imaging via interpretation of current distributions*, 53rd annual meeting, Europ. Ass. Explor. Geophys., 392–393.
- Jödicke, H., 1990, *Zonen hoher elektrischer Krustenleitfähigkeit im Rhenoharzynikum und seinem nördlichen Vorland*, Ph.D. thesis, Universität Münster.
- Jones, A.G., 1987, *MT and reflection: an essential combination*, Geophys. J. Roy. astr. Soc. **89**, 7–18.
- Jones, F. W., and Pascoe, L. J., 1972, *The perturbation of alternating geomagnetic fields by three-dimensional conductivity inhomogeneities*, Geophys. J. **27**, 429–485.
- Jupp, D.L.B., and Vozoff, K., 1975, *Stable iterative methods for the inversion of geophysical data*, Geophys. J. R. astr. Soc. **42**, 957–976.
- Jupp, D.L.B., and Vozoff, K., 1977, *Resolving anisotropy in layered media by joint inversion*, Geophys. Prosp. **25**, 460–470.
- Kamenetsky, F.M., and Porstendorfer, G., 1983, *Die Skin-Tiefe in der Magnetotellurik und bei elektromagnetischen Sondierungen mit künstlichen Quellen in der Fernzone*, Gerlands Beitr. Geophysik **92**, 465–470.
- Kamenetsky, F.M., 1985, *On some specific features of inductional electromagnetic soundings*, in: Academy of Science CCCP, *Inductional investigations of the upper part of the Earth crust*, 20–38, (in Russian).
- Karlik, G., and Strack, K.-M., 1990, *"All-time" scheinbare Widerstandskurven für LOTEM*, in Haak, V., and Homilius, J., (eds.), *Protokoll über das 13. Kolloquium "Elektromagnetische Tiefenforschung"*, Hornburg, NLfB, 135–144.
- Kaufman, A.A., and Keller, G.V., 1983, *Frequency and transient soundings*, Elsevier, Amsterdam.
- Keller, G.V., Pritchard, J.I., Jacobson, J.J., and Harthill, N., 1984, *Megasource time-domain electromagnetic sounding methods*, Geophysics **49**, 993–1009.
- Keller, G.V., 1971, *Electrical characteristics of the Earth's crust*, in Wait, J.R., (ed.), *Electromagnetic probing in geophysics*, Golem Press, 13–76.
- Keller, G.V., 1988, *Rock and mineral properties*, in: Nabighian, M.N., (ed.), *Electromagnetic Methods in applied Geophysics*, Vol. 1 – Theory, Soc. Expl. Geophys., Tulsa, 13–52.
- Keller, G.V., and Frischknecht, F.C., 1966, *Electrical Methods in geophysical prospecting*, Pergamon Press Inc.
- Kern, H., 1982, *P- and S-wave velocities in crustal and mantle rocks under the simultaneous action of high confining pressure and high temperature and the effect of the rock microstructure*, in Schreyer, W., (ed.), *High pressure researches in geoscience*, E. Schweizerbart'sche Verlagsbuchhandlung, 15–45.
- Kraev, A.P., 1937, *Transient process in a homogeneous submerged medium*, Sci. Rep., Leningrad State Univ. **14**, Ser. Phys. Sci. **3** (III).
- Kriegshäuser, B., 1991, *Einige Aspekte der 3-D Interpretation von LOTEM Daten*, Diplomthesis, University of Cologne, (unpublished).
- Kulhanek, O., 1976, *Introduction to digital filtering in geophysics*, Elsevier, Amsterdam.
- Kuth, Ch., 1987, *Zwei- und dreidimensionale Simulationsrechnungen zum Induction log*, in: Ebel, A., Neubauer, F.M., Raschke, E., Speth, P., (Hrsg.), *Mitteilungen aus dem Institut für Geophysik und Meteorologie der Universität zu Köln* **56**.
- Kuth, Ch., and Neubauer, F.M., 1988, *Multi-frequency inversion of induction logs*, Geophys. Prosp. **36**, 66–82.
- LaCoste, L.J.B., 1982, *Deconvolution by successive approximation*, Geophysics **47**, 1724–30.
- Lanczos, C., 1961, *Linear Differential Operators*, Van Nostrand, Princeton, 665–679.
- Lawson, C.L., and Hanson, R.J., 1974, *Solving least squares problems*, Prentice Hall Inc.
- LeRoux, C.L., 1987, *Frequency domain grounded dipole source EM: A study of near-field effects and the response due to a vertical conductive plate in a conducting host*, M. Sc. thesis, University of Toronto.

- Lines, L.R., and Treitel, S., 1984, *Tutorial, A review of least-squares inversion and its application to geophysical problems*, *Geophys. Prosp.* **32**, 159–186.
- Lüschen, E., Wenzel, F., Sandmeier, K.-J., Menges, D., Rühl, T., Stiller, M., Janoth, W., Keller, F., Söllner, W., Thomas, R., Krohde, A., Stenger, R., Fuchs, K., Wilhelm, H., and Eisbacher, G., 1987, *Near-vertical and wide-angle seismic surveys in the Black Forest, SW Germany*, *J. Geophys.* **62**, 1–30.
- Macnae, J.C., and Lamontagne, Y., 1987, *Imaging quasi-layered conductive structures by simple processing of transient electromagnetic data*, *Geophysics* **52**, 545–554.
- Macnae, J.C., and Spies, B.R., 1989, *Paper 13—Accomplishment of wide-band, high-power EM*, 109–121, in: Garland, G.O., (ed.), *Proceedings of Exploration '87: Third Decennial International Conference on Geophysical and Geochemical Exploration for Minerals and Groundwater*, Ontario Geological Survey, Spec. Vol. 3.
- Macnae, J.C., Smith, R., Polzer, B.D., Lamontagne, Y., and Klinkert, P.S., 1991, *Conductivity-depth imaging of airborne electromagnetic step-response data*, *Geophysics* **56**, 102–114.
- Matthews, D.H., 1986, *Seismic reflections from the lower crust around Britain*, in Dawson, J.B., Carswell, D.A., Hall, J., and Wedepohl, K.H., (eds.), *The nature of the lower continental crust*, *Geol. Soc. Spec. Pubs.* **24**, 11–21.
- Mayne, S.J., Nicholas, E., Bigg-Wither, A.L., Rasidi, J.S., and Raine, M.J., 1974, *Geology of the Sydney Basin – A review*, BMR Bulletin 149, Australian Government Publishing Service, Canberra.
- Mason, R., 1973, *The Limpopo mobile belt – southern Africa*, *Philos. Trans. R. Soc. London, Ser. A.* **273**, 463 – 485.
- Menke, W., 1984, *Geophysical data analysis: discrete inverse theory*: Academic Press.
- Nabighian, M.N., 1979, *A quasi-static transient response of a conducting half-space – An approximate representation*, *Geophysics* **44**, 1700–1705.
- Nabighian, M.N., 1988, *Electromagnetic methods in applied geophysics, Vol.1 – Theory*, Soc. Expl. Geophys., Tulsa.
- Nabighian, M.N., and Oristaglio, M.L., 1984, *On the approximation of finite loop sources*, *Geophysics* **49**, 1027–1029.
- Nabighian, M.N., and Macnae, J.C., 1991, *Time domain electromagnetic prospecting methods*, in: Nabighian, M.N., (ed), *Electromagnetic methods in applied Geophysics, Vol. 2*, Soc. Expl. Geophys., (in press).
- Naess, O.E., and Brulan, L., 1985, *Stacking methods other than simple summation*, in: A. A. Fitch, *Developments in Geophysical Exploration – 6*, Elsevier, 189 – 224.
- Nekut, A.G., 1987, *Direct inversion of time-domain electromagnetic data*, *Geophysics* **52**, 1431–1435.
- Nekut, A.G., and Spies, B.R., 1989, *Petroleum exploration using controlled source electromagnetic methods*, *Proc. IEEE* **77**, 338–362.
- Newman, G.A., Hohmann, G.W., and Anderson, W.L., 1986, *Transient electromagnetic response of a three-dimensional body in a layered earth*, *Geophysics* **51**, 1608 – 1627.
- Newman, G.A., 1989, *Deep transient electromagnetic soundings with a grounded source over near-surface conductors*, *Geophysical J.* **98**, 587–601.
- Oehler, D.Z., and Sternberg, B.K., 1984, *Seepage-induced anomalies, "false" anomalies, and implication for electrical prospecting*, *Bull. Am. Assn. Petr. Geol.* **68**, 1121–1145.
- Oristaglio, M.L., and Hohmann, G.W., 1984, *Diffusion of electromagnetic fields into a two-dimensional earth: A finite difference approach*, *Geophysics* **49**, 870–894.
- Orsinger, A., and Van Nostrand, R., 1954, *A field evaluation of the electromagnetic reflection method*, *Geophysics* **19**, 478–489.
- Palacky, G.J., 1983, *Tutorial: Application in electrical and electromagnetic methods*, *Geophys. Prosp.* **31**, 861–872.
- Palacky, G.J., 1988, *Resistivity characteristics of geologic targets*, in: Nabighian, M.N., (ed.), *Electromagnetic Methods in applied Geophysics, Vol. 1 – Theory*, Soc. Expl. Geophys., Tulsa, 53–122.
- Parker, R.L., 1984, *The inverse problem of resistivity sounding*, *Geophysics* **49**, 2143–2158.

- Petry, H., 1987, *Transient elektromagnetische Tiefensonderung – Modellrechnungen und Inversion*, Diplom thesis, University of Cologne, (unpublished).
- Polzer, B.D., 1986, *The interpretation of inductive transient electromagnetic sounding data*, M.Sc. thesis, University of Toronto, (unpublished).
- Pridmore, D. F., Hohman, G. W., Ward, S. H., and Sill, W. R., 1981, *An investigation of finite-element modeling for electrical and electromagnetic data in three dimensions*, *Geophysics* **46**, 1009–1024.
- Prieto, C., Perkins, C., and Berkman, E., 1985, *Columbia River Basalt Plateau – An integrated approach to interpretation of basalt covered areas*, *Geophysics* **50**, 2709 – 2719.
- Raiche, A.P., 1974, *An integral equation approach to three-dimensional modelling*, *J. Geophysical* **36**, 363–376.
- Raiche, A.P., and Gallagher, R.G., 1985, *Apparent resistivity and diffusion velocity*, *Geophysics* **50**, 1628–1633.
- Raiche, A.P., Jupp, D.L.B., Rutter, H., and Vozoff, K., 1985, *The joint use of coincident loop transient electromagnetic and Schlumberger sounding to resolve layered structures*, *Geophysics* **50**, 1618–1627.
- Qian, F., Zhao, Y., Yu, M., Wang, Z., Liu, X., and Chang, S., 1983, *Geoelectric resistivity anomalies before earthquakes*, *Scientia Sinica (Series B)*, Vol. XXVI, 326 – 366.
- Qian, F., Zhao, Y., Xu, T., Ming, Y., and Zhang, H., 1990, *A model of an impending-earthquake precursor triggered by tidal forces*, *Physics of the Earth & Planetary Interior* **62**, 284–297.
- Qian, J., Gui, X., Ma, H., Ma, X., Guang, H., and Zhao, Q., 1979, *Observations of apparent resistivity in the shallow crust before and after several great shallow earthquakes*, *International Symposium on earthquake Prediction*, Unesco SC-79/Conf. 801/Col 14/I –13.
- Qian, W., and Pedersen, L.B., 1991, *Industrial interference magnetotellurics: An example from the Tangshan area, China*, *Geophysics* **56**, 265 – 273.
- Rossow, J., 1987, *An investigation of deconvolution techniques for transient electromagnetic records*, Ph. D. thesis, Colorado School of Mines, 140.
- Robertson, J.D., 1987, *Carbonate porosity from s/p travel time ratios*, *Geophysics* **52**, 1346–1354.
- Rozenberg, G., Henderson, J., and MacDonald, J.C., 1985, *The use of transient electromagnetic data on permafrost distribution for CDP static correction*, Expanded Abstracts, 55th Annual Meeting, Society of Exploration Geophysicists.
- SanFilipo, W.A., and Hohmann, G.W., 1985, *Integral equation solution for transient response of a three-dimensional body in a conductive halfspace*, *Geophysics* **50**, 798 – 809.
- Schlumberger, 1985, *Well evaluation conference China 1985*, Schlumberger Documentation Services.
- Schlumberger, 1987, *Log interpretation principles / applications*, Schlumberger Educational Services.
- Schneider, W.A., Sixta, D.P., Janak, P.M., Grupp, S.R., Rimmer, and Guderjahn, C.G., 1982, *A comparison of land seismic sources*, 44th Annual Meeting, Abstract vol., Europ. Ass. Expl. Geophys., Venice.
- Schruth, P., 1989, *Die Bestimmung der Leitfähigkeitverteilung unter der Basaltbedeckung des Vogelsberges mit einem Transient Elektromagnetischen Tiefensonderungsverfahren*, Diplom thesis – geology, University of Cologne, (unpublished).
- SEG, 1980, *Digital tape standards*, Soc. Expl. Geophys.
- Shankland, T.J., and Ander, M.E., 1983, *Electrical conductivity, temperatures, and fluids in the lower crust*, *J. Geophys. Res.* **88**, 9475–9484.
- Shanks, J.L., 1967, *Recursive filters for digital processing*, *Geophysics* **32**, 33–52.
- Sheriff, R.E., 1984, *Encyclopedic dictionary of exploration geophysics*, Soc. Expl. Geophys.
- Smith, R. S., and West, G. W., 1989, *Field examples of negative coincident-loop transient electromagnetic responses modeled with polarizable half-planes*, *Geophysics* **54**, 1491–1498.

- Smith, R.S., and Buselli, G., 1991, *Examples of data processed using a new technique for presentation of coincident- and in-loop impulse response transient electromagnetic data*, *Exploration Geophysics* **22**, 363–368.
- Smith, R.S., Edwards, R.N., and Buselli, G., 1991, *A new technique for presentation of coincident- and in-loop impulse-response transient electromagnetic data*, *Geophysics* **56**, (in press).
- Spies, B.R., 1983, *Recent developments in the use of surface electrical methods for oil and gas exploration in the Soviet Union*, *Geophysics* **48**, 1102–1112.
- Spies, B.R. and Eggers, D.E., 1986, *The use and misuse of apparent resistivity in electromagnetic methods*, *Geophysics* **51**, 1462–1471.
- Spies, B.R., 1988, *Local noise prediction filtering for central induction transient electromagnetic sounding*, *Geophysics* **53**, 1068–1079.
- Spies, B.R., 1989, *Depth investigation in electromagnetic sounding methods*, *Geophysics* **54**, 872–888.
- Stanley, W.D., Saad, A.R., and Ohofugi, W., 1985, *Regional magnetotelluric surveys in hydrocarbon exploration*, Parana Basin, Brazil, *Bull. Am. Assn. Petr. Geol.* **69**, 346–260.
- Staude, H., 1989, *Geologische Karte von Nordrhein Westfalen, Blatt 3910 Altenberge*, Geologisches Landesamt Nordrhein Westfalen, Krefeld, FRG.
- Stephan, A., 1989, *Interpretation von transient elektromagnetischen Messungen (LOTEM) im Bereich der Halterner Sande und Entwicklung der lokalen Rauschkompensation*, Diplom thesis – Geophysics, University of Cologne, (unpublished).
- Stephan, A., Schniggenfittig, H., and Strack, K.-M., 1991, *Long-offset transient EM sounding north of the Rhine-Ruhr-Coal-District, F. R. Germany*, *Geophys. Prosp.* **39**, 505–525.
- Stephan, A., and Strack, K.-M. 1991, *A simple approach to improve the signal to noise ratio for TEM data using multiple receivers*, *Geophysics* **56**, 863–869.
- Sternberg, B.K., and Clay, C.S., 1977, *Flambeau Anomaly: A high conductivity anomaly in the southern extension of the Canadian shield*, in: Heacock, J.G., (ed.), *The Earth's Crust*, *Geophys. Monogr.* **20**, 501–530.
- Sternberg, B.K., 1979, *Electrical resistivity structure of the crust in the southern extension of the Canadian Shield – Layered earth models*, *J. Geophys. Res.* **84**, 212–228.
- Sternberg, B.K., Washburne, J.C., and Pellerin, L., 1988, *Correction for the static shift in magnetotellurics using transient electromagnetic soundings*, *Geophysics* **53**, 1459–1468.
- Stoyer, C.H., 1981, *TDEM data acquisition and processing principles*. GP 671 class notes, Colorado School of Mines (unpublished).
- Stoyer, C.H., and Damron, L.A., 1986, *Integrated geophysical study in the Eastern basin and range Milford Valley, UT*, Integrated Geosciences Inc., (unpublished technical report).
- Stoyer, C.H., *Efficient computation of transient sounding curves for wire segments of finite length using an equivalent dipole approximation*, *Geophys. Prosp.* **38**, 87–99.
- Strack, K.-M., 1984, *The deep transient electromagnetic sounding technique: First field test in Australia*, *Exploration Geophysics* **15**, 451–459.
- Strack, K.-M., 1985, *Das Transient-Elektromagnetische Tiefensondierungsverfahren angewandt auf die Kohlenwasserstoff- und Geothermie-Exploration*, in: Ebel, A., Neubauer, F.M., Raschke, E., Speth, P., (Hrsg.), *Mitteilungen aus dem Institut für Geophysik und Meteorologie der Universität zu Köln* **42**.
- Strack, K.-M., 1987, *"All time" Definition des scheinbaren spezifischen Widerstandes für die LOTEM-Methode*, in: Haak, V. and Homilius, J., (eds.), *Elektromagnetische Tiefenforschung*, NfB, 341–347.
- Strack, K.-M., Hanstein, T.H., and Eilenz, H.N., 1989, *LOTEM data processing for areas with high cultural noise levels*, *Physics of the Earth & Planetary Interior* **53**, 261–269.

- Strack, K.-M., Hanstein, T., LeBrocq, K., Moss, D.C., Vozoff, K., and Wolfgram, P.A., 1989b, *Case histories of long-offset transient electromagnetics (LOTEM) in hydrocarbon prospective areas*, First Break 7, 467 – 477.
- Strack, K.-M., Lüschen, E., and Kötz, A.W., 1990, *Long offset transient electromagnetic (LOTEM) soundings applied to deep crustal studies in Southern Germany*, Geophysics 55, 834–842.
- Tabarovski, L. A., 1982, *Boundary conditions for vector potential at interface between conductor and isolator*, Elektromagnitnye metody geofizicheskikh issledovaniy, Novosibirsk, 36–50. (in Russian).
- Tezkan, B., 1988, *Electromagnetic sounding experiments in the Schwarzwald central gneiss massif*, J. Geophys. 62, 109 – 118.
- Tikhonov, A.N., 1946, *On the transient electric current in a homogeneous conduction half-space*, Izv. Akad. Nauk. SSSR, Ser. Geograf. Geofiz. 10.
- Tsubota, K., 1979, *The frequency and time domain response of a buried two dimensional inhomogeneity*, Ph.D. thesis T-2130, Colorado School of Mines.
- Tulinius, H., 1980, *Time-Domain electromagnetic survey in Krafla, Iceland*, M. Sc. thesis T-2325, Colorado School of Mines.
- Vanyan, L.L., 1967, *Electromagnetic depth soundings*: Consultants Bureaus, New York.
- Van Zijl, J.S.V., 1969, *A deep Schlumberger sounding to investigate the electrical structures of the crust and upper mantle in South Africa*, Geophysics 34, 450 – 462.
- Van Zijl, J.S.V., Hugo, P.L.V., and deBellocq, J.H., 1970, *Ultra deep Schlumberger sounding and crustal conductivity structure in South Africa*, Geophys. Prosp. 18, 615 – 634.
- Van Zijl, J.S.V., and Joubert, S.J., 1975, *A crustal model for South African Precambrian granitic terrains based on deep Schlumberger soundings*, Geophysics 40, 657 – 663.
- Van Zijl, J.S.V., 1977a, *Electrical studies of the deep crust in various tectonic provinces of southern Africa*, J.G. Heacock (ed.), *The Earth's Crust*, Am. Geophys Union Monogr. 20, 470 – 500.
- Van Zijl, J.S.V., 1978, *The relationship between the deep electrical resistivity structure and tectonic provinces in southern Africa, Part 1. Results obtained by Schlumberger soundings*, Trans. Geol. Soc. S. Afr. 81, 129 – 142.
- Vasseur, G., and Weidelt, P., 1977, *Bimodal electromagnetic induction in non-uniform thin sheets with an application to the northern Pyrenean induction anomaly*, Geophys. J. R. astr. Soc. 51, 669–690.
- Velikhov, Y.P., Zhamaletdinov, A.A., Belkov, I.V., Gorbunov, G.I., Hjelt, S.E., Lisin, A.S., Vanyan, L.L., Zhdanov M.S., Demidova, T.A., Korja, T., Kirillov, S.K., Kuksa, Yu.I., Poltanov, A.Y., Tokarev, A.D., and Yevstigneyev, V.V., 1986, *Electromagnetic studies on the Kola peninsula and in northern Finland by means of a powerful controlled source*, J. Geodynamics 5, 237 – 256.
- Verma, R.K., and Mallik, K., 1979, *Detectability of intermediate conductive and resistive layers by time domain electromagnetic sounding*, Geophysics 44, 1862–1878.
- Vozoff, K., 1972, *The Magnetotelluric method in the exploration of sedimentary basins*, Geophysics 37, 98–141.
- Vozoff, K., and Jupp, D.L.B., 1975, *Joint inversion of geophysical data*, Geophys. J. R. astr. Soc. 42, 977–991.
- Vozoff, K., (ed.), 1986, *Magnetotelluric methods*, Geophysics Reprint Series, Soc. Expl. Geophys., Tulsa.
- Vozoff, K., LeBrocq, K., Moss, D., Zile, M., and Pridmore, D., 1986, *Deep transient electromagnetic soundings for petroleum exploration*, Final Report to NERDDC, CGER, Macquarie University.
- Vozoff, K., 1991, *The magnetotelluric method*, in: Nabighian, M.N., (ed.), *Electromagnetic methods in applied Geophysics*, Vol. 2, Soc. Expl. Geophys., (in press).
- Wait, J.R., 1951a, *A conducting sphere in a time varying magnetic field*, Geophysics 16, 666–672.

- Wait, J.R., 1951b, *The basis of electrical prospecting methods employing time varying fields*, Ph. D. thesis University of Toronto.
- Wait, J.R., 1956, *Method of geophysical exploration* U.S. Patent No. 2,735,980 (To Newmont Mining Corporation, Feb. 21, 1956).
- Walker, R.C., Harthill, N., Strack, K.-M., and Lee, D.S., 1982, *Sensitivity analysis of transient electromagnetic sounding inversion*, 52nd annual meeting, Soc. Expl. Geophys.
- Walther, Ch., Trappe, H., and Meissner, R., 1986, *The detailed velocity structure of the Urach geothermal anomaly*, J. Geophys. 59, 1-10.
- Wannamaker, P.E., Hohmann, G.W., and San-Filipo, W.A., 1984, *Electromagnetic modelling of three-dimensional bodies in layered earths using integral equations*, Geophysics 49, 60-74.
- Ward, S.H., and Hohmann, G.W., 1988, *Electromagnetic theory for Geophysical applications*, in: Nabighian, M.N., (ed.), *Electromagnetic Methods in applied Geophysics*, Soc. Expl. Geophys., 131-311.
- Watt, T., and Bednar, J.B., 1983, *Role of alpha-trimmed mean in combining and analyzing common-depth-point gathers*, Expanded Abstracts, 53rd annual meeting, Soc. Expl. Geophys., 276-277.
- Weidelt, P., 1975, *Electromagnetic induction in three-dimensional structure*, J. Geophys. 41, 85-109.
- Weidelt, P., 1985, *Einführung in die elektromagnetische Tiefenforschung*, unpublished lecture notes, University of Braunschweig (in German).
- White, J.E., Martineau-Nicoletis, L., and Monash, C., 1983, *Measured anisotropy in Pierre Shale*, Geophys. Prosp. 31, 709-725.
- Wilhelm, H., Berkold, A., Bonjer, K.-P., Jäger, K., Stiefel, A., and Strack, K.-M., 1988, *Heat flow, electrical conductivity in the Black Forest crust, SW Germany*, special issue: *Lower crust properties and processes*, Am. Geophysical Union, 215-232.
- Wohlenberg, J., 1982, *Seismo-acoustic and geoelectric experiments within the Urach 3 borehole*, in: Haenel, R., (ed.), *The Urach geothermal project*, E. Schweizerbart'sche Verlagsbuchhandlung, 97-100.
- Woodall, R., 1984, *Success in mineral exploration*, Geoscience Canada II (1), 41-46, II (2), 83-90, II (3), 127-133.
- Yang, S., 1986, *A single apparent resistivity expression for long-offset transient electromagnetics*, Geophysics 51, 1291 - 1297.
- Yost, W.J., 1952, *The interpretation of electromagnetic reflection data in geophysical exploration - Part 1: General theory oscillating dipole*, Geophysics 17, 89-106.
- Yost, W.J., Caldwell, R.L., Beor, C.L., McChere, C.D., and Skomal, E.N., 1952, *The interpretation of electromagnetic reflection data in geophysical exploration Part II, metallic model experiments*, Geophysics 17, 806-826.
- Zhdanov, M.S., and Matusevich, V.Yu., 1984, *Restoration of the spatial pattern of wave propagation in an elastic medium*, Annales Geophysicae 2, 1-16.
- Ziegon, J.A., 1989, *Transient Elektromagnetische Tiefensondierung - Planung, Aufbau und Anwendung eines analogen Modells zur Unterstützung von 3-D - Interpretationen*, Diplom thesis - geophysics, University of Cologne, (unpublished).
- Zonge, K.L., Ostrander, A.G., and Emer, D.F., 1986, *Controlled source audio-frequency magnetotelluric measurements*, in: Vozoff, K. (ed), *Magnetotelluric Methods*, Soc. Expl. Geophys., 749 - 763.

The author explicit authorizes unrestricted use of this material as long
as proper reference is given.

KMS Technologies – KJT Enterprises Inc.
6420 Richmond Ave., Suite 610
Houston, Texas, 77057, USA
Tel: 713.532.8144

Please visit us
<http://www.kmstechnologies.com>

This material is not longer cover by copyright. The copyright was
released by Elsevier to Dr. Strack on November 5th, 2007.

The author explicit authorizes unrestricted use of this material as long
as proper reference is given.

KMS Technologies – KJT Enterprises Inc.

Appendix 6 Subject Index

extract from

Strack, K.-M., 1992, reprinted 1999
***Exploration with deep transient
electromagnetic:*** Elsevier, 373 pp.

This material is not longer cover by copyright. The copyright was released by Elsevier to Dr. Strack on November 5th, 2007.

The author explicit authorizes unrestricted use of this material as long as proper reference is given.

Appendix 6

Subject Index

A

- | | | | |
|---------------------------------------|----------------------------------|---|--|
| Aa | 12 | angular frequency | 25 |
| acquisition | 184 | anhydrite | 174 |
| - comments | 300 | anisotropic model | 16 |
| - procedure | 161 | anisotropy | 15, 16, 19, 307, 308 |
| - system | 70, 127, 136, 154, 165, 190, 300 | - coefficient | 16, 206 |
| - time | 171 | anomalous area | 44 |
| A/D converter | 141 | anomalous body | 109, 187 |
| A/D converter temperature drift | 49 | anomalous conductor | 117 |
| A/D offsets | 62 | anomalous fields | 110 |
| Africa | 247 | anomalous response | 109 |
| aftershocks | 276 | anomalous structure | 219 |
| airborne electromagnetics | 3 | anomalous transients | 215 |
| airborne TEM | 5 | anomalous zone | 112, 189 |
| aircraft generators | 133 | anomaly maps | 73 |
| all time apparent resistivity | 32, 33, 35, 36, 38, 40, 45, 46 | anthropogenic electromagnetic noise | 47 |
| alpha-trimmed mean | 58 | anthropogenic influence | 47 |
| Alpine orogen | 253 | apparent resistivity | 2, 21, 26-29, 31-33, 37, 38, 45, 187, 218, 270, 275 |
| Ampere's law | 24, 289 | - curve | 62, 65, 71, 72, 117, 143, 178-180, 207, 210, 307-309 |
| amplifier | 49, 129, 131, 140, 144, 155 | - formula | 32, 46 |
| - gains | 271 | - transforms | 69, 104 |
| amplitude | | Appollonian circle | 54 |
| -distortion | 57 | APRE | 314 |
| -response | 48, 57, 253, 259 | a priori information | 74, 83, 125, 173, 184, 186, 190, 246, 259, 266 |
| -spectra | 198 | a priori knowledge | 109 |
| AMT | 214 | aqueous fluids | 281 |
| analog | | Arapaho | 206 |
| - filter | 31, 120, 146, 161, 230 | Archie formation factor | 11 |
| - modeling | 307 | Archie's formula | 11, 12, 182, 238, 307 |
| - modeling classification | 107 | Archie's law | 20, 307 |
| - modeling experiment | 106 | area-defined rejection | 60, 61 |
| - notch filter | 70, 144, 258, 261, 309 | array dimension | 27 |
| - recordings | 284 | artificial noise | 182, 183 |
| - scale model | 105 | ASCII data | 298 |
| - transmission circuitry | 146 | Asia | 8, 19 |
| -to-digital converter | 140, 143 | asymptotic apparent resistivity | 45 |
| | | A-type | 41, 87 |

– curve	307
– model	88
– three-layer models	41
audio magnetotellurics	27, 214, 257
Australia	9, 19, 173, 184, 185, 190, 194, 225, 226, 227, 229, 235, 246, 309
average	
– predicted residual error	314
– quadratic deviation	76
– seismic velocity	245
– velocity	244
axial conductor	104, 105, 114

B

bandwidth	52–55, 57, 144–147
– limitations	144
basalt	100
– cover	227
base camp	150, 171
base frequency	254
base stack	163, 171, 309
base station	163–165, 167, 169, 171
base transient	171
Baxian Depression	192, 184, 190
Beijing	276
bentonite	152
Berkshire Park	214
Bessel function	25
best fit model	79, 83
BHP	208
bias control	143, 144
bias voltage	143
binary steps	131
Biot Savart's law	39, 65, 295
bipolar continuous waveform	133, 172, 307, 308
bipolar current waveforms	133
bipolar waveform	133, 307, 308
BIRPS	257
Black Box	48, 50
Black Forest	117, 119, 252, 256–265, 281, 283
blocked well log	242
BMFT	9
Bohai Gulf Basin	182
borehole	96, 195, 204, 209, 215
– information	204
– measurements	99
Brazil	192

bright spot	258
brine	3, 224
British Institutions Reflection Profiling Syndicate	257
broad-band artificial	161
building blocks	145
bulk porosity	190
bulk resistivity	20
Buntsandstein	196

C

Cabora Bassa	248
– power line	247
calibration	
– curve	4, 240
– factor	50, 62, 63, 65–67, 72, 117, 118, 157, 231, 251, 307, 315
– gear	155
– signal	155
– unit	130, 131
– well	119
Cambrian	240
Canadian Shield	249, 251
candidate models	250
Canning Basin	235, 236, 246
carbonate layer	183, 184
carbonates	4, 173, 182, 184, 192, 238, 240, 241, 244, 245,
carbonate unit	173
Carboniferous	196, 201, 203, 204, 226, 241, 244
card image header	300
case history	43, 99, 100, 165, 814, 193, 204, 225, 227, 229, 235, 240, 246, 247, 250, 251, 284
cementation factor	11
characteristic of noise	58
charge	229
– accumulation	228
– density	228
China	9, 167, 168, 171, 173, 182, 190, 227, 240, 246, 247, 251, 274, 277, 281–283
– survey	167
Chinese State Seismological Bureau	277
clastic sediments	182
clastic unit	238, 240
clay shales	212
clock drift	138, 153, 154, 158, 164, 165, 169
– measurement log	312
clock rate	136, 307

- clock trigger 154
- coal 11, 212
 - measures 213
- coefficient of anisotropy 17, 206, 307
- coincident loop TEM 225
- Cologne 193
- Colorado 205, 225
 - School of Mines 7, 19
 - – test area 193, 205
- compensated data 169
- complex plane 54
- complex structures 121
- component 125
- composition of rocks 12
- compressional-to-shear-wave velocity .. 263
- conductance 38, 109, 122, 200, 262, 279, 280, 307
 - referencing 199, 279, 307, 310
- conductive
 - bodies 118
 - dikes 187
 - patch 117, 120, 125
 - plate 121
 - targets 229
- conductivity 27, 33, 40
 - image 38
- conductor resistivity test 255
- conductor thickness test 255, 256
- confidence 232, 239, 255
 - bounds 76, 267, 314
 - envelope 37, 70
 - intervals 314
 - level 51, 145
 - limit 260
 - values 266
- confined bodies 121
- conglomerates 212
- consolidated sediments 11
- consolidated rocks 13
- continuity of the normal current density component 228
- continuous electric field measurement . 138, 158, 159
- contour map 201, 203, 241, 242
- contour sections 45
- control measurement 164–169
- control site 278, 279
- controlled source
 - EM 247
 - – methods 161, 247
 - – surveys 200
 - audio–frequency magnetotellurics 27, 89, 215, 308
 - electromagnetic methods 246
 - electromagnetic techniques .. 6, 21, 62, 241, 308
 - method 227
- convolution 48, 70, 156, 266, 285
 - of synthetic data 51
 - theorem 50, 52, 53, 285
- copper–copper sulphate electrodes 130
 - , non-polarizing 130, 229
- correction factor 66, 67
- correlated noise 162
- correlation matrix 314
- cost effectiveness 274
- costs per station 182
- Coulomb's law 24
- coupling effects 48
- covariance matrix 314
- CPU time 102, 122
- Cramer–Rao multipliers 314
- craton 271, 273, 274
- cratonic crust 268
- Cretaceous 196, 220, 243
- crustal applications 22, 145, 247
- crustal conductor 252
- crystal clock 128
- crystal oscillator 154
- crystalline environment 111
- crystalline basement 266
- crystalline overthrusting 227
- crystalline rock 20, 99, 255, 279, 282
- CSAMT 89, 215, 224, 308
- CSIR 9, 247
- CSIRO 208
- CSM test area 205–207
- cultural noise 68, 193, 204, 258, 259, 266, 308
 - sources 58
- cumulative conductance 174–176, 196, 308
- current 27, 62, 153, 172, 228, 230, 246, 250, 251, 253, 309
 - channeling . 62, 67, 71, 178, 230
 - controlled transmitter 156
 - density 24, 45, 228, 289, 294
 - – vector 65
 - filament 39, 40
 - flow 65, 117, 228

- image	39, 245	deep crustal transients	247
- reversal	133	deep drilling project	252
- step	270	deep exploration	7
- switching	172, 251, 309	deep geothermal applications	250
- waveform	49, 307, 308	deep reflection seismic	253
curve fitting process	183	deep transient	171
cyclic deposition process	15	- EM equipment	9
		- electromagnetics	1, 9, 45, 47
		- electromagnetic signals	68
		- electromagnetic sounding	
		method	2, 5, 124
		deeply weathered overburden	4, 19
		dehydration processes	282
		DEKORP	257
		delay time	304
		delta function	49
		DEMS I	8
		DEMS II	9
		DEMS III	208
		DEMS III	9
		DEMS IV	9, 129, 131, 132, 140, 144, 146-148, 172, 229, 270, 284, 300
		DEMS V	9
		Dendron	269
		Denver	206
		- Julesberg Basin	16, 205
		depth	
		- bounds	272
		- conversion	244, 245
		- of investigation	83, 89, 161, 274, 278
		- resolution	229
		- soundings	5
		- to the conductor	145
		- to-base	232
		Deutsches Kontinentales Reflektions-	
		seismik Programm	257
		deviation of mean	314
		Devonian	241, 253
		- Famenian	235
		diabase	184
		diapirism	4, 19
		dielectric constant	24, 26
		dielectric permittivity	289
		difference equation	26, 52-54
		diffusion	229
		- depth	38, 84, 119, 120
		- patterns	22
		- process	21, 22, 24, 45
		- speed	22
		- velocity	38
Dakota sandstone	206		
damped error multipliers	315		
damped multipliers	314		
damping factors of the original			
parameters	83, 232, 315		
damping factors of the transformed parameters			
80,	82		
damping factor	79, 80, 83, 287, 315, 316		
data acquisition	145, 173, 282		
- system	129, 131		
data			
- density	201		
- influence matrix	315		
- processing sequence	259		
- processing	127, 150, 169, 193, 210, 232, 247, 258		
- quality	161, 171		
- redundancy	258, 277		
- space	316		
DC			
- drifts	142, 271		
- level	69, 104, 142, 143, 272, 309		
- effect	142		
- monopole	65, 66		
- resistivity	3, 62, 247-250, 269, 270, 274, 281-283		
- resistivity methods	27		
- resistivity soundings	27, 229, 247		
- step	68		
- to AC converter	9		
Debye potentials	24, 289, 290		
deconvolution	50, 51, 68, 70, 72, 120, 133, 154, 156, 207, 216, 251, 286		
- effects	251		
deconvolved data	37, 45		
deep EM	310		
deep TEM research	250		
deep crust	247		
deep crustal problems	251		
deep crustal studies	4, 19, 140, 192, 247, 252, 283,		

- digital
 - data acquisition system 254
 - data processing techniques 128
 - electromagnetic system, IVth generation 8, 129, 132, 229
 - filters 54, 70, 141, 309
 - notch filter 57
 - processing techniques 71
 - recursive filter . 49, 52-57, 70, 259
 - telemetry 138
 - to-analog conversion 143
 - dike 114, 115
 - dipole 122, 207
 - equator 85
 - length 117
 - -dipole mapping 3, 138, 159
 - -sounding 229
 - direct presentation 37
 - discrepancy vector 78, 92, 287
 - displacement currents 26
 - distorted data 108
 - distorted responses 106
 - distorted signals 102, 108
 - distorted transient 103, 107, 109
 - distortions due to external influences 52, 53
 - DJ Basin 205, 226
 - DMT 9
 - dolerite 184-186, 190
 - dolomite 174
 - double peaks 247
 - double reversal 116
 - drift-induced offset 142
 - drift 144, 154, 163
 - dynamic range .. 27, 57, 76, 140, 141, 172, 270, 271, 284
 - limitation 139
 - dynamic resolution 254
- E**
- early stage transform 168
 - early time
 - amplitudes 222
 - apparent resistivity formulation . 187
 - apparent resistivity . 27, 28, 30, 37, 45, 46, 123, 199, 272
 - approximation 37
 - curves 251
 - depression 116
 - half-space voltage 29
 - resistivity curves 143
 - reversals 104
 - earth model 73, 75, 76, 96, 146
 - earth resistance 153
 - earth response, 39, 48, 104
 - earthed dipole 215
 - earthquake 275, 276, 283
 - prediction 251, 275, 284
 - ECORS 257
 - eigenparameter 232, 314-316
 - domain 232
 - eigenvalues 80, 82, 83
 - eigenvector 232, 287, 316
 - electric
 - and magnetic field data 233
 - component 85
 - current density 151
 - dipole 63
 - displacement 24, 289
 - fences 58
 - model 178
 - power line transients 70
 - railroads 204
 - receiver signal 15
 - transients 239, 240
 - electric field 15, 21, 26, 31, 39, 45, 46, 67, 86, 87, 130, 157, 158, 159, 183, 187, 189, 190, 192, 198, 202, 228, 229, 231, 232, 234, 244, 246, 249, 289
 - component 16, 24, 72, 85, 128, 178, 184, 243, 289
 - data 183, 234, 238
 - intensity 24
 - interpretation 184
 - inversion 233
 - joint inversion 159
 - measurements 67, 71, 201, 227, 229, 249, 250
 - parallel to the wire 30
 - perpendicular to the wire 31
 - response 116, 87
 - sensors 25, 128
 - strength 23
 - transient 187, 199, 231, 249
 - electrical
 - anisotropy 14, 16, 20, 308
 - charges 228
 - conductivity 9, 24
 - coupling 117
 - fences 261
 - field strength 21
 - log 176, 185
 - methods 26, 27

- properties of rocks 9
 - resistivity 9, 18
 - section 183
 - electrode ... 117, 118, 151, 153, 156, 159, 172, 210
 - plants 156
 - plates 172
 - sites 152
 - electromagnetic
 - data 9, 37, 74, 80
 - depth sounding method 309
 - field 26, 83, 116, 293, 309
 - components 30, 201
 - equations 24
 - interference 309
 - measurements 138
 - methods 2, 26, 27, 75, 227, 247, 297
 - noise 47, 131, 179, 210, 310
 - reflections 26
 - response 128
 - soundings 229
 - surface method 174
 - technique ... 19, 125, 127, 277, 310
 - theory, 138
 - waves 76
 - electromagnetics 2, 4, 6, 67, 309, 310
 - electromechanical switchbox 133, 134
 - embedded conductor 120
 - EM
 - data 240
 - depth soundings 263
 - field data 73
 - fields 37, 161
 - measurements 138, 226, 283
 - method 161, 227
 - noise 277
 - sounding data 73
 - techniques 182, 227
 - EM37 7, 308
 - energy 228
 - environmental concerns 152
 - epicentres 281
 - equator of the dipole transmitter .. 109, 230
 - equivalence 308
 - equivalent loop 278
 - equivalent resistivities 173
 - error
 - bar .. 37, 78, 79, 99, 98, 145, 168, 199, 259, 260, 272, 279
 - bounds 79, 255
 - ellipse 273
 - estimate 84
 - function 28
 - propagation 76
 - ridge trace 79
 - statistics 231
 - vector 77
 - estimated model 79
 - Etude Continentale et Oceanique par Reflexion et Refraction Seismique . 257
 - Europe .. 93, 100, 229, 233, 246, 247, 257, 281, 183
 - European Community 9
 - exploration depth 27
 - exploration
 - environment 183
 - geophysicist 10
 - problems 182
 - strategy 184
 - target 190
 - task 184
 - explorationist 19
 - external magnetic field 49
 - external noise 146, 163
 - external potential 295
 - extreme topography 4, 19
- ## F
- Faraday's law 24, 289
 - fast digital filters 116
 - fault 91
 - zones 187
 - feasibility study ... 173, 176, 179, 182, 186, 187, 189, 190, 315
 - field
 - array 110
 - behaviors 38
 - data 116
 - gradients 123
 - layouts 38
 - procedures 10, 127, 151
 - survey productive 156
 - system 154, 227
 - techniques 10
 - file header 300
 - filter bandwidth 57
 - filter coefficients 54
 - filter effects 120
 - filter response function 54
 - finite difference program 121
 - finite difference scheme 116, 123

- finite element method 116
 - fitting error 255, 273, 314
 - Flambeau anomaly 249
 - flux gate magnetometers 130
 - formation 12
 - factor 11
 - water 11
 - forward calculations 116
 - forward modeling 74, 75, 96, 123, 174, 176, 181, 184, 190, 216, 219, 222, 242–245, 270, 271
 - Fourier components 290
 - Fourier transform 52, 53, 64
 - four-layer model 33
 - Foxhills 206
 - France 8
 - frequency 26, 27, 87, 161
 - deconvolution 50
 - domain 6, 72
 - – deconvolution 51, 70
 - – EM system 49
 - – methods 27
 - – primary field 6
 - – soundings 27
 - – system 20
 - response 49, 54
 - – wavenumber domain 291
 - FRG 192
 - fudge factor 62
- G**
- gain 178
 - amplifier 141
 - factors 131
 - , improper definition of 62
 - ranging 140
 - galvanic part 228
 - galvanic source systems 215
 - Gauss–Newton 76
 - generator 128, 133–135, 153, 161
 - power 127, 158
 - geoelectric 173
 - boundaries 21
 - data presentation 225
 - mapping 173, 176
 - model 205
 - properties 246
 - sections 205, 206
 - – geologic cross section 14
 - geologic age 196
 - geologic boundaries 161
 - geologic noise 236
 - geological 181
 - cross section 213
 - meaning 196, 200
 - section 49, 107
 - strata 177
 - structure 37, 47, 74, 79, 91, 99, 100, 104, 111, 116, 140, 146, 162, 173, 190, 191, 193, 196, 204, 205, 209, 215, 222, 224, 229, 241, 261, 264, 268
 - target 7
 - Geopacific Resources 181
 - geophysical appearance 79
 - geophysical data 193
 - geophysical techniques 11, 79
 - geophysicist 282
 - geothermal gradient 9
 - German 240
 - Ministry for Research and Technology 9
 - TEM Pilot–Demonstration Project 240
 - deep drilling project 251, 252
 - deep transient EM systems 251
 - railroad power grid 56
 - Germany 9, 19, 57, 59, 68, 89, 95, 101, 107, 109, 133, 134, 145, 152, 164, 165, 193, 225, 254
 - Gibb's phenomenon 57
 - global minimum 78
 - gneisses 206, 266
 - gradual resistivity increase 90
 - granites 206
 - graphite 282
 - gravity 2, 4, 309
 - Greta coal measures 213, 214
 - grounded 229
 - dipole transmitter 228
 - electrical dipole 23, 45, 65, 117
 - wire dipole 117
 - wire TEM 15, 21, 23, 128
 - Group Seven 7, 19, 205
- H**
- half-space 21–24, 26, 27, 32, 34, 35, 40, 45, 46, 63, 65, 104, 116, 117, 228, 262, 272
 - resistivity 45
 - response 16, 105

- reversal 116
- interpretation 73, 83, 88, 91, 100, 102, 104, 124, 125, 127, 147, 150, 159, 168, 171, 187, 196, 201, 213, 224, 245, 249, 254, 255, 257, 261, 264, 282-284
- process 183
- team 11
- workstation 150
- interpreter 11, 104
- interval conductivity 39
- interval image 42, 46
- interval resistivity image 41, 42
- interval resistivity 37-39, 42
- inverse modeling 74, 75
- inverse resistivity 38
- inversion ... 51, 70, 73-76, 79, 82 84, 88-94, 99-102, 118, 121, 124-126, 212, 214, 215, 219, 226, 231, 237, 244, 245, 250, 251, 254, 259, 261, 266, 267, 279, 280, 282, 308, 314, 315
- parameters 287
- process 67
- result 200, 201, 212, 230
- stability 79
- starting model 210
- statistics .. 73, 79, 81, 83, 199, 245, 279, 314
- with hard bounds 91
- with soft bounds 91
- ionospheric currents 49
- IP 225
- iteration model 74
- iterative deconvolution 285

J

- Jacobian (sensitivity) matrix 77, 84, 92, 126, 232, 233, 287, 315, 316
- jagged structures 99
- Japan 190
- Jiangsu province 240
- joint inversion 83-90, 126, 138, 184, 215, 238, 239, 246, 282, 308, 315
- Jurassic 206
- sediments 253

K

- K-type 41
- curve 308
- model 41, 46, 84
- synthetic data 86
- three-layer models 41
- Kaapvaal craton 268, 174, 283, 284

- Kronecker symbol 78
- Kurrajong Heights 214

L

- Lagrange multiplier 100
- laminated lower crust 258, 263
- Lamontagne Geophysics Ltd. 310
- land techniques 3
- Laramie 206
- large loop EM methods 228
- late apparent resistivity formula 45, 199
- lateral effects 160
- lateral inhomogeneities 50, 62, 71, 111
- lateral moveout 228
- lateral resistivity variations ... 47, 141, 149, 159, 279
- laterally inhomogeneous conductive plate 109
- laterolog 90
- late time
 - apparent resistivity . 27-30, 37, 46, 244, 251, 272
 - - transforms 103
 - approximation 37
 - half-space voltage 29
 - resistivity 251
 - - curves 143
 - - transform 267
 - reversal 104- 106
- Latin America 8
- laundry detergent 152
- layer-cake 15, 76, 174, 175, 308, 310
- layered
 - earth model 26, 65, 118
 - earth structures 102
 - earth . 24, 43, 45, 64, 75, 103, 104, 113, 120
 - half-space 122
 - quarter-spaces 121
- layer equivalence 308
- layer equivalencing 174, 176, 190
- leapfrogging technique 159
- lightening 58
- lime 152, 172
- limestone 12, 174, 195, 196, 206, 235, 242-245
- Limpopo Belt 268, 274, 282, 283
- LNC application 170
- LNC technique ... 158, 162, 165, 166, 168, 170, 171, 308
- line characteristics 68
- linear digital filters 52, 53

- linear drift 198
 - linearized inversion 88
 - LNPF 161
 - lithological boundaries 191
 - lithological parameters 183
 - lithology 12, 78, 174, 176, 210, 235, 282
 - local minimum 78
 - local noise compensation technique 49, 149, 158, 161, 172, 277, 308
 - local noise prediction filtering 161
 - local structure 280
 - lockin filter 57, 68
 - log resistivities 266
 - logarithmic domain 198
 - logarithmic parameters 76, 126
 - logarithmic transforms 146
 - long offset transient electromagnetic sounding system 128
 - long offset transient electromagnetics 128, 161, 309
 - long-spread reflection survey 266
 - longitudinal direction 14
 - longitudinal resistivity 15, 16, 309
 - Long Offset Transient EM 7
 - Long Offset Transient Electromagnetics 5, 21
 - LOPIS 297, 298
 - LOPS 298, 300, 304
 - LOTEm 5, 7, 9, 10, 15–17, 20, 21, 22, 27, 31, 32, 100, 104, 111, 116, 117, 127–132, 134, 145, 150, 151, 155, 161, 162, 172–179, 182–197, 201, 204, 205, 207–210, 212–216, 219, 222, 224–230, 233, 236, 237, 240–247, 250–254, 256, 258, 262–269, 272–285, 290, 295, 297, 308, 309, 314
 - electric field 250
 - field system 172
 - forward modeling 176
 - image section 245
 - magnetic field 250
 - method 16
 - processing and interpretation 16
 - system 297
 - sounding method 281
 - soundings 60
 - survey 241
 - low cut filters 142
 - lower crust 247, 257
 - lower crustal conductor 283
 - low frequency noise 70
 - low pass filtering 169
 - low-velocity anomalous region 266, 281
 - low-velocity channel 257
 - low-velocity zone 263, 281, 283
- M**
- Macquarie University 208
 - magnetic
 - component 15, 24, 159, 238
 - data 183, 238
 - field 24, 26, 32, 33–35, 38–40, 45, 65, 67, 87, 89, 94, 126, 130, 138, 142, 159, 172, 187, 189, 190, 198, 202, 217–219, 228, 229, 231, 233, 234, 246, 289
 - field component 72, 85, 138, 158, 161, 243
 - field derivative 15, 16, 244
 - field joint inversion 159
 - field measurements 15, 201
 - field receiver 270
 - field response 244
 - field sensors 128, 157
 - field transient 187, 199, 231, 249, 284
 - induction 24, 289
 - permeability 289
 - response 232, 233
 - transient data 238–240
 - magnetics 2, 4, 309
 - magnetometers 229
 - magnetometric resistivity 62
 - magnetotelluric data 83, 182–184
 - magnetotelluric measurements 241, 264
 - magnetotelluric method 161
 - magnetotellurics 6, 19, 27, 62, 83, 186, 190, 215, 252, 257, 263, 265, 309
 - main amplifier 229
 - maintenance 149
 - mapping of porosity variations 4
 - marine sediments 209
 - Marl 195
 - Marquardt algorithm 215
 - Marquardt–Levenberg method 79, 82, 83, 126
 - Marquardt solution 100
 - Marquardt type inversion 100, 271
 - massive sulphide mineralization 5
 - master clock 138
 - material equations 288
 - Maxwell's equations 2, 24, 45, 288, 289

- measured voltage 27, 29, 45, 64
 - median stacking technique 271, 272
 - megasource 249, 250
 - TEM 250
 - Mesozoic 264, 266
 - metallic sulphides 282
 - metamorphosed sedimentary rocks 12
 - Metronix GmbH 9
 - MHD generators 247
 - microprocessor 143
 - Middle East 8
 - mid-time depressions 104
 - mid-time reversal 104, 105
 - migration 44
 - Milford Valley 104-107, 113-115
 - mineral exploration 5
 - minimum depth of investigation 258
 - minimum model 99
 - minimum thickness test 262
 - mining applications 5
 - mining industry 189
 - misalignment errors of the receiver 49
 - MMR 62
 - correction 50
 - mobile
 - processing center 150
 - processing systems 150
 - receiver station 168, 171
 - site 169
 - stations 163, 171
 - model
 - function 74, 75, 77, 78
 - parameters 74, 81
 - resolution 232
 - response 38
 - setup 113
 - moment 283
 - Monte Carlo inversion 250
 - MPPO-1 5
 - MT 6, 67, 84-89, 161, 162, 186, 190, 215, 216, 224, 228, 259, 262, 279, 282, 309
 - soundings 186
 - Münsterland 88, 193
 - area 225, 226
 - basin 215
 - multi-dimensional modeling 45, 76
 - multichannel
 - acquisition systems 129, 172
 - field procedures 160
 - measurements 148
 - procedures 172
 - processing techniques 127
 - remote units 131
 - system 49, 127, 139, 158, 165, 171
 - transient EM system 138, 139
 - multifold reflection data 266
 - multiple images 39
 - multitasking 150
 - multiturn loops 229
- N**
- Napier formation 235
 - Narrabeen Group 213
 - natural
 - electromagnetic fields 247
 - electromagnetic noise 178
 - noise 161
 - noise sources 58
 - source electromagnetic methods 246
 - near-surface lateral resistivity inhomogeneities 47, 49
 - near-surface anomalous zones 222
 - near-surface conductor 217
 - Negro Mag Fault 105, 113
 - New South Wales 208
 - Newton-Raphson method 34
 - noise 83, 84, 91, 144-146, 149, 161, 163-165, 171, 178, 184, 207, 259, 262, 278, 279, 308, 309
 - cancellation technique 148, 162
 - characteristic 162, 259
 - compensation 49, 138, 165, 170, 193, 282
 - frequencies 231
 - interference 144
 - limitations 144
 - processing 148
 - reduction 161, 169, 172
 - -compensated signal 163
 - -free signal 171
 - -free synthetic input signal 56
 - -to-signal ratio 315
 - noisy field data 182
 - non-recursive filter 52, 53
 - nonseismic techniques 2, 4, 309
 - normal fields 110
 - normalized
 - Jacobian 234
 - damping parameter 81

- eigenvalue	81
- singular value	315
- spectral value	315
Northern Ireland	8
notch filter	49, 50, 54, 56, 68, 258
notch frequency	54
number of effective parameters ...	83, 315
number of iterations	78, 316
number of stacks	178
NSR	315
Nyquist frequency	54, 70

O

Oberpfalz	252, 254, 256, 261, 281, 283, 284
Occam inversion	73, 99-102, 124, 125, 147-149, 196, 197
Occam model	100
off-time	247, 308, 309
offset	16, 21, 25, 27, 35, 66, 105, 141, 173, 178, 181, 190, 192, 249, 258, 270, 272, 309,
Ogallala	206
oil and gas pool systems	182
oil exploration	6, 121
oil field	229, 233
oil shales	212
oil-water contact	3, 19
1-D interpretation	44
1-D inversion	73
1-D source imaging	44
onset-reversal	103
onset	103, 304
operational amplifiers	144
optimum survey layout	182
optimum survey strategy	182
optimum transmitter-receiver offset ...	182
original parameters	83, 87, 126
orthonormal data space eigenvectors ...	287
orthonormal data space	81
oscillator clocks	229
outliers	70
output signal	47
overinterpretation	99
overshoot	40-42
overthrust	4, 19, 192

P

Pacific North-West	252
Pahoehoe	12

Paleozoic	264, 266
parameter	
- bounds	97
- combinations	82
- difference vector	77, 92, 287
- influence matrix	315
- resolution	80
- space	81, 287, 316
- vector	78, 84
- weights	92
parametric inversion	231
passive EM techniques	227, 247
Pennsylvanian	206
Peoples Republic of China	167
percentage sandstone	238-240
periodic noise	48, 49, 52, 53, 57, 68-70, 164, 170, 198, 253, 259, 309
permafrost	3, 19
Permian	196, 206, 213, 241, 242, 244, 253
petroleum exploration	21
petrophysical behavior	11
phase and amplitude preserving digital recursive filter	52, 53
phase curves	27
phase shifts	55
phase-correlated	57
physical background	21, 127, 228
physical parameter	76, 314, 315, 316
physical properties of rocks ..	10, 227, 247
Pierre Shale	206
Pietersburg	269
pipeline	102, 107, 230, 309
- response	116, 230
Poisson's ratio	263, 281, 282
polarity	116
- reversals	49
- reversing transmitter	49, 308
polarization	230
- effects near the electrodes	49
pole-zero technique	54
poles and zeroes	54, 70
poloidal density	289
poloidal mode	289
poloidal potentials	24
pore fluid	12, 14
porosity	4, 11, 12, 20, 184, 235, 238, 240, 244, 246
- maps	4
- predictions	182
- variation	11, 19, 184, 190, 192

- variations 238
- portable system 9
- poststack 57, 58, 68 - 71
 - filtered data 70
 - processing 68, 69, 103
- postvolcanic gas exhalations 282
- potassium 152, 172
- potential theory 24
- power consumers 49
- power line 49, 70, 108, 161, 204, 219, 241
 - noise 254, 258
- power network 49
- PRBS 49, 309
- PRC 243, 277, 278
- preamplifier 49, 129-131, 140, 144, 155, 229
- precursor 275
- prestack 47, 57, 68, 69, 210
 - filtered data 70
 - filtering 166, 258
 - processing 9, 68, 71, 166, 254, 271
- presurvey feasibility study 17, 182
- pretrigger 136, 304
- primary field 6
- processing 91, 145, 171, 184, 208
 - comments 300
 - sequence 253
 - steps 231
 - theory 11
 - time 144, 171
- production mode 182
- production problems 182
- profile inversion 73, 91-99, 125, 126
- pseudo random binary sequence .. 49, 309
- pseudo-sections 37
- pseudo-static 67
- P-wave velocity 281, 282

Q

- quality control 127, 150, 171, 198, 229, 231, 259
- quasi-stationary Maxwell equations 24, 288
- Q-type 41, 46, 88
 - curve 309
 - three-layer models 41
- Quaternary 253

R

- railroad 70, 108
 - grids 161
- power grid noise. 57
- tracks 102, 107, 219
- ramp function 49
- ramp time 133, 154, 156, 309
- random access file 298
- raw field data 169, 171, 182, 198, 254, 258
- raw records 253
- raw signals 198
- raw transient 231
- real time quality control 129
- receiver .. 9, 22, 27, 45, 79, 105, 109-112, 117, 121, 125, 128, 131, 135, 141, 146, 148, 156-159, 161, 165, 167, 171, 173, 178, 183, 196, 205, 207, 210, 212, 217, 229, 230, 249, 253, 259, 261, 266, 270, 309, 310
 - analog filter effects 258
 - area 62
 - coil 165, 179, 181
 - filters 47
 - gain 278
 - location 187
 - misalignment 50, 62
 - misorientation 48
 - moments 192
 - setup 22, 162
 - site 21, 40, 150, 165, 182
 - system 127, 129, 171, 172
- reciprocal modified impedances ... 25, 292
- record 68
 - pointer 298, 299
- recording system 154
- recording time 230
- rectifier-current-switch assembly 128
- recursion formulae 45
- recursive filter . 52, 53, 55, 57, 58, 70, 231
- reduced model 174
- reduced well log 90
- reference level 103, 143
- reference zero level 102
- referencing 200
- refection
 - coefficient 294
 - seismic data 240, 263
 - seismic sections 263
 - seismic surveys 235
 - seismic ... 204, 227, 257, 264, 309
- reflections of the electromagnetic waves 6
- reflectors 241, 245
- refraction seismic 257, 264
- regional noise 165

regional velocity gradient	264	Ruhr District	193, 204
regression	73	S	
rejection criteria	70	safety devices	127, 133
relative error	84	safety interlocks	136
remote clocks	135	saline connate water	3
remote operations	151	saline water	281
remote unit	9, 138, 146, 149, 154, 160	salinity	12, 240
remote-reference technique	49, 161	salt	152, 172
removable hard disk	9	— concentration	12, 14, 20
repeatability	277, 279	— sediment boundary	99
repetition rate	133, 307, 309	sampling rate	230
resistive fault zones	125	sand-to-shale ratio	4, 20, 230, 238, 240, 246
resistive medium	40	sandstone	12, 20, 174, 184, 206, 212
resistive targets	229	— target	181
resistivity	11, 14, 16, 26, 40, 233	satellite clocks	135
— anisotropy	15	scalar potential	24, 45, 290
— anomaly	275	scale factor	61, 67, 71, 316
— contrast	22, 38, 45	Schlumberger soundings	274
— depth section	145, 280	screening layer	229
— image	38	SEAMEX	9
— of the formation	11	secondary field	6
— of the pore fluid	11	secondary signal	6
— range	11	sedimentary	
— section	97	— areas	76, 254
— structure	21, 41, 125	— basin	79, 93, 220
— test	262	— cover	266
— transform	31, 70, 104, 111, 115, 146, 148, 168, 199, 266	— environment	91, 110, 111, 117, 124, 125, 152, 158, 308
— variations	19	— rocks	12, 282
resolution	81, 240, 243	sedimentation process	15
— analysis	174, 227, 231, 234, 245	sediments	15, 99, 100, 192
— criteria	84	SEG Y standard	297, 300, 305
— limit	271	seismic	
— statistics	190	— cable	130
— study	183, 184	— data	240, 245, 297
— threshold	140	— distortion	310
reverberation of the seismic waves	4	— field procedures	160
reversal	44, 73, 102–104, 108–112, 116, 122, 125, 126, 219, 230, 249, 284, 309	— industry	128
Rheinisches Schiefergebirge	193	— information	238, 239, 242
Rhine–Ruhr industrial district	165	— interpretation	174, 213, 261
ringing effects	57	— line	184, 241, 264
rock failure	275	— mapping	238
rock resistivity	12	— modeling	263
rock type	11, 12	— reflection line	197
roll along technique	160	— reflection pattern	269
roll over time	104	— reflection profile	269
roughness	100	— reflection	252
Ruhr Area	225	— reflector	213, 245
		— section	138, 172, 182–184, 186, 196, 235, 237, 240, 241, 245, 257, 258

- survey 172, 257, 263,
- systems 138
- technology 141
- velocities 3
- seismically laminated zone 257
- seismics . 37, 127, 184, 186, 190, 195, 227, 246, 265, 310
- selective stack 60, 69, 258
- selective stacking algorithm 61, 62, 70, 199
- selective stacking methods 58
- selective stacking . 48, 68-70, 168, 170, 171
- selectively stacked transient 51, 163, 259, 278
- sensitivity 125, 233, 234, 246, 314
 - analysis 77
 - matrix 315
 - study 176, 177
- sensor 131, 144, 146
- shale 174, 206, 212
- shallow TEM soundings 186
- Shoalhaven Group below 213
- sign reversal 43, 187, 216, 217, 225
- signal
 - drifts 139
 - level 181
 - transmission line 130
 - to-noise improvements 47, 127, 148
 - to-noise limitations 139
 - to-noise ratio . 27, 47, 49, 51, 59-61, 68, 70, 71, 102, 127, 128, 145, 158, 161, 172, 198, 204, 230, 245, 258, 259, 278
- siltstones 243
- simplest model 231
- single channel processing 139
- single record 57, 171
- single site processed data 148
- single site system . 129, 131, 139, 144, 148, 158, 159
- singular value 232, 315, 316
 - decomposition . 79, 80, 287, 316
- SIROTEM 5, 7, 214, 215, 309
- skin depth 27, 84
- slave clock 138
- SLDM 116, 121-124, 223
 - program 187, 222
- slowness 38, 40
- small bipole 21
- smoke ring 23
 - concept 21, 45, 228
- smooth inversion algorithm 196
- smooth model 99
- smooth resistivity versus depth function 124
- smoothing and stacking 169
- SMZ 268, 274
- S/N ratios 264
- SQUID magnetometers 62, 207
- soft bounds 94, 95, 98
- soldering joint 105
- soundings 91, 93, 189, 193, 200
- source currents 192
- source image conductivity 39
- source image 39, 40-44, 46, 246
- source moment 133, 281
- sources of noise 48
- South Africa 9, 19, 57, 268, 281-283
- Southern Germany 253
- Southern Marginal Zone 268, 283
- Soviet Union 7, 37, 247
- sparse data 138
- spectral Lanczos decomposition
 - method 116, 121, 122, 124
- spectral values 315
- spherics 161
- spike 49, 58, 59, 70, 107, 310
 - detector 58
- spitter 157, 310
- split spread configuration 160
- sporadic noise . 48, 49, 58, 60, 70, 164, 170, 171, 231, 310
- spread 160
- square wave current 128
- square wave signal 131
- stability 79
- stack 249
- stacked data 279
- stacked signals 278
- stacked transient 103, 167, 170, 278
- stacking 76, 271, 282
 - algorithms 72
 - methods 61
 - technique 60, 161
 - velocities 245, 266
- standard average 72
- standard deviations 77, 84, 314, 316
- standard geothermal gradient 20
- standard inversion 91
- starting model . 83, 85, 87, 93-95, 97, 196, 212, 219, 231, 233, 254, 316

- three-dimensional geology 99
- three-dimensional modeling 124
- three-dimensional structure 89, 104
- 3-D
 - algorithms 73
 - anomaly 217
 - data 121
 - distortions 310
 - effect 200, 215, 219, 222, 224, 225, 249, 250, 274
 - interpretation 188, 193
 - model 43, 44, 112
 - modeling 73, 121, 189
 - response 112, 116, 118, 120
 - simulations 122
 - structure ... 38, 39, 43, 44, 47, 49, 51, 67, 68, 73, 76, 82-89, 91, 159
- three-layer earth 30
- three-layer model 35, 40, 41
- threshold value 82, 100
- Tiangjin 276
- tidal forces 275
- time derivative of the vertical magnetic field .. 21, 109, 128, 187, 199, 193, 232
- Time Domain ElectroMagnetics 310
- time domain ... 6, 72, 116, 286, 296, 310
 - methods 27
 - signal 6
 - system 20
- time window 173, 179, 181, 182
- time-frequency equivalent 50, 64
- time-variant Hanning window 271
- timing marker 283
- timing markers 248
- TM mode 25, 289
- toroidal mode 289
- toroidal current density 289
- toroidal potentials 24
- total conductance .. 38, 174, 175, 307, 308, 310
- total magnetic field 218
- trace header 304, 305
- traces 245
- tracing layer 94
- trains 58
- transform domain 285, 286
- transformation matrix 232
- transformed parameters ... 81, 83, 87, 126, 316
- transient 54, 102, 103, 107, 115, 125, 128, 140, 142, 144, 154-156, 162, 163, 168, 171, 187, 210, 212, 229, 231, 247-249, 253, 254, 258, 259, 271, 278, 283, 285, 298, 299
 - data 143
 - electromagnetics .. 6, 7, 19, 21, 116, 249, 286, 310
 - electromagnetic
 - data 45, 297
 - fields 21
 - method 7, 21
 - sounding systems 171
 - soundings 125
 - EM 37, 227, 249, 297, 308
 - field system 5
 - methods 27, 161
 - sounding 310
 - system 7, 138, 309
 - techniques 3
 - leader 68
 - response 122, 187, 188
 - signal 70
 - sounding 249, 251
 - trailer 68
- transmitter 22, 25, 27, 35, 45, 46, 71, 105, 109, 112, 117, 118, 120-122, 125, 127, 128, 133, 135, 138, 141, 151, 153, 155-157, 160-162, 171-173, 178, 193, 194, 200, 210, 215, 217, 229-234, 241, 252, 258, 261, 265, 270, 278, 281, 283, 297, 308-310
 - clocks 158
 - control sheet 153
 - current ... 127, 158, 217, 284, 309
 - dipole 21, 39, 210
 - moment 25
 - electrodes 133
 - moment 49, 278
 - overprints .. 47, 116, 117, 126, 200, 231, 241, 251, 261
 - record sheet 313
 - setup 22
 - site 21
 - switching 68, 247
 - system 127, 129, 133, 172
 - waveform 47, 48, 271
 - wire 156, 157
 - receiver offset 178
 - receiver separation 65
- transverse
 - electric (TE) mode 24
 - magnetic (TM) mode 24

- resistance	175, 200,	310
- - referencing		310
- resistivity		15
Triassic	196, 213, 240-245,	253
true		
- amplitude filters		254
- amplitude notch filter		57
- amplitude recursive filters	52,	53
- signal		49
- system response		49
tuff		12, 212
Turkey		8
two-dimensional section		188
2-D interpretation		188
2.5-D model		121
two-layer earth model	23,	24
two-layer model		22,
	32, 34, 35, 40	
typical field setup		128

U

U-matrix		316
unconsolidated sediments		11
unconsolidated rocks		13
unconstraint inversion		202
undamped parameter		92
undershoot		33
unit circle		54
United States		225
University of Cologne	9, 165,	193
University of Toronto		310
- EM system	7,	310
Urach	264, 265, 267,	282
- Geothermal Area	252, 264, 265,	281,
	283	
USA	8, 192, 205, 281,	283
USSR		247
Utah		104, 114
UTEM	7, 214, 215,	310

V

vacuum permeability		24
valley fill		117
van Cittert iteration	50, 285,	286
vertical		
- component of the electric field		228
- current flow		15

- current loops		289
- electric field		63
- magnetic field	30, 63, 65,	192
- resistivity,		17
- shift		66
- stacks		160
vibroseis		309
V-matrix		316
volcanic covers	4, 19,	192
volcanic material		240
volcanic rocks	12,	152
voltage		27
- - current relationship		26
- response	33-35,	270

W

walkaway profile		126, 178
walkaway test	178, 230, 242, 278,	310
water pumps		58
water saturation		240
wave equation		26
wave number		25
WBK		9
weakly-cemented detrital rocks		12
weighting matrix	77, 80, 84, 287,	288
weights	84, 92, 94, 98,	259
well completion report		212, 213
well log	16, 17, 74, 83, 89-92,	94,
	173-176, 183, 184, 190, 191, 193, 195,	
	196, 201, 202, 205, 214, 215, 233, 237,	
	239, 240, 242, 266	
- reduction		96
well-cemented sediments		20
Wenner arrays		275
Windjana / Nullara limestone		235
wind noise		165, 169

Y

Yangtze and Huabei paraplatforms		240
----------------------------------	--	-----

Z

z-domain		50
Zechstein	196, 202,	226
Zimbabwe craton		268
Zonge GDP 12		229
z-plane		55
z-transform	52, 53,	310

KMS Technologies – KJT Enterprises Inc.
6420 Richmond Ave., Suite 610
Houston, Texas, 77057, USA
Tel: 713.532.8144

Please visit us
<http://www.kmstechnologies.com>

This material is not longer cover by copyright. The copyright was released by Elsevier to Dr. Strack on November 5th, 2007.

The author explicit authorizes unrestricted use of this material as long as proper reference is given.

KMS Technologies – KJT Enterprises Inc.

Appendix 7 Color Figures

extract from

Strack, K.-M., 1992, reprinted 1999
***Exploration with deep transient
electromagnetic:*** Elsevier, 373 pp.

This material is not longer cover by copyright. The copyright was released by Elsevier to Dr. Strack on November 5th, 2007.

The author explicit authorizes unrestricted use of this material as long as proper reference is given.

Appendix 7

Color Figures

Following are the descriptions for the figures on the next two pages.

Fig.A7.1 Example of colour resistivity sections derived with *Occam inversion*. The top section shows the display of the inversion results as they are output. The center frame shows the same data after filtering it with a lowpass filter with a width of half of the total depth. This filter is applied horizontally. For the bottom frame only every third data set was used simulating sparse measurements.

Fig.A7.2 Comparison of different inversions using single sets of the synthetic data. On the left column the starting model was without the resistive unit, on the right column the resistive unit was included from the beginning on. Both layer thickness and layer resistivity were allowed to vary during the fitting procedure.

Fig.A7.3 Comparison of different inversions using single sets of the synthetic data. On the left column the starting model was without the resistive unit, on the right column the resistive unit was included from the beginning on. The layer resistivities were allowed to vary during the fitting procedure, while the layer thicknesses were forced to stay at the preset values. This simulates the use of a priori information from seismics.

Fig.A7.4 Comparison of different *joint inversions* using combinations of the synthetic data sets for increased resolution. On the left column the starting model was without the resistive unit, on the right column the resistive unit was included from the beginning on. The layer resistivities were allowed to vary during the fitting procedure, while the layer thicknesses were forced to stay at the preset values. This simulates the use of a priori information from seismics.

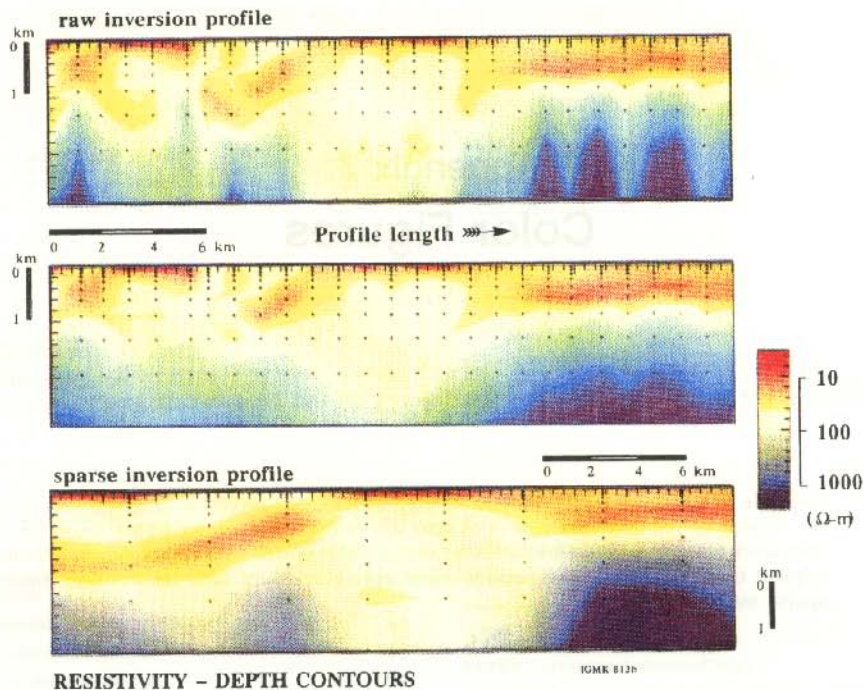


Fig.A7.1

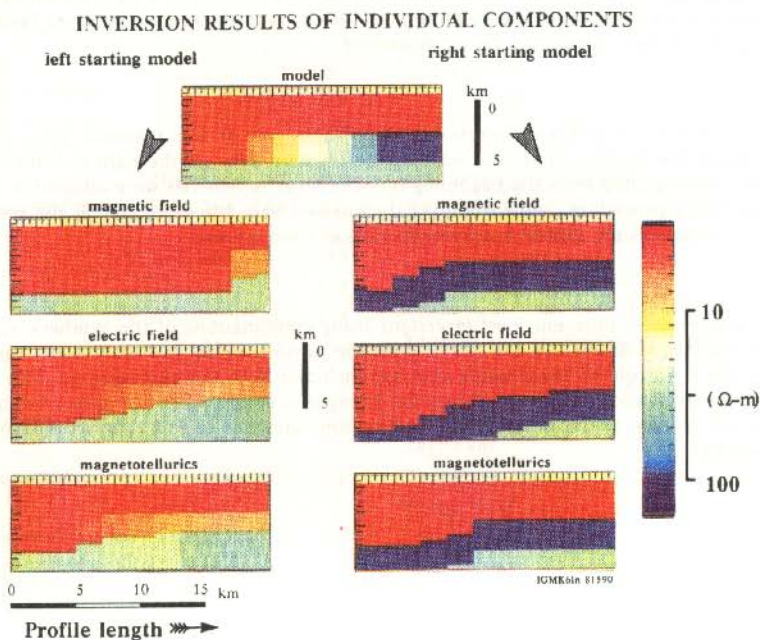
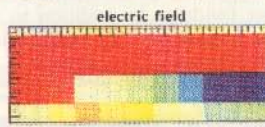
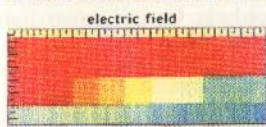
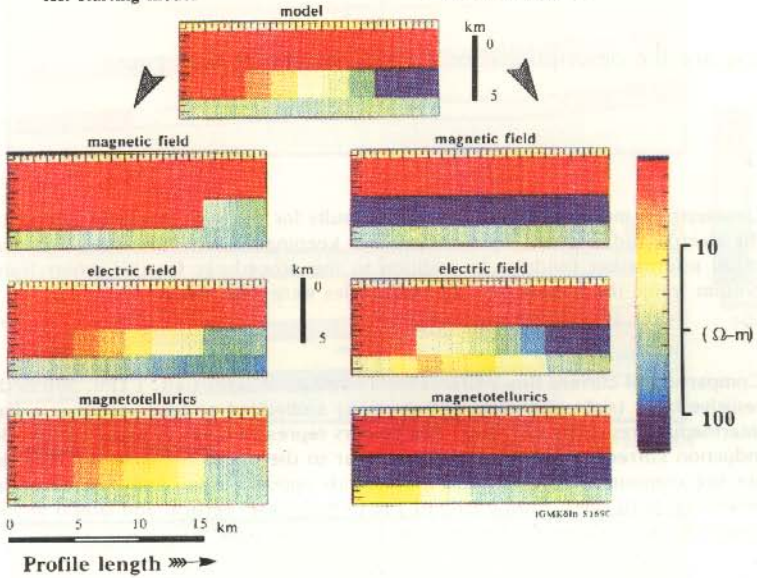
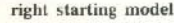
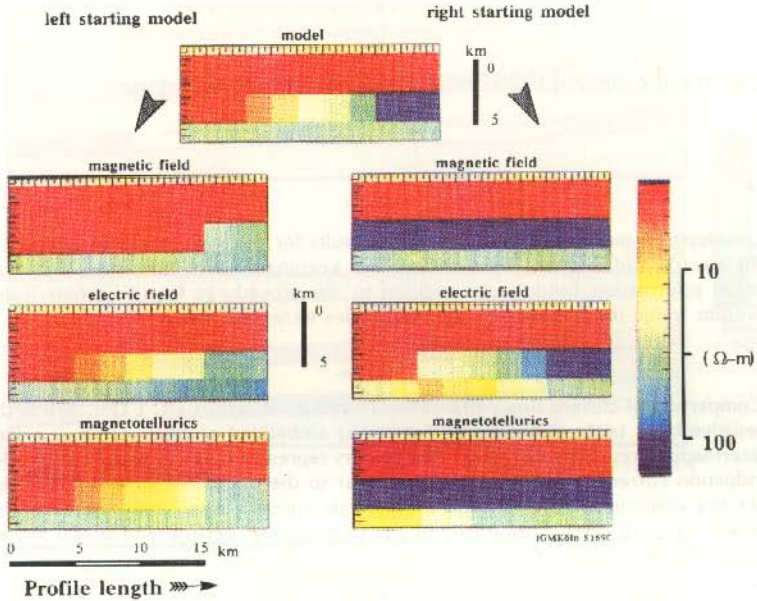


Fig.A7.2

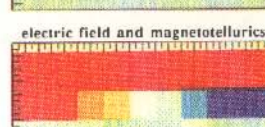
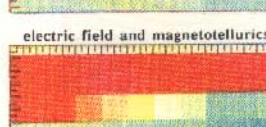
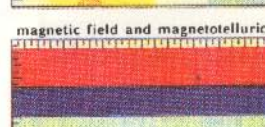
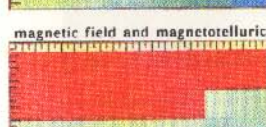
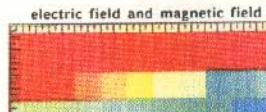
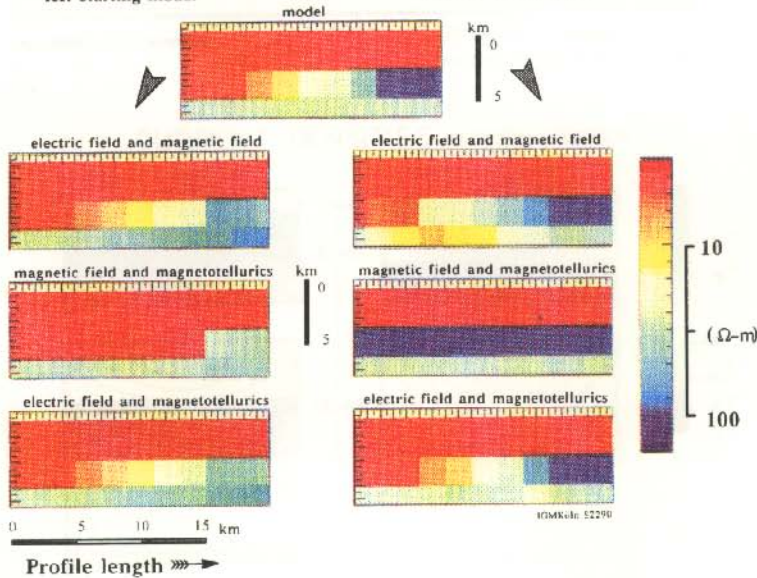
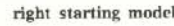
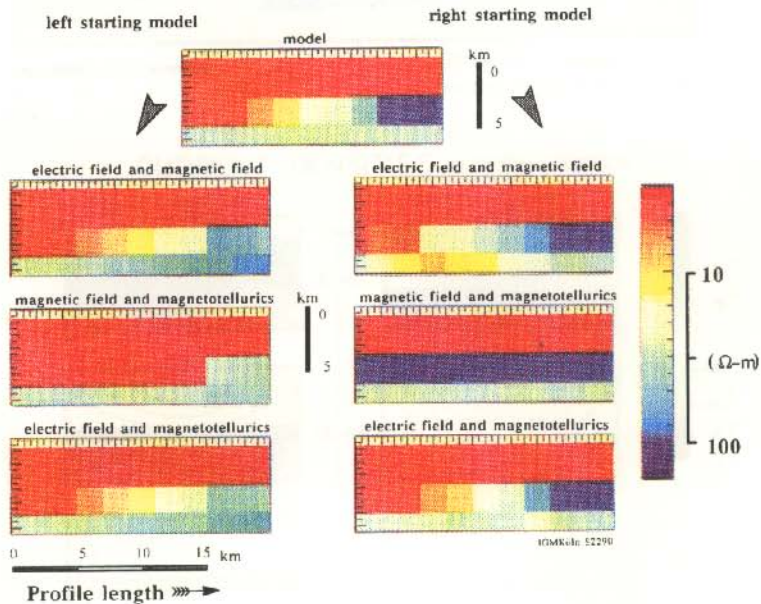
INVERSION OF INDIVIDUAL COMPONENTS (structure fixed)



Profile length

Fig.A7.3

JOINT INVERSION OF INDEPENDENT COMPONENTS (structure fixed)



Profile length $\ggg \rightarrow$

Fig. A7.4

Following are the descriptions for the figures on the next pages.

Fig.A7.5 Geoelectrical model (top) and inversion results for the joint inversion (along a profile) of the electric and magnetic field components keeping the structure fixed from the seismic a priori information (middle). In addition to the procedures for the center frame, for the bottom frame the bottom and top resistivities were kept fixed.

Fig.A7.6 Comparison of current flow patterns for a conductive layer (left, $1 \Omega\text{m}$, 500 m thick) and a resistive layer (right, $400 \Omega\text{m}$, 500 m thick) embedded at 2 km depth in a half space of intermediate resistivity ($20 \Omega\text{m}$). The colours represent areas of equal current density. The induction currents are flowing perpendicular to the plane of the figure. The dashed lines are the contours of the return currents with opposite sign. Time increases from top to bottom on both sides, from 0.01 s to 1 s. In both cases vertical and lateral moveout can be observed, but is faster for the resistive case on the right.

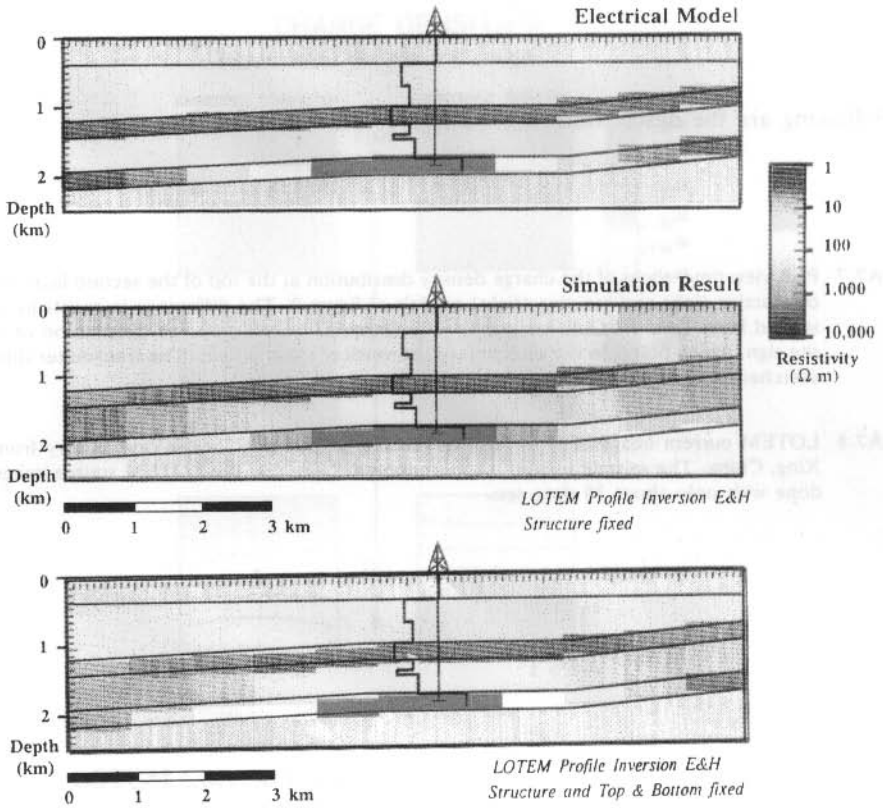


Fig.A7.5

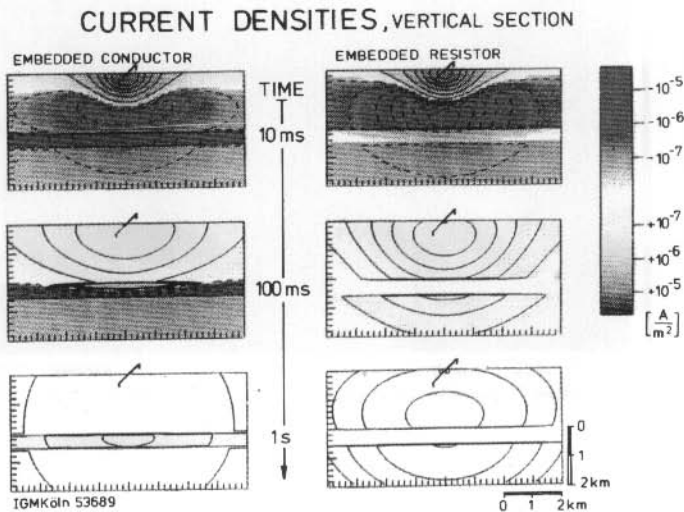


Fig.A7.6

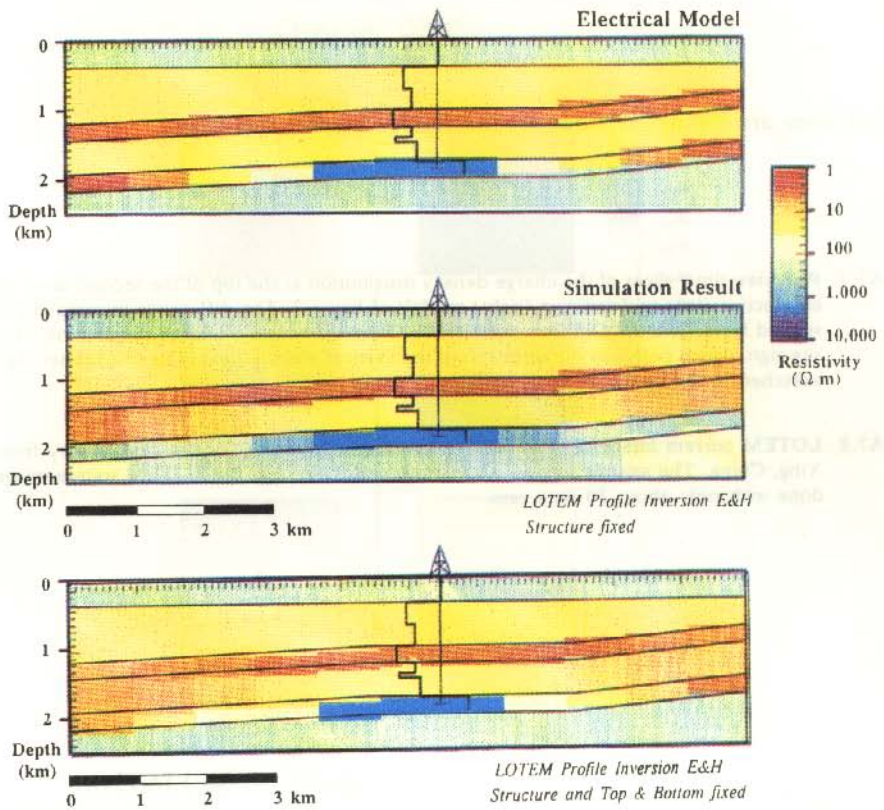


Fig.A7.5

CURRENT DENSITIES, VERTICAL SECTION

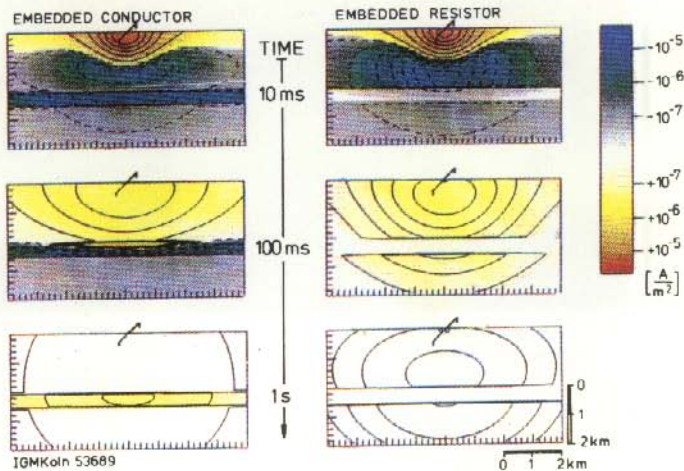


Fig.A7.6

Following are the descriptions for the figures on the next pages.

Fig.A7.7 Plan view time-slices of the charge density distribution at the top of the second layer for the conductive (left) and resistive (right) models of figure 2. The difference in resistivity of the second layer (left – 1 Ohm-m; right – 400 Ohm-m) causes a charge distribution of opposite sign, which points in the direction of the vertical electric field. The transmitter dipole is sketched in the center of each frame.

Fig.A7.8 LOTEM current image of a profile parallel to a seismic line for the case history from Tai Xing, China. The seismic section is superimposed. Note that the LOTEM source image was done with only about 30 data sets.

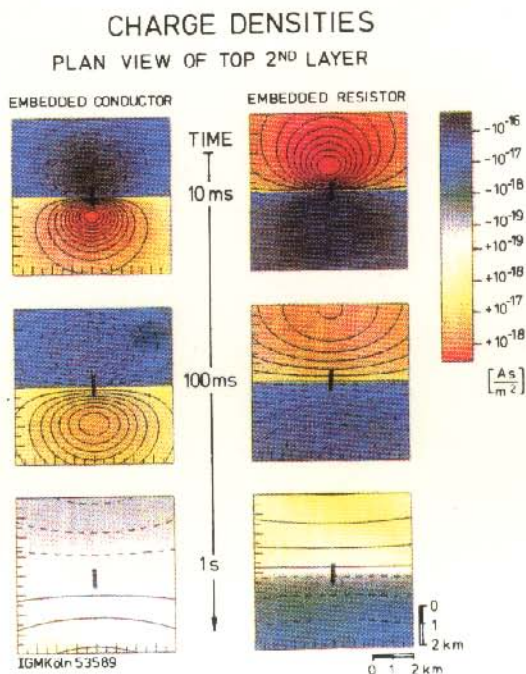


Fig.A7.7

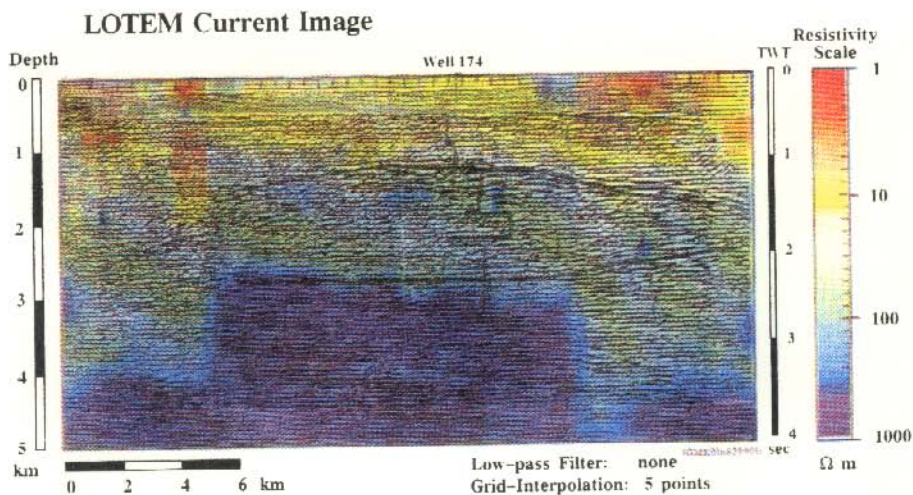


Fig.A7.8

KMS Technologies – KJT Enterprises Inc.
6420 Richmond Ave., Suite 610
Houston, Texas, 77057, USA
Tel: 713.532.8144

Please visit us
<http://www.kmstechnologies.com>

This material is not longer cover by copyright. The copyright was released by Elsevier to Dr. Strack on November 5th, 2007.

The author explicit authorizes unrestricted use of this material as long as proper reference is given.